2007

CARBON NANOTUBE AUGMENTATION OF A BONE CEMENT POLYMER

Brock Holston Marrs
University of Kentucky, brock.marrs@uky.edu

ABSTRACT OF DISSERTATION

Brock Holston Marrs

The Graduate School

University of Kentucky

2007

CARBON NANOTUBE AUGMENTATION OF A BONE CEMENT POLYMER

ABSTRACT OF DISSERTATION

A dissertation submitted in partial fulfillment of the requirements for the degree of Doctor of Philosophy in Biomedical Engineering at the University of Kentucky.

By

Brock Holston Marrs

Lexington, Kentucky

Director: Dr David Pienkowski, Professor of Biomedical Engineering

Lexington, Kentucky

2007

ABSTRACT OF DISSERTATION

CARBON NANOTUBE AUGMENTATION OF A
BONE CEMENT POLYMER

Acrylic bone cement is widely used as a structural material in orthopaedics, dentistry, and orofacial surgery. Although bone cement celebrates four decades of success, it remains susceptible to fatigue fracture. This type of failure can directly lead to implant loosening, revision surgery, and increased healthcare expenditures. The mechanism of fatigue failure is divided into three stages: 1) fatigue crack initiation, 2) fatigue crack propagation, and 3) fast, brittle fracture. Adding reinforcing fibers and particles to bone cement is a proposed solution for improving fatigue performance. The mechanical performance of these reinforced bone cements is limited by fiber ductility, fiber–matrix de-bonding, elevated viscosity, and mismatch of fiber size and scale of fatigue induced damage. In this dissertation, I report that adding small amounts (0% - 10% by weight) of multiwall carbon nanotubes (MWNTs) enhances the strength and fatigue performance of single phase bone cement. MWNTs (diameters of 10^{-9} – 10^{-8} m; lengths of 10^{-6} – 10^{-3} m) are a recently discovered nanomaterial with high surface area to volume ratios (conferring MWNT – bone cement composites with large interfaces for stress transfer) that are capable of directly addressing sub-microscale, fatigue induced damage. MWNTs (2wt%) significantly increased the flexural strength of single phase bone cement by a modest 12%; whereas, similar additions of MWNTs dramatically enhanced fatigue performance by 340% and 592% in ambient and physiologically relevant conditions, respectively. Comparing the fatigue crack propagation behaviors of reinforced and unreinforced single phase bone cements revealed that the reinforcing mechanisms of MWNTs are strongly dependent on stress intensity factor, K, a numerical parameter that accounts for the combinatorial effect of the applied load and the crack size. As the crack grows the apparent stress at the crack tip intensified and the MWNTs

lost their reinforcing capabilities. For that reason, it is likely that the predominant role of the MWNTs is to reinforce the bone cement matrix prior to crack initiation and during the early stages of crack propagation. Therefore, MWNTs are an excellent candidate for improving the clinical performance of bone cement, thereby improving implant longevity and reducing patient risk and healthcare costs.

KEYWORDS: Bone Cement, Carbon Nanotubes, Carbon Nanotube Composites, Fatigue Failure, Fracture Mechanics

Brock Holston Marrs

April 16, 2007

CARBON NANOTUBE AUGMENTATION OF A BONE CEMENT POLYMER

By

Brock Holston Marrs

Dr David Pienkowski
Director of Dissertation

Dr Abhijit Patwardhan
Director of Graduate Studies

April 16, 2007

RULES FOR USE OF THE DISSERTATION

Unpublished dissertations submitted for the Doctor's degree and deposited in the University of Kentucky Library are as a rule open for inspection, but are to be used only with due regard to the rights of the authors. Bibliographical references may be noted, but quotations or summaries of parts may be published only with the permission of the author, and with the usual scholarly acknowledgments.

Extensive copying or publication of the dissertation in whole or in part also requires the consent of the Dean of the Graduate School of the University of Kentucky.

A library that borrows this dissertation for use by its patrons is expected to secure the signature of each user.

Name	Date

DISSERTATION

Brock Holston Marrs

The Graduate School

University of Kentucky

2007

CARBON NANOTUBE AUGMENTATION OF A BONE CEMENT POLYMER

DISSERTATION

A dissertation submitted in partial fulfillment of the requirements for the degree of Doctor of Philosophy in Biomedical Engineering at the University of Kentucky.

By
Brock Holston Marrs

Lexington, Kentucky

Director: Dr David Pienkowski, Professor of Biomedical Engineering

Lexington, Kentucky

2007

For Ravin, Mom, and Dad,
whose love and support throughout this work was immeasurable.
My gratitude extends beyond words.

ACKNOWLEDGEMENTS

I would like to acknowledge the unwavering support and guidance of Dr David Pienkowski throughout the duration of my time at the University of Kentucky. Along with Dr Pienkowski, I must recognize the staff and students of the Orthopaedic Biomechanics laboratory for their help with instrumentation and the Department of Orthopaedic Surgery for their ongoing support of my work. I would also like thank Dr Rodney Andrews for providing me the opportunity to expand and grow my technical skills during the past five years at the Center for Applied Energy Research (CAER). Additionally, I thank the carbon materials group at CAER for their help with processing, testing, instrumentation, analysis, and, in general, for their advice. Specifically, I thank Terry Rantell for his help with starting this project in the right direction, Matt Weisenberger for his help and thoughts on carbon nanotube composites, and Dr Dali Qian for his work with transmission electron microscopy. I also thank Dr David Puleo and Dr Charles Knapp for their support and advice. Additionally, I thank the faculty, staff, and students of the Center for Biomedical Engineering at the University of Kentucky for their support, both inside and out of the classroom. I give special thanks to Polly Sinnett-Jones and Dr Ian Sinclair of the University of Southampton in the United Kingdom. Their help, support, thoughts, and conversations were invaluable during my six months abroad.

TABLE OF CONTENTS

ACKNOWLEDGEMENTS ..... **iii**

TABLE OF CONTENTS ..... **iv**

LIST OF FIGURES ..... **vi**

LIST OF TABLES ..... **vii**

CHAPTER ONE BONE CEMENT **1**

1.1 Composition and Additives 1
1.2 Applications 2
1.2.1 Total joint arthroplasty *2*
1.2.2 Vertebroplasty and kyphoplasty *4*
1.2.3 Dental prostheses *5*
1.3 Quasi-Static Mechanical Performance 6
1.4 Fatigue and Fracture Properties 7
1.4.1 Fracture toughness *7*
1.4.2 Fatigue crack propagation *8*
1.4.3 Fatigue performance *9*

CHAPTER TWO FATIGUE AND FRACTURE MECHANICS **12**

2.1 Initiation of Fatigue Cracks 15
2.2 Crack Propagation 16
2.2.1 Fatigue crack propagation and the stress intensity factor *17*
2.2.2 Growth of the plastic zone under cyclic loading *18*
2.3 Cyclic Softening and Other Damage Mechanisms in Polymers 20
2.3.1 Fatigue striations and discontinuous growth bands *21*
2.3.2 Crazing *22*

CHAPTER THREE CARBON NANOTUBES **26**

3.1 Fullerenes and Carbon Nanotubes 26
3.2 Characterization, Properties, and Applications 27
3.2.1 Production of carbon nanotubes *28*
3.2.2 Properties of carbon nanotubes *30*
3.3 Carbon Nanotube Composites 31
3.3.1 Dis-aggregation and dispersion of carbon nanotubes *31*
3.3.2 The carbon nanotube – matrix interface *33*
3.3.3 Mechanical properties of carbon nanotube composites *33*
3.4 Carbon Nanotube – Bone Cement Composites 35

CHAPTER FOUR AUGMENTATION OF ACRYLIC BONE CEMENT WITH MULTIWALL CARBON NANOTUBES **36**

4.1 Introduction 36
4.2 Methods 37
4.2.1 Nanotube production *37*
4.2.2 Specimen preparation *38*
4.2.3 Mechanical testing *39*
4.2.4 Data analysis *40*
4.3 Results 41
4.4 Discussion 47

CHAPTER FIVE MULTIWALL CARBON NANOTUBES ENHANCE THE FATIGUE PERFORMANCE OF PHYSIOLOGICALLY MAINTAINED METHYL METHACRYLATE – STYRENE COPOLYMER 51

5.1 INTRODUCTION 51
5.2 EXPERIMENTAL 53
5.2.1 Sample preparation 53
5.2.2 Fatigue testing and scanning electron microscopy 54
5.2.3 3-parameter Weibull analysis 55
5.3 RESULTS AND DISCUSSION 57
5.3.1 Fatigue testing results 57
5.3.2 Mechanisms of reinforcement 60
5.3.3 Carbon fibers versus multiwall carbon nanotubes 62
5.3.4 Effects of aging and testing in a physiologically relevant environment 62
5.3.5 The effects of MWCNTs is reduced at high concentrations 63
5.4 CONCLUSIONS 63

CHAPTER SIX MONOTONIC AND DYNAMIC FRACTURE PROPERTIES OF SINGLE PHASE BONE CEMENT REINFORCED WITH MULTIWALL CARBON NANOTUBES 64

6.1 INTRODUCTION 64
6.2 EXPERIMENTAL 66
6.2.1 Multiwall carbon nanotubes 66
6.2.2 Specimen production 67
6.2.3 Fracture toughness 67
6.2.4 Fatigue crack propagation 68
6.2.5 Scanning electron microscopy 69
6.3 RESULTS 69
6.4 DISCUSSION 72

CHAPTER SEVEN DISCUSSION AND CONCLUSIONS 77

7.1 MECHANISMS OF REINFORCEMENT 77
7.1.1 Crack initiation 78
7.1.2 Plastic deformation and crack propagation 78
7.1.3 Stress Intensity Factor (K) 80
7.1.4 MWNT Agglomerations 80
7.2 EFFECT OF STRESS AMPLITUDE 81
7.3 INTERSTITIAL CRYSTALLINITY 82
7.4 DOSE DEPENDENCY 82
7.5 LIMITATIONS 83
7.6 IMPLICATIONS 84
7.7 CONCLUSIONS 84

APPENDIX 85

A. WEIBULL ANALYSIS 85
A.1 3-Parameter Weibull Analysis with Visual Estimation of N_o 86
A.2 3-Parameter Weibull Analysis with Calculated N_o 87

REFERENCES 88

VITA 98

LIST OF FIGURES

Figure 2.1 Mode I Fracture 13
Figure 2.2 S-N Curve 13
Figure 2.3 Zones of Fatigue Failure 14
Figure 2.4 Fatigue Crack Initial State 18
Figure 2.5 First Tensile Half-Cycle 18
Figure 2.6 Relaxation to Zero Stress 19
Figure 2.7 Residual Compressive Stress 19
Figure 2.8 Compressive Half-Cycle 19
Figure 2.9 Compressive Relaxation 20
Figure 2.10 Second Tensile Half-Cycle 20
Figure 2.11 Fatigue Striations 22
Figure 2.12 Formation of Craze Network 23
Figure 2.13 Craze Failure 25
Figure 2.14 Crack Growth Through Crazes 25
Figure 3.1 Multiwall Carbon Nanotube 28
Figure 3.2 Nesting Dolls 28
Figure 3.3 Entangled MWNTs 29
Figure 3.4 MWNT Agglomeration 32
Figure 4.1 MWNT Structure 38
Figure 4.2 Cycles to Failure 42
Figure 4.3 Weibull Means 44
Figure 4.4 Probability of Survival 45
Figure 4.5 MWNT - Bone Cement Composite 46
Figure 4.6 Polymer Sheathing 47
Figure 5.1 Multiwall Carbon Nanotube 53
Figure 5.2 Minimum Fatigue Life 56
Figure 5.3 Micro-crack 59
Figure 5.4 MWNT - Bone Cement Composite 60
Figure 6.1 Multiwall Carbon Nanotube 66
Figure 6.2 Secant Method for Measuring Growth Rate 71
Figure 6.3 Fatigue Crack Propagation 71
Figure 6.4 MWNT Agglomerations 73
Figure 6.5 MWNT – Matrix De-Bonding 75

LIST OF TABLES

Table 4-1 Mean ± Standard Deviation of Mechanical Test Parameters Obtained from Quasi-Static 3-Point Bending Testing of Bone Cement Augmented with MWNTs.....42

Table 4-2 Summarized Fatigue Data and Weibull Parameters for Each MWNT Concentration Studied.....43

Table 5-1 Weibull Test Parameters vs MWCNT Loading at 20 MPa Peak Stress.....57

Table 5-2 Weibull Test Parameters vs MWCNT Loading at 30 MPa Peak Stress.....58

Table 5-3 Weibull Test Parameters vs MWCNT Loading at 35 MPa Peak Stress.....58

Table 6-1 Fracture Toughness of MWNT - Single Phase Bone Cement Composites 70

Table 6-2 Paris Law Parameters.....72

Acrylic bone cement is a proven material that is frequently used in orthopaedics and dentistry. This polymer-based implantable material is attractive because it is an injectable, two phase system that hardens within a reasonable time frame. Bone cement offers structural support and mechanical stability to a wide range of reparative surgeries. Semantically, bone cement is a misnomer. The function of bone cement is not to bind materials together; rather, it stabilizes one material (usually a metallic implant) with respect to another (the host bone) through mechanical interlocking.

1.1 Composition and Additives

Bone cement is commercially available as a two phase system based on polymethymethacrylate (PMMA). PMMA is chosen because it is injectable and the polymerization reaction is well documented and can be easily controlled. The powder phase of bone cement is primarily composed of PMMA beads, or beads of related copolymers such as methyl methacrylate – styrene copolymer (MMA-co-Styrene) and polymethylmethacrylate – methyl methacrylate copolymer (PMMA-co-MMA). The polymer beads constitute between 82 and 89% (by weight) of the powder phase. Most of the currently used bone cements contain an inorganic radiopacifying agent (barium sulfate or zirconia) at concentrations of 10 – 15 wt%. For select applications of bone cement, elevated concentrations (>15wt%) of radiopacifier are beneficial (i.e. vertebroplasty). The radiopacifier enables the surgeon to view the bone cement post-operatively with x-rays. The powder also contains a relatively small amount of benzoyl peroxide (BPO; ~ 0.5 – 2.6%), which catalyzes the polymerization reaction. The liquid phase is dominated by methyl methacrylate (MMA) monomer (~ 98wt%). Along with MMA, the liquid contains approximately 2wt% N,N-Dimethyl-*p*-toluidene (DMPT), which accelerates the polymerization reaction. A miniscule amount of hydroquinone is usually added to the liquid phase to prevent premature “on the shelf” polymerization. A few commercial bone cements contain antibiotics. When the liquid and powder phases are mixed the initiator (BPO) reacts with the accelerator (DMPT) to form free radicals, which start the free radical polymerization of MMA into PMMA. The monomer phase polymerizes around the pre-polymerized beads and radiopacifier. During polymerization, the mixture of the two phases is worked into dough that can be molded or injected. In a short amount of time (10 – 15 minutes) the bone cement hardens.

The relative amounts and types of materials vary among the different commercial bone cements and can be adjusted to tailor the handling and mechanical properties of the bone cement. Nearly all bone cements contain inorganic radiopacifiers (barium sulfate or zirconia), but the effect of adding non-reactive particles is the subject of debate. Some published results conclude that the radiopacifier, or agglomerates of the radiopacifier, can negatively affect the quasi-static and fatigue properties of bone cement. [1, 2] Conversely, if the particle size of the radiopacifier is low and agglomerates are not formed, then the radiopacifier can improve mechanical performance. [3] Iodine containing polymers are studied as alternatives to barium sulfate and zirconia [4-7]; however, they result in only modest changes to the quasi-static mechanical properties of bone cement. [5-7] Although the iodine containing bone cements possess superior fracture toughness, they do not show the same resistance to crack propagation as traditional bone cements. van Hooy-Corstiens et al report elevated fatigue performance in bone cements that contain iodine. [7]

1.2 Applications

Bone cement is widely used in orthopaedics and dentistry. In orthopaedics, bone cement is frequently used as a structural material in total joint arthroplasty and, more recently, in vertebroplasty and kyphoplasty. Bone cement is also used to anchor some dental implants. Alternatively, the PMMA form of radiolucent bone cement is used to form the bridgework for restorative dental prostheses (dentures).

1.2.1 Total joint arthroplasty

Acrylic bone cement celebrates a history of use in total joint arthroplasty that is over four decades old. Charnley first proposed using self-polymerizing PMMA bone cement to stabilize the metallic implant during total joint arthroplasty procedures. [8] Taking advantage of the doughy, polymerization stage, he proposed to inject the bone cement into the clean intermedullary canal and insert the metallic stem of the implant into the dough. Within a reasonable amount of time, the bone cement hardens and sets the implant with respect to the neighboring bone. The hardened cement not only stabilizes the implant, but it also provides a buffer zone between the implant and the bone, which have markedly different mechanical properties. The implant, bone cement mantle, and host bone work together as a single unit to restore functionality to the patient's joint.

The implant construct is divided into three critical zones: 1) the bone – bone cement interface, 2) the bone cement mantle, and 3) the bone cement – implant interface. [9, 10] Although the *in vivo* behavior of each is obviously different, each is critical to the success of the construct. At Zone 1 (the bone – bone cement interface), the response of the bone tissue to the bone cement varies from case to case. Several parameters affect the clinical development of this interface, including: chemical necrosis from residual monomer seeping into the bone, thermal necrosis from the exothermic polymerization, and the micro-motion at the interface, which can produce debris particles that irritate surrounding tissues. [11] Each of these factors can negatively affect the outcome of the procedure by inducing an inflammatory response, which ultimately leads to the fibrous encapsulation of the bone cement and implant. The formation of a fibrous layer directly leads to migration and loosening of the implant. In the best case scenario, bone – bone cement interface is a site of good interlocking.

The bone cement – implant interface (Zone 3) is the focus of extensive research and is, more often than not, the reason for re-designing the stem of the metallic implant. More recently, implant stems are manufactured with precoated surfaces, sintered surfaces (beads or fibers), grooved, or serrated patterns with the goal of improving mechanical interlocking between the implant and the bone cement mantle. A good interface enhances the transfer of body loads from the artificial joint to the surrounding bone; however, as Bauer et al point out, an everlasting bond between these two components is unrealistic and some level of de-bonding is likely. [11] Extensive de-bonding can lead to construct failure at this interface [12], but small amounts of de-bonding appears to minimally affect the lifetime of the construct (with a smooth stem). [13] Attention should be paid to the development of wear particles and debris, especially for implants with surface texture. Such by-products of micro-motion can migrate to the articulating surface of the joint as well as into surrounding tissues. [11]

The bone cement mantle (Zone 2) is equally as important to the success of the construct as the other two zones. As previously mentioned, the bone cement is a buffer between the implant and bone. For complete restoration of the joint's load bearing capabilities, the joint reaction and body forces must be adequately transferred from the implant to the bone. The dynamic joint reaction forces of the hip and knee are attributed to everyday activity such as standing, walking, and climbing stairs. If these forces and those attributed to body mass are inefficiently distributed, then the host bone may remodel around the construct. Bone tissue is strain-dependent (Wolff's Law). If the

implant shields the bone from stresses developed from the joint reaction and body forces, then the bone may resorb. [11] Thus, the bone cement aides the distribution of forces and prevents stress shielding; however, loss of mechanical integrity (i.e. fatigue failure) greatly dampens the effectiveness of the bone cement mantle. Mechanical failure of the mantle or de-bonding at either interface directly leads to a loss in stability. Implant loosening is one of the leading causes of clinical failure.

To date, the most popular total joint arthroplasty procedures are knee replacements (~381,000 cases of primary surgery in 2002) and hip replacements (~193,000 cases of primary surgery in 2002). [14] Other cemented arthroplasties include shoulder [15] and elbow [16] replacements. Clinical failure of the primary implant is corrected with revision surgery. Revisions are more prevalent among younger [17] and active or overweight patients. [18] The American Academy of Orthopaedic Surgeons revealed that in 2003 the cost of revision knee and hip surgeries in the United States reached $1.5 billion and $1.7 billion, respectively. [19] Additionally, Burns *et al* project that the total cost of knee revisions will rise to $24.3 billion by the year 2030. [20] Even slight improvements to any part of the implant construct could have major impact on the healthcare system. Clinical failure is often the result of fatigue failure of the bone cement mantle; thus, improving the fatigue performance of bone cement is necessary for increasing the clinical life of the implant and reducing healthcare expenditures.

1.2.2 Vertebroplasty and kyphoplasty

Vertebral compression fractures (VCFs) are common among patients with fragile bone structure, such as those suffering from osteoporosis. Phillips estimates that these types of fractures occur in one out of every five people over the age of 70 years. [21] A compressed vertebra distorts posture and shifts the center of gravity away from the spinal column, which negatively alters the biomechanics of the spine. Chronic pain and discomfort may develop from improper healing and spinal kinematics. The current treatments for VCF are vertebroplasty and kyphoplasty. [21-23] In the former, low viscosity bone cement is percutaneously injected into the collapsed vertebrae to stabilize the fracture. In the latter, a balloon is inserted into the fracture site and inflated to restore the height of the vertebral body. Bone cement is then used to stabilize the restored structure of the vertebrae. Low viscosity bone cements increase the infiltration into the fracture site, but they typically have longer setting times. In a number of cases bone cement was shown to leak out of the injection site and into the surrounding tissues.

[21, 22, 24] The extravasation of bone cement may lead to unwarranted health risks such as pulmonary embolism, inflammation, or possible neurological effects. Additionally, operative and post-operative visualization of the injection site is difficult, so a number of experimental bone cements with elevated concentrations of radiopacifier are under investigation. [25] The Food and Drug Administration strictly limits the number of bone cements approved for vertebroplasty and kyphoplasty and recently increased the number of approved bone cements from two in 2004 to twelve in 2006. [26]

Vertebral collapse may also result from the treatment of osteolytic tumors within the spinal column. Although recent advances in oncology greatly extend patients' lives, they often contribute to the loss of bone mass within the vertebral body, which can lead to vertebral collapse. [27] The immediate impact on the patient is deformation of the spine and added stress on the tissues anterior to the spinal column (pulmonary, neurological, etc). Early treatment of vertebral fractures with vertebroplasty show significant relief of pain. [27] However, the extravasation of low viscosity bone cement from the vertebroplasty site and inefficient restoration of vertebral height make kyphoplasty the better choice for treating osteolytic tumors. Higher viscosity bone cements that are less likely to leak into neighboring tissues can be used in kyphoplasty (considering the larger injection site).

1.2.3 Dental prostheses

In some dental applications, radiolucent bone cement exclusively composed of PMMA is used for structural purposes. The application of PMMA in dentistry is quite different from that in total joint arthroplasty, vertebroplasty, and kyphoplasty. Rather than initiating the polymerization reaction of PMMA by mixing two phases, the reaction is induced by heating the monomer phase. The polymerizing monomer can be molded or cast into desired shapes. Full and partial restorative dental prostheses (dentures) are partially made of dental PMMA. A metallic framework is constructed to hold the artificial teeth in place. MMA monomer is polymerized around this framework to create a custom fit for the patient. The role of PMMA in dentures is to provide structural support for the artificial teeth and metalwork. The PMMA also provides mechanical stability and strength to the denture. The use of PMMA in dentures does not share some of the drawbacks of two phase PMMA-based bone cements such as cement leakage, chemical necrosis, and thermal necrosis. The pre-formed prosthetic interfaces with the interior of the mouth through topical contact surfaces; thus, the biocompatibility and cytotoxicity

issues are minimal. However, dental PMMA is not immune from mechanical failure. Roughly one out of every three failed prostheses results from midline fractures of the PMMA retainer. [28] Other types of fracture account for an additional 38% of the failed prostheses.

1.3 Quasi-Static Mechanical Performance

An extensive amount of literature is reported on the quasi-static mechanical properties of bone cement. Typically, quasi-static testing (tension, compression, bending, shear, etc) is a quick and easy way to compare and contrast various commercial bone cements. All applications of bone cement involve some form of monotonic loading; thus, these tests are valid for predicting the performance of bone cement. ASTM F 451 – 95 is dedicated to the characterization of bone cement; yet, the only included quasi-static mechanical test is the compression test. [29] The literature is not limited to just compression. In two reviews, Lewis [10] and Kuehn *et al* [30] compare the many quasi-static properties of several commercial bone cements.

Although bone cement is used successfully, there exists room for improvement. [10] Increasing the strength of bone cement would aide in improving clinical performance. Engineering high performance bone cement can be addressed from many directions. For example, reducing the number and size of pores increases the quasi-static strength of bone cement. [31-33] This can be accomplished through vacuum mixing. Sterilization, which can alter molecular weight, also plays a role in the quasi-static strength of bone cement (though sometimes negative). [34-36] Addition of a reinforcing phase can also positively affect the quasi-static properties of bone cements, although most of the changes are modest. [36-46] Fiber reinforcement enables the bone cement mantle to withstand higher loads by dissipating the strain energy associated with loading. Polyzois et al report negative effects for the addition of glass fibers and woven fibers to PMMA. [47] Alternatively, Vallo reports a significant increase in the flexural modulus of bone cement with the inclusion of glass beads. [48]

Although these studies produce positive and insightful results, there remains room for improvement. The static mechanical properties (strength, modulus, deflection) largely remained unchanged with a few exceptions. This lack of improvement can be attributed to the de-bonding of the fibers from the matrix (which, ironically, improves fracture properties). The success of a composite material (i.e. stress transfer) is dependent on the interfacial strength between the fibers and the matrix. Adding

macroscopic fibers to the bone cement matrix may heighten viscosity, which could directly lead to the incorporation of pores or voids within the bone cement mantle. Additionally, elevated viscosity may lead to inadequate dispersion of the fibers, formation of fiber agglomerations, and development of regions of non-homogeneity. Pores and agglomerations curb the positive effects of fiber reinforcement by elevating local stresses.

1.4 Fatigue and Fracture Properties

In addition to the quasi-static mechanical properties, the dynamic and fracture related properties are also relevant and widely studied. Fracture toughness, fatigue crack propagation, and fatigue testing to failure provide valuable information regarding the dynamic performance of bone cement, which can be used to predict the clinical longevity of the bone cement when subjected to dynamic loading. Technically, fracture toughness should be grouped with the quasi-static properties; however, it has great implications for the dynamic performance of the bone cement. In fact, fracture toughness is defined as the material's resistance to fracture when the specimen is pre-cracked. In some cases, the pre-crack is formed from dynamically loading a notched specimen. Characterizing and understanding the fracture and fatigue properties is beneficial to optimizing the clinical performance of bone cement, especially considering the array of dynamic loads in the *in vivo* bone cement mantle, the micro- and macropores discovered in retrieved bone cement mantles, and the role of fatigue failure of bone cement in the success of the implant. A review of these fracture properties by Lewis and Nyman [49] establishes standard conditions, parameters, and analytical techniques to be used when characterizing the fatigue and fracture properties of bone cement.

1.4.1 Fracture toughness

The fracture toughness (ΔK_{IC}) is defined as the resistance of a material to fracture when the material contains a pre-formed crack. Fracture toughness takes into consideration the applied load as well as the size of the pre-crack. Increasing the energy absorbing capacity is believed to elevate the toughness of bone cement since energy absorptive mechanisms delay catastrophic fracture. Crazing and micro-cracking are thought to enhance toughness for these very reasons. [50] Thermoplastic elastomer beads increase the probability of crazing and micro-cracking and, thus, can be used to

enhance the fracture toughness of bone cement. [51] Several intrinsic factors that affect the fracture toughness of bone cement include composition [52, 53], radiopacifier [5, 54], and relative amounts of the reactive components. [55] Extrinsic factors also contribute to the fracture toughness of bone cement. Sterilization techniques (gamma irradiation, ethylene oxide) indirectly affect fracture toughness [52, 53, 56] by altering the molecular weight of polymer. [35, 55] Fracture toughness decreases with increasing prevalence of porosity, which can be minimized by vacuum mixing. [52, 57] Analysis of extracted bone cement mantles confirms that porosity is one of the most important factors affecting fracture toughness. [57] Plasticization of the bone cement, which is known to occur in saline environments, increases toughness by promoting the formation of crazes and other energy absorbing mechanisms.

Adding a reinforcing phase to bone cement directly affects fracture toughness. Adding polymer fibers of ultra high molecular weight polyethylene [36], Kevlar 29 [58, 59], plasma-treated PE [60, 61], and PMMA [39, 40] significantly increase the fracture toughness of bone cement. The reasons for such increases are numerous. Some authors propose that the increases are the result of a collection of energy dissipating mechanisms, such as crack deflection and increased ductility of the fibers. [39] SEM images of the Kevlar 29 – bone cement composites reveal fiber failure mechanisms (splitting and kinking) that are energy absorptive and likely contributors to elevated toughness. [58] Metal fibers such as stainless steel [62] and titanium (12 μm and 22 μm diameter) [63] also increase the fracture toughness of bone cement. The steel fibers are shown to deflect the path of crack growth, which leads to the postulation that mechanical interlocking between the “rough” crack faces is partly responsible for the increased fracture toughness. Similarly, the addition of glass beads enhances toughness. [48] Rather than reinforcing the matrix, the glass beads serve to alter the monomer to polymer ratio, which likely leads to the increase. Although poor fiber – matrix bonding is known to negatively affect several quasi-static properties, several authors postulate that de-bonding absorbs energy and may boost fracture toughness. [36, 48, 58, 62, 63]

1.4.2 Fatigue crack propagation

Fatigue failure of bone cement (and other polymers) is divided into three stages: fatigue crack initiation, fatigue crack propagation, and fast, brittle fracture. [64] Depending upon the applied stress of the dynamic test, the crack propagation stage may dominate the fatigue failure of bone cement. The crack propagation stages of polymers

similar to bone cement include the formation of crazes and micro-cracks (as described in Chapter Two) [64]; thus, the stress intensity factor (K), which takes into consideration the applied stress and the extent of damage accumulation, plays a role in determining the rate of crack growth. Accumulation of fatigue related damage is nonlinear; thus, changes in the stress intensity factor (K) and rate of crack growth are expected. [65] Understanding the role of fatigue crack propagation in fatigue failure will be useful to engineering new, high performance bone cements. Published results show that inorganic radiopacifiers (i.e. barium sulfate, zirconia) decrease the rate of crack propagation, thus, improving the fatigue performance of the bone cement. [2, 5, 66] The presence of barium sulfate is thought to sufficiently weaken the interstitial matrix (region formed form polymerized MMA). The path of the fatigue crack is then limited to the interstitial matrix and, ultimately, lengthened. Similar evidence from fractography suggests that low rates of crack growth produce the roughest fracture surfaces, an effect most likely attributed to the crack following a path around the polymer beads as opposed to through them. [50] Secondary to lengthening the crack path, the radiopacifier creates voids in the bone cement, which blunt crack growth. [2, 5] Similar to radiopacifiers, reinforcing phases such as acrylonitrile – butadiene – styrene (ABS) and fibers slow the rate of crack growth, thus, improving the resistance to fatigue crack propagation. [60, 63, 67] The role of porosity in the fatigue performance of bone cement is both contradictory and controversial. [68-70] Pores are simultaneously sites of crack initiation and mechanisms for blunting crack growth. [67, 69, 70] Therefore, bone cement can be tailored by adding reinforcing phases and altering the intrinsic properties to maximize the propagation stage, which will enhance fatigue performance.

1.4.3 Fatigue performance

Typically, dynamic testing is more complex than monotonic testing. Dynamic tests are lengthy and the test parameters must be chosen carefully. [71] During dynamic loading, the material is forced through several changes that may not manifest during monotonic loading; therefore, careful consideration must be given to fatigue data, especially as each sample is analyzed and compared. Analysis of fatigue data is not straightforward and uncertainties arise from many factors. Four such factors to consider are: 1) variability in microstructure among the specimens, 2) variability in the fatigue test (e.g. cycle to cycle variance in the path of the actuator), 3) variability in the testing environment, and 4) variability in modeling the fatigue process. [72]

In a review of reports pertaining to bone cement, Lewis writes that a collection of intrinsic and extrinsic factors greatly affect fatigue performance. [71] The intrinsic factors include composition, molecular weight, radiopacifier (type and size), relative amounts of components, viscosity, and the presence of a reinforcing phase and/or antibiotics. Extrinsic factors include storage temperature, mixing method, specimen production, configuration and size, aging, curing, sterilization, sample size, and test conditions. Lewis identified several areas of disagreement within the literature: storage temperature, viscosity, handling (centrifugation, vacuum mixing, and pressurization) of the bone cement, fabrication of specimens, selection of specimens, role of porosity, test frequency and environment. [71] The commercial brand of the bone cement usually accounts for the discrepancies; however, some of these issues appear to be interdependent, regardless of brand. Despite the numerous inconsistencies reported by Lewis, several factors are shown to alter the fatigue performance of bone cement: adding a reinforcing phase, adding a radiopacifier, increasing molecular weight, and increasing test frequency.

In theory, adding a reinforcing phase to bone cement increases fatigue performance. Typically, fibers of various materials are added with the hope of delaying fatigue crack initiation and/or slowing the propagation of the fatigue crack. Current reports show several positive outcomes, but the successes are relatively limited. Decreasing the number and size of pores increases the fatigue performance of bone cement. [31, 52, 73-78] This is typically achieved through vacuum mixing and pressurized injection. While most would agree that reducing the amount of pores in the mantle would greatly improve the mechanical performance, others suggest it may adversely affect other properties including shrinking. [79] Changes in molecular weight (often through sterilization [34]) also alter the fatigue performance of bone cement — decreasing molecular weight decreases fatigue performance.[35, 52, 55, 74] Adding a reinforcing phase (typically fibers) can improve fatigue performance much in the same way that quasi-static strength is increased. The reinforcing phase shields the bone cement from dynamic loads and slows the development of fatigue related damage. Self-reinforcing bone cements exhibit elevated dynamic properties. [39] Additionally, metal fibers improve the fatigue performance of bone cement, especially at lower stress amplitudes. [62, 63, 80] Similarly, carbon fibers positively affect fatigue performance. [81]

Similar to quasi-static properties, the fatigue performance of fiber reinforced bone cements are limited by heightened viscosity and fiber ductility. Additionally, macroscale fibers do little to address the microscale and sub-micron mechanisms of fatigue failure (i.e. crazing, micro-cracking). The fibrils of a craze are typically several hundred nanometers to a few microns in length and far less in width [72, 82]; thus, the discrepancy in size between the craze and traditional fibers limits the enhancement of fatigue performance. Therefore, the reported increases in fatigue performance are more likely due to increased fracture toughness and crack bridging than craze reinforcement. Ideally, the reinforcing phase would simultaneously improve quasi-static strength and address the issue of crazing and micro-cracking. A smaller fiber of high strength should meet these requirements.

The long term survivability of materials (whether metal, ceramic, or plastic) is, without doubt, critical to their functionality and applicability. Each type of material responds differently to dynamic loading and those responses depend on the characteristics of the material (i.e. strength, ductility, brittleness). Typically, fatigue is characterized as a series of microscopic and sub-microscopic events that culminate in the catastrophic failure of the material. These events directly relate to the accumulation of fatigue related damage. The extent and rate of damage accumulation varies from material to material. For most polymers, the mechanisms of fatigue failure are well known and will be described in detail.

In general, polymers can be sub-divided into groups based on the orientation of their smallest functional unit – the molecular chain. Those polymers with regions of highly ordered molecular chains are said to be crystalline or semi-crystalline and include polyethylene (PE), polypropylene (PP), and polyethylene terapthalate (PET). Alternatively, amorphous polymers are those that have no ordering among their molecular chains (polystyrene (PS), polymethylmethacrylate (PMMA), and polysulfone (PSF)). The behaviors of each classification are different; however, amorphous and semi-crystalline polymers share some of the same responses to dynamic loading. In addition to crystallinity, the amount of cross-linking, or lack thereof, and the molecular weight also play significant roles in the fatigue failure of polymers. Polymers can further be broken down into two distinct categories: thermoplastics (usually comprised of linear polymer chains that are held together with secondary attractive forces) and thermosets (polymers that form a rigid structure through chemical cross-links). Typically, thermoplastics exhibit superior resistance to fracture; thus, they should exhibit greater fatigue performance than thermosets.

For the purposes of this exploration, only controlled stress fatigue in Mode I will be considered. (Figure 2.1) Typically, the fatigue life of a polymer is studied by applying a stress of constant amplitude at a pre-determined frequency and counting the number of stress cycles it takes to fail the specimen completely. Traditionally, the mechanism of fatigue failure is divided into three distinct phases [64, 83]: 1) initiation of a fatigue crack, 2) propagation of the crack through the polymer, and 3) fast, brittle fracture. The length of the first two stages determines the fatigue life of the polymer (since the third stage is fast). It is currently unclear which mechanism (initiation or propagation) is dominant in

the fatigue failure of polymers. Generally, high stress amplitudes result in shorter fatigue lives whereas low stress amplitudes lead to longer fatigue lives. This is exemplified by the classic S – N curve. (Figure 2.2) The lower horizontal asymptote of the S-N is commonly reported as the endurance limit (σ_e), which is defined as the stress below which the specimen theoretically survives an infinite number of cycles. In industry, the endurance limit is often used describe the lifetime performance of the material.

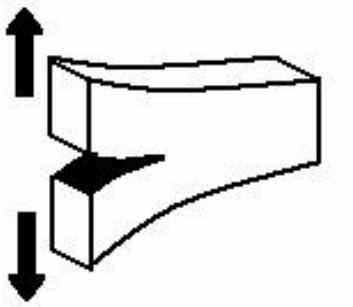

Figure 2.1 Mode I Fracture

Mode I fracture entails the separation of the crack faces in the direction of the principal stress (indicated by the arrows). The crack grows perpendicular to the direction of the principal stress.

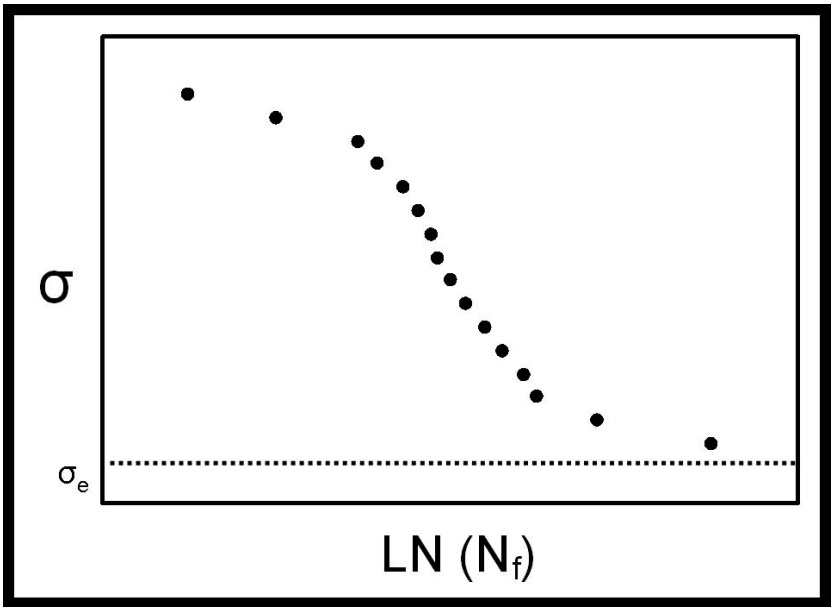

Figure 2.2 S-N Curve

The classic S-N curve plots the applied stress against the natural log of the number of cycles to failure. The lower asymptote of the curve denotes the endurance limit of the material (σ_e).

The S-N curve of a polymer is divided into three regions (I, II, and III) and the each region is determined by the ratio of the applied stress to the quasi-static strength of the polymer. (Figure 2.3) Region I includes fatigue tests with applied stresses nearest the ultimate strength of the polymer. The probability of failure is high within this region and most specimens fail after a short cycling period; thus, tests within this regime are said to be of low cycle fatigue (LCF). The applied stress of LCF typically exceeds the strength required to form crazes; thus, crack initiation and craze formation typically occur during the initial cycle of the fatigue test. [72] Therefore, polymers tested within Region I are thought to reside almost exclusively in crack propagation. In the instances when the applied stress is not large enough to induce crazing, then Region I may become an extension of Region II.

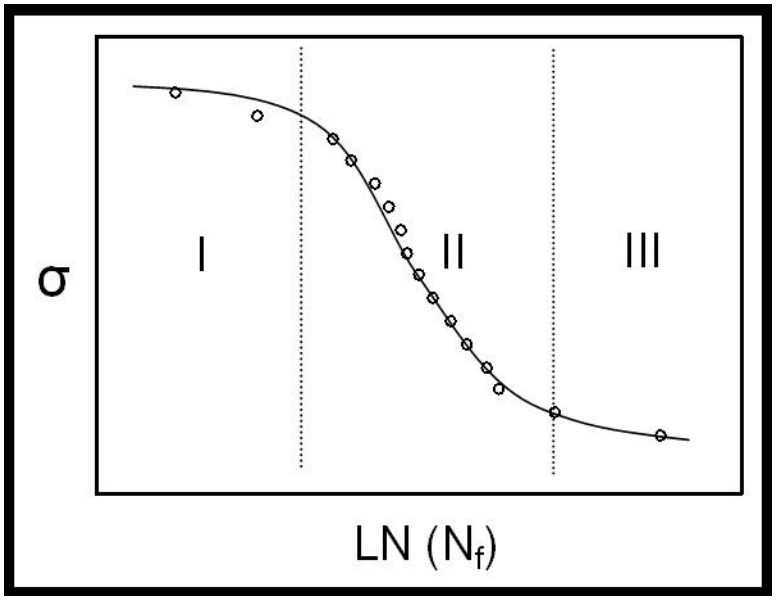

Figure 2.3 Zones of Fatigue Failure

The S-N curve is divided into three regions. Each region differs in slope, which indicates the underlying mechanisms of fatigue failure are different.

Region II is developed from fatigue testing with applied stresses between the endurance limit (σ_e) and strength required to form crazes (σ_c). Most fatigue tests fall within this region. Suresh explains that the slow growth of crazes and subsequent nucleation of fatigue cracks dominate the failure of polymers within this region. [72] Although crazes do not form during the initial cycle of the fatigue test, they eventually form with continued cycling. [83] The onset of damage can manifest as the formation of

micro-cracks, which eventually nucleate into a larger fatigue crack. Crazes usually precede the growth of the fatigue crack. The fatigue crack mechanistically grows by the formation and subsequent failure of crazes until the crack reaches a critical size. At this critical crack size, which is related to fracture toughness, stable growth gives way to unstable crack propagation and, ultimately, catastrophic failure.

Region III, the region of high cycle numbers, is comprised of specimens that show little sign of crazing. In fact, the size of the craze zone shrinks as the applied stress decreases. [84] This is largely due to the minimization of stress localization at defects, pores, and voids. In such cases, the strength required to form crazes is never reached. For this reason, the fatigue performance of the polymer is thought to be dominated by crack initiation. [83] Thus, the nucleation of a fatigue crack at a microstructural defect may precede the formation of crazes. Specimen failure prior to reaching the run-out limit of the fatigue test is primarily due to the rapid onset of crack formation and growth without the presence of plastic deformation.

2.1 Initiation of Fatigue Cracks

Fatigue failure of polymers is thought to be dominated by two mechanisms: fatigue crack initiation and fatigue crack propagation. The former is classified as the period of cycling prior to the formation of a fatigue crack. The length of the initiation phase is dependent on several things including the strength of the material, the magnitude of the applied stress, and the presence of voids, flaws, pores and material inhomogeneities. Localization of the applied stress at such structural defects creates an elevated apparent stress at the defect site. The elevated apparent stress increases the likelihood of crack initiation, especially if the localization of stress is accompanied by an increase in local temperature. With large, macroscopic defects, crack initiation may lead directly to catastrophic failure.

In some polymers, the formation of crazes precedes the initiation of fatigue cracks. In these cases, the period of crack initiation extends until the area of cyclic deformation becomes so large that the mechanical integrity of the polymer is compromised. As long as the applied stress produces elastic strains in the polymer, the craze zone will continue to grow without the formation of a fatigue crack; however, inelastic straining within the craze leads to its deterioration, which enables the nucleation of a fatigue crack. In cases where crazing does not occur (such as polymers in Region III of Figure 2.3), crack initiation dominates the fatigue performance of the polymer until

failure occurs. Once the initiation of the fatigue crack is complete, the specimen departs the period of crack initiation and enters the period of crack propagation.

2.2 Crack Propagation

Crack propagation (for both monotonic and dynamic loading) is best described as the stable crack growth that onsets at initiation and lasts until fast, brittle fracture occurs. The mechanisms of crack propagation are best described through the use of linear elastic fracture mechanics (LEFM). As Schultz explains [84], if crack initiation results in the formation of a fatigue crack of length *a*, then the subsequent growth of the crack (*δa*) is related to the applied stress (σ) and the elastic work (δW_a) by the Griffith criterion:

$$\delta W_a = \left[\frac{\pi \sigma^2 a\left(1-\upsilon^2\right)}{E} \right] \delta a \qquad (1)$$

where E is the Young's modulus and ν is the Poisson's ratio. Since the $(1 - \nu^2)$ term is close to unity, the Griffith criterion is reduced to:

$$\delta W_a = \left[\frac{\pi \sigma^2 a}{E} \right] \delta a \qquad (2)$$

As propagation ensues, the surface area of the crack increases; thus, a second work term is added to account for the surface energy of the crack (δW_s),

$$\delta W_s = 2\gamma_s \delta a \qquad (3)$$

where γ_s is the surface energy per unit length of the crack. If the work due to the surface area exceeds the work term for moving the crack by *δa* ($\delta W_s > \delta W_a$), the crack will not grow. For example, when the initial length of the crack is small, the crack does not readily advance. Conversely, at larger values of *a*, δW_a exceeds δW_s and the crack grows spontaneously. The two work terms are equivalent when the length of the crack is at a critical value, a_{cr}. Equations 2 and 3 can then be combined to calculate the stress (σ_{cr}) at this critical crack length:

$$\sigma_{cr} = \left[\frac{2E\gamma_s}{\pi a_{cr}} \right]^{1/2} \qquad (4)$$

Since energy can be stored in the plastic deformation of polymers, Equation 4 must be modified to include a term for the work spent by plastic flow (γ_p) during the growth of the crack by *δa*. Thus, the modified equation becomes

$$\sigma_{cr} = \left[\frac{2E\left(\gamma_s + \gamma_p\right)}{\pi a_{cr}} \right]^{1/2} \qquad (5)$$

2.2.1 Fatigue crack propagation and the stress intensity factor

Although the Griffith criterion originally described the propagation of cracks during monotonic loading, the principles can be applied to dynamic loading. An important parameter of fatigue crack propagation is the development of the stress intensity factor, K, which accounts for the relationship between the applied stress and the extent of plastic deformation. The stress intensity factor (reported as MPa√m) can be substituted into the Griffith criterion:

$$\delta W_a = \left(\frac{K^2}{E} \right) \delta a \qquad (6)$$

where $K = \sigma(\pi a)^{1/2}$. As Schultz explains, the (K^2/E) term relates to the energy stored in the plastic zone surrounding the crack tip and, thus, is equivalent to the energy required to lengthen the crack by δa. [84]

The formation of a plastic zone, as noted by the inclusion of a plastic work term (γ_p), is not independent of the stress intensity factor, and vice versa. In fact, the length of the plastic zone, R_p, accompanying large cracks is directly proportional to the square of the stress intensity factor. It is known, by definition, that calculation of the stress intensity factor (K) considers both the size of the crack (a) and the applied stress (σ) [72, 84] – as the plastic zone increases so does the stress intensity factor. In order for a crack to advance the strength of the plastic zone must be overcome; therefore, it can be inferred that propagation of a fatigue crack is a function of the stress intensity factor, K.

Recall that crack propagation is related to the amount of energy spent in advancing the crack, which is directly related to the stress intensity factor. [84] It can then be assumed that the rate of crack growth in a fatigue test (da/dN) is some function of K. Paris et al devised an equation based on a power law that directly relates the rate of crack growth with the stress intensity factor range (ΔK) [85]:

$$da/dN = C(\Delta K)^m \qquad (7)$$

where C and m are material constants and ΔK is the range of stress intensity factors between the maximum and minimum stresses of the fatigue test ($K_{\sigma max} - K_{\sigma min}$). The material constants, C and m, account for the environment, temperature, material properties, microstructure, loading mode, mean stress, and test frequency. [72]

2.2.2 Growth of the plastic zone under cyclic loading

Schultz further describes fatigue crack propagation through a series of drawings depicting the growth of the plastic zone as it relates to the applied stress. [84] The fatigue test is assumed to be fully reversed tension – compression with a mean stress amplitude of zero. As the stress cycle starts (σ_o = 0 MPa), a fatigue crack of unknown length is assumed to be closed and surrounded by a previously developed plastic zone of unspecified dimensions. (Figure 2.4) As the applied stress is raised to the maximum tensile stress ($+\sigma_o$), the yield strength of the plastic zone (σ_y) is surpassed and plastic deformation results. (Figure 2.5) The energy of this plastic deformation is dissipated through the enlargement of the plastic zone in the direction of the principal stress. In cases of low stress amplitude and small plastic zone, the yield strength may not be exceeded and the energy from the application of stress would be stored elastically in the material.

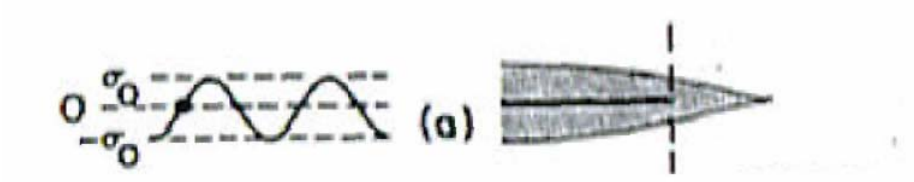

Figure 2.4 Fatigue Crack Initial State

The initial state (σ = 0) of the fatigue crack (solid horizontal line) and the surrounding plastic zone (gray area). Reprinted with permission from J Shultz. [84]

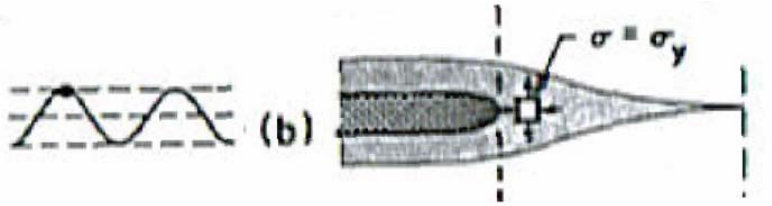

Figure 2.5 First Tensile Half-Cycle

Raising the applied stress rises from zero to the maximum (σ_{max}) opens the crack. The stress within the plastic zone surpasses the yield stress of the polymer. The plastic zone grows normal to the direction of the principal stress. Reprinted with permission from J Shultz. [84]

During relaxation, the stress within the plastic zone reaches zero before the applied stress. (Figure 2.6) The plastic zone was enlarged during the previous quarter-cycle; thus the plastic zone does not elastically return to the same state as the start of

the cycle. As the applied stress is completely relaxed (σ = 0 MPa) and the crack faces begin to close and a nominal compressive stress ($-\sigma^*$) develops in the plastic zone. (Figure 2.7) Since the plastic zone is compressed in the direction of the applied stress, a residual orthogonal tensile stress is created. The crack faces do not close completely at σ = 0 MPa (recall the growth of the plastic zone). Compressing the polymer ($-\sigma_o$) closes the crack faces and causes the plastic zone to deform in the direction perpendicular to the principal stress. (Figure 2.8)

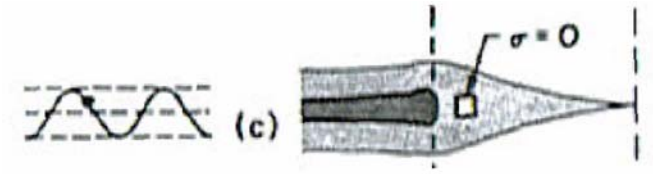

Figure 2.6 Relaxation to Zero Stress

Relaxation of the tensile stress shows slight closure of the crack. The stress within the plastic zone reduces to zero setting up a residual compressive stress. Reprinted with permission from J Shultz. [84]

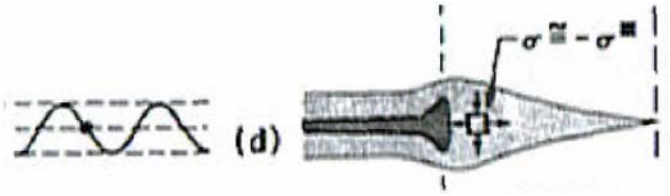

Figure 2.7 Residual Compressive Stress

Further relaxation of the applied stress to zero shows the development of the compressive residual compressive stress ($-\sigma^*$). Reprinted with permission from J Shultz. [84]

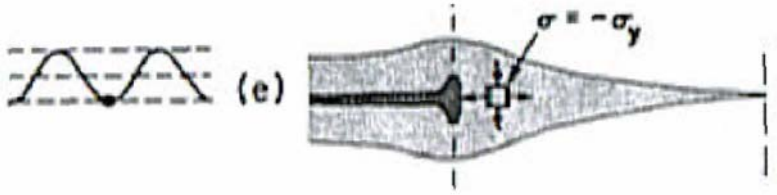

Figure 2.8 Compressive Half-Cycle

As the applied stress reaches the maximum in the compressive state the plastic zone again extends in the direction of crack growth. The stress within the plastic zone reaches the compressive yield stress ($-\sigma_y$) and the plastic zone grows. Reprinted with permission from J Shultz. [84]

As the applied stress returns to zero, the residual tensile stress at the crack front slightly opens the crack faces. (Figure 2.9) Although the plastic zone is now much larger than in the initial state, the fatigue crack does not advance. As the applied stress is increased to the maximum tensile stress (+σ), the plastic zone again increases as the crack faces open. (Figure 2.10) At this point the crack front and the plastic zone are greatly enlarged. However, the fatigue crack will not advance until the plastic zone fails; thus, the fatigue crack may remain stagnate while the plastic zone grows. At some point, the crack front and, more importantly, the plastic zone will become so large that the further stressing will cause the plastic zone to deteriorate and the fatigue crack will advance.

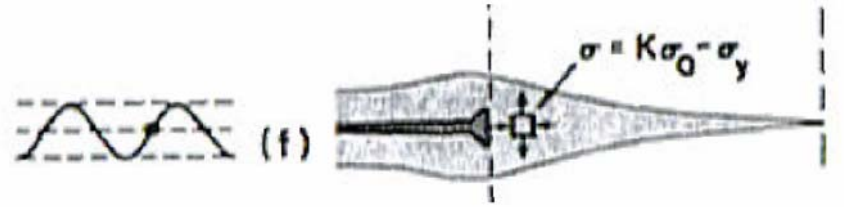

Figure 2.9 Compressive Relaxation

The return of the applied stress to zero shows slight closure of the fatigue crack. The stress within the plastic zone is set to a tensile bias. Despite the large growth of the plastic zone, the fatigue crack remains stationary. Reprinted with permission from J Shultz. [84]

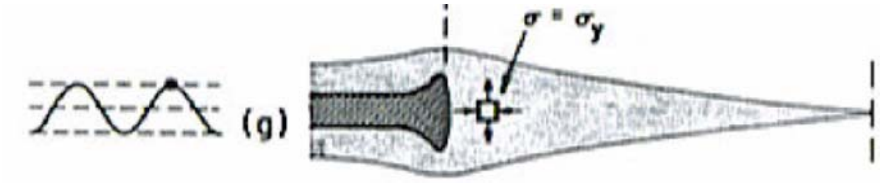

Figure 2.10 Second Tensile Half-Cycle

The return of the applied stress to the maximum tensile stress (+σ) separates the crack faces. The plastic zone again increases in size. Once the crack front is strained inelastically, the plastic zone breaks down and the fatigue crack grows for the first time. Reprinted with permission from J Shultz. [84]

2.3 Cyclic Softening and Other Damage Mechanisms in Polymers

The deformation and subsequent failure of amorphous and semi-crystalline polymers depend on their entangled molecular chains. Applying a mechanical load to the polymer may induce the redistribution of the molecular chains such that the polymer can better resist the load. Given the viscoelastic nature of polymers, this redistribution

can be elastic, plastic, or Newtonian. Amorphous polymers may deform homogeneously throughout the bulk of the material or heterogeneously along microscopic phenomena, such as crazing or shear banding. [72, 86] Such inhomogeneous deformation is typical of composite materials. [83] The response of polymers to dynamic loading is collectively termed cyclic deformation, which can be lengthy, gradual, or short depending on the amplitude of the applied load and the extent of plastic deformation within the polymer. In brittle polymers cyclic deformation manifests itself as cyclic softening [72, 83, 87], which is aptly named so because the strain in the polymer under dynamic loading increases with the number of cycles. Beardmore and Rabinowtiz explain that the resistance of the specimen to deformation decreases over time; thus, the material is said to "soften." [83]

2.3.1 Fatigue striations and discontinuous growth bands

Fatigue striations are often seen on the fracture surfaces of failed polymers. Crack blunting during the step-wise growth of fatigue cracks form these material phenomena perpendicular to the direction of crack growth. (Figure 2.11) Unlike metals, the distance between striations in polymers is directly proportional to the rate of fatigue crack growth. [72] It should be noted, however, that the relationship between fatigue striations and crack growth rate is empirical. A small number of striations indicates that crack initiation dominates the fatigue failure of the polymer. [83] Striations frequently result from dynamically testing at high values of ΔK. Alternatively, discontinuous growth bands are common in polymers dynamically loaded at low values of ΔK. Observationally, discontinuous growth bands resemble fatigue striations, but the spacing between discontinuous growth bands is much larger than between striations. The larger separation results from the growth of the craze zone over several cycles and the subsequent "jump" growth in the fatigue crack. [72]

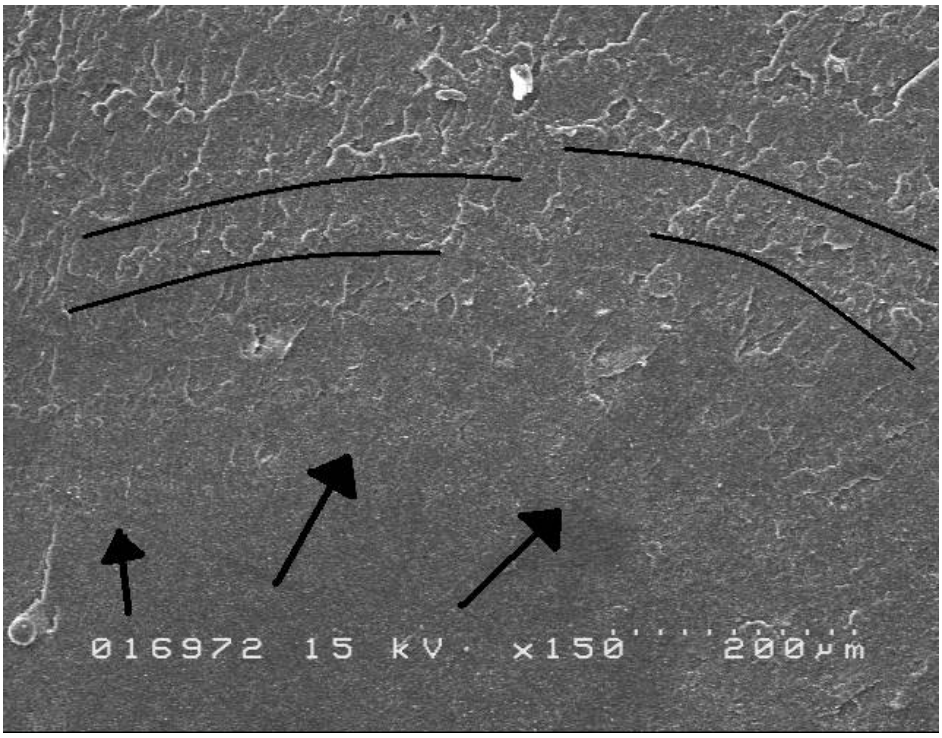

Figure 2.11 Fatigue Striations

This micrograph of a MMA-co-Sty fracture surface show the presence of fatigue striations. The striations form perpendicular to the direction of crack growth (indicated by the arrows. The black lines indicate the regions of crack blunting. Craze breakdown is seen beyond the lines.

2.3.2 Crazing

Crazing is one of dominant mechanisms of cyclic softening in polymers. Typically, dynamic testing with stress amplitudes above the endurance limit results in the formation of crazes, or craze zones. Crazing typically precedes the initiation and propagation of fatigue cracks; thus, it is an ongoing process that results in the unremitting accumulation of microscopic damage. [72, 86] Crazes form when the applied stress localizes and concentrates at a flaw or void in the polymer (initiation) or at the crack front (propagation). The elevated local stress is counteracted by the alignment of disordered, entangled molecular chains in the direction of the principal stress. Michler effectively describes the formation of a craze as a series of microscopic events in a network of molecular chains. [88] (Figure 2.12) As the molecular chains align, zones of weaker matrix are created. The aligned chains are strained under dynamic loading and the weaker domains begin to yield. Further deformation of the network ruptures the

yielded domains such that micro-voids are formed where the weak domain once existed and fibrils of oriented molecules materialize. The collection of fibrils and micro-voids forms the structure of the craze.

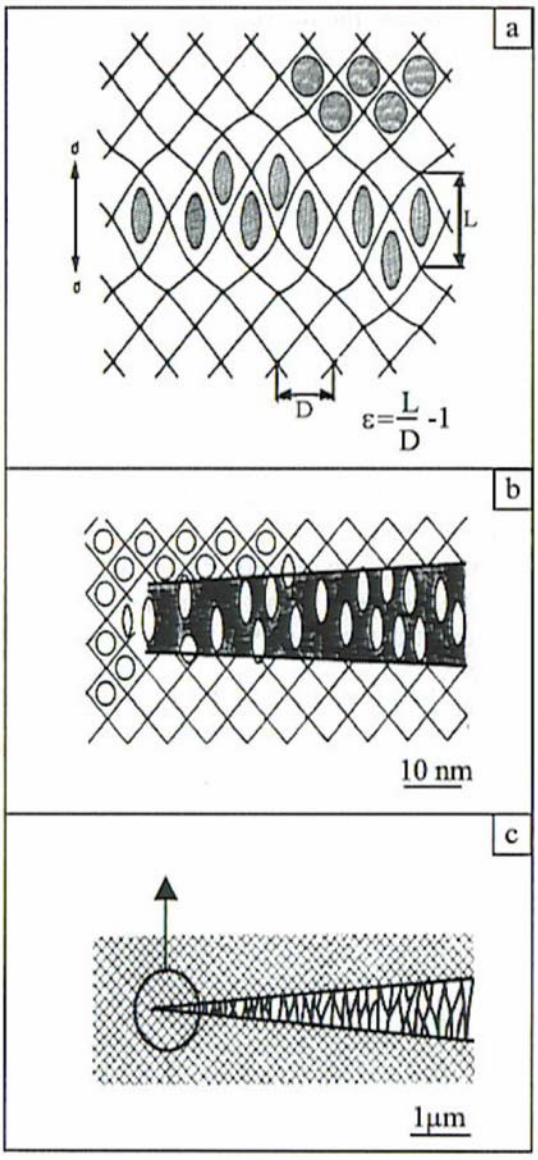

Figure 2.12 Formation of Craze Network

Michler depicts the formation of crazes as a network of entangled polymer chains. As the network is strained (a) the weaker regions of the matrix (dark circles) begin to yield. Further straining (b) causes the weaker regions to fail creating a system of micro-voids and fibrils. This network formation is shown relative to a much larger craze zone (c). With kind permission of Springer Science and Business Media. [88]

Although the molecules of the fibrils are highly ordered, the density of the craze is only a fraction of that of the bulk polymer. [72] Micro-hardness testing reveals that the mechanical properties of the fibrils are much greater than those of the bulk polymer. [88] The fibrils are parallel to the direction of loading, but the length of the craze is normal to the principal stress. Since a fatigue crack cannot initiate or propagate until the fibrils of the craze fail, the formation of fibrils initially toughens the polymer. [72]

Recall the division of the S – N curve into three distinct regions. (Figure 2.3) Region I is dominated by crack propagation primarily because crazes form during the onset of the first tensile half-cycle within this region. Beardmore reports that craze formation and failure comprise the entire life of the specimens in Region I. [83] In Region II, the periods of initiation and propagation are somewhat balanced, but the role of crazing in the initiation period is not as prevalent as in propagation. During propagation, the crazes grow with each cycle rather than fail (as in Region I). Within Region II, the localized stress increases the size of the craze although it does not exceed the strength of the fibrils. Eventually, the craze grows to a point where the fibrils closest to the crack front fail during ensuing tensile half-cycles. The actual mechanism of craze failure is unclear, but it is thought to initiate at the fibril – matrix interface. [72] (Figure 2.13) As the craze breaks down, the crack advances through the length of the craze zone. Crack growth is blunted at the tip of the deteriorated craze and a new craze develops. (Figure 2.14) In Region III, the formation of crazes is rare as the polymer's fatigue life is dominated by crack initiation. In general, the applied stress is too small to initiate the formation of crazes; thus, the extent of crazing diminishes as the applied stress decreases.

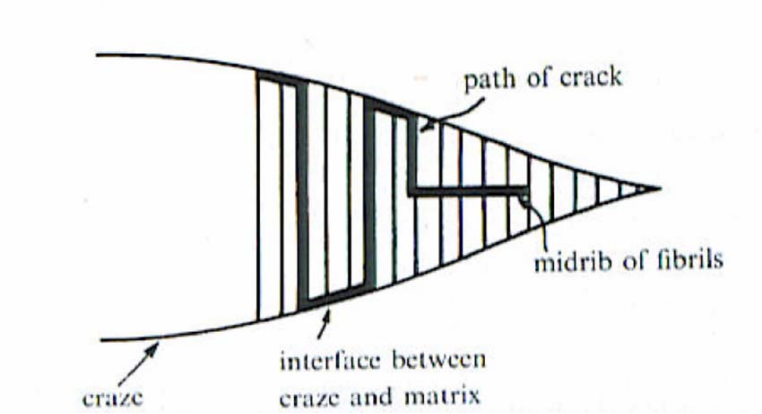

Figure 2.13 Craze Failure

The proposed mechanism of craze failure shows that the fibrils closest to the crack front fail at the fibril – matrix interface. The path of failure follows the fibrils until a point where it deviates through the midrib of shorter fibrils. Reprinted with the permission of Cambridge University Press. [72]

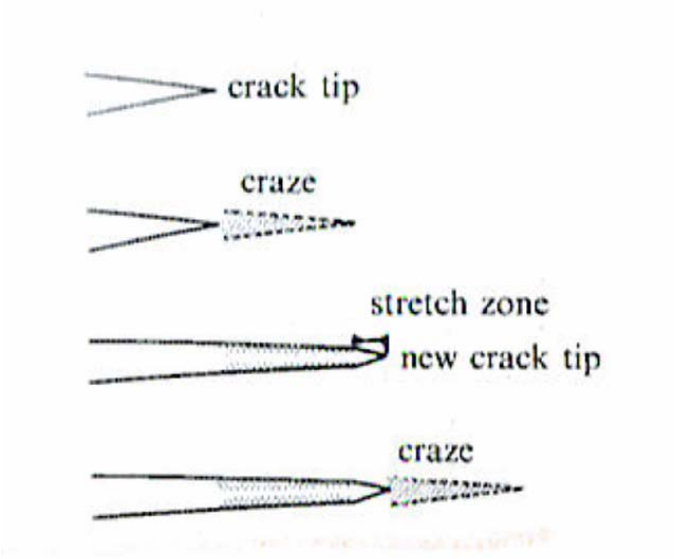

Figure 2.14 Crack Growth Through Crazes

The mechanism of step-wise growth is shown. A region of crazing develops ahead of the crack tip. The craze breaks down and the crack advances through the broken down region. A new craze develops ahead of the new crack tip. Reprinted with the permission of Cambridge University Press. [72]

3.1 Fullerenes and Carbon Nanotubes

Perhaps by coincidence, one year after Drexler's description of nanotechnology [89] a team of researchers headed by Dr Harold Kroto from the University of Sussex and Dr Richard Smalley from Rice University reported the discovery of nanoscale carbon spheroids now known as Buckminster fullerenes (C_{60}, C_{70}, etc). [90] Their discovery helped lay the groundwork for nanoscale carbon science. "Bucky balls", as they are loosely termed, are comprised of a series of carbonaceous pentagons and hexagons that form a sphere-like lattice. The structure is exclusively carbon and the thickness of the wall is equivalent to the diameter of one carbon atom. Although their atomic structures are strongly dependent on the hexagonal ring of carbon, the structure of fullerenes differs from that of graphite through the inclusion of pentagonal rings. The interplay of the hexagons and pentagons provide fullerenes with their spherical shape. The carbon – carbon bonds that comprise the structure of the fullerenes also confer these nanomaterials with unique and extraordinary properties. The discovery, and subsequent characterization, of fullerenes sparked interest in nanoscale carbon science, which eventually led to the experimental description of another nanoscale carbon form — the carbon nanotube.

In the late 1980's and early 1990's, a team of carbon scientists including Kroto and Smalley first conceived the notion of carbon nanotubes: tubular structures with vast similarities to fullerenes. [91] Specifically, Dresselhaus predicted that carbon nanotubes could exist as symmetrical cylinders with end caps resembling fullerene hemispheres. [92] Soon after this theoretical description, Dr Sumio Iijima reported, for the first time, the experimental production of carbon nanotubes. [93] As predicted, the structure of carbon nanotubes resembles that of the Buckminster fullerene in many ways. Conceptually, splitting a fullerene into equal hemispheres and extending the carbon lattice between the hemispheres creates the structure of a carbon nanotube. Like fullerenes, the thickness of a single carbon nanotube is equivalent to the diameter of one carbon atom. Saito further describes the structure of a carbon nanotube as "a graphene sheet rolled into a cylindrical shape so that the structure is one-dimensional with axial symmetry, and in general exhibiting a spiral conformation, called chirality." [91] Many of

the properties of fullerenes translate to carbon nanotubes; thus, interest in carbon nanotubes is increasing and extensive amounts of research are dedicated to the characterization and application of these nanomaterials.

3.2 Characterization, Properties, and Applications

Carbon nanotubes are produced in two varieties: single wall and multiwall. As the names imply, single wall carbon nanotubes (SWNT) consist of one carbon nanotube, whereas multiwall carbon nanotubes (MWNT) consist of a single nanotube core surrounded by evenly spaced, concentric carbon nanotubes (Figure 3.1). [91] The diameter of a single wall carbon nanotube ranges from less than one nanometer up to a few nanometers; the inner diameter of a multiwall carbon nanotube is equivalent to the diameter of a SWNT and the outer diameter ranges between a few nanometers and several tens of nanometers. In MWNTs, the concentric nanotubes are spaced 0.34 – 0.39 nanometers apart (depending on the chirality of the individual nanotubes) [94]; thus, the structure of the MWNT satisfies the analogy of the Russian doll. (Figure 3.2) Since each layer of a multiwall carbon nanotube resembles graphite, which possesses very low inter-graphene sheet frictional forces, actuation of MWNT layers (rotary and linear) relative to one another is nearly frictionless. [95] Both varieties of carbon nanotubes can reach several hundred microns in length giving these nanomaterials large aspect ratios (length/diameter); therefore, CNTs are virtually one dimensional when compared to other, more recognizable fibers. Additionally, the carbon nanotubes have large surface area to volume ratios, which play an important role in the application of carbon nanotubes in composite materials.

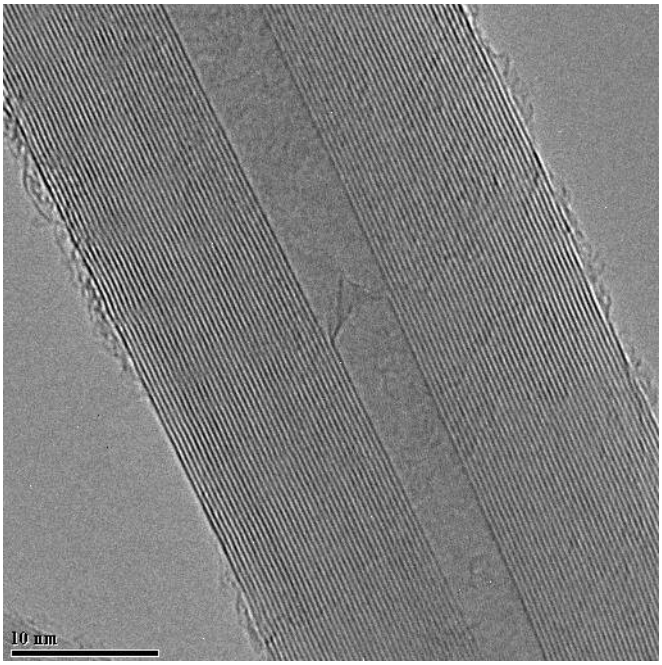

Figure 3.1 Multiwall Carbon Nanotube

This transmission electron micrograph reveals the highly ordered structure of a multiwall carbon nanotube. The interior single wall nanotube is encompassed by evenly spaced, concentric carbon nanotubes.

Figure 3.2 Nesting Dolls

The structure of the multiwall carbon nanotube is analogous to the nesting dolls popular in Russian culture. Removal of the outermost nanotube reveals an identical, yet smaller, carbon nanotube.

3.2.1 Production of carbon nanotubes

Carbon nanotubes are manufactured with a variety of production techniques including the laser vaporization of graphite, the carbon arc method, and the chemical vapor deposition (CVD) method. [91, 96-98] Recent developments in the CVD process

at the Center for Applied Energy Research at the University of Kentucky enable the growth of multiwall carbon nanotubes in highly purified, aligned mats. [96, 99-101] Furthermore, large batch, continuous production of aligned MWNTs via optimized CVD has driven down the price of the carbon nanotube production, which, for the first time, facilitates the large scale use of carbon nanotubes for commercial applications. [99] Carbon nanotubes produced with the CVD process are harvested from the quartz substrates as a powder-like substance. High magnification observation with scanning electron microscopy shows the powder to be a collection of mats of aligned, yet slightly entangled multiwall carbon nanotubes. (Figure 3.3) As Figure 3 shows, the MWNTs preferentially grow parallel to each other. As the MWNTs grow, they naturally tend to sway into each other. The high surface energies and van der Waal attractive forces of the MWNTs cause the entanglements.

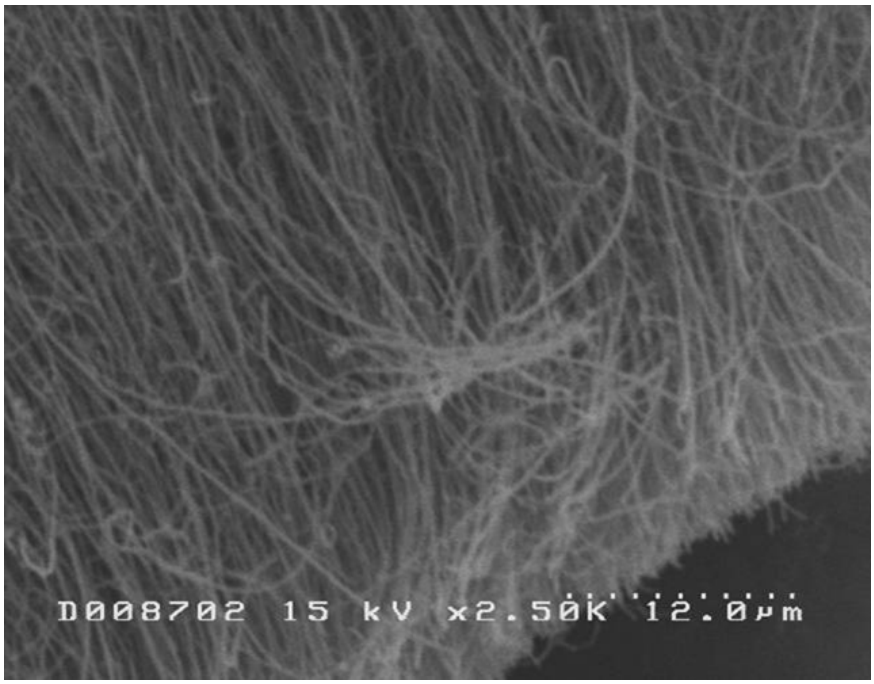

Figure 3.3 Entangled MWNTs

This micrograph is representative of as-produced multiwall carbon nanotubes. The preferentially aligned, entangled nanotubes are harvested in mats. These entanglements are a source of difficulty in the processing of carbon nanotube composites.

3.2.2 Properties of carbon nanotubes

The characterization of carbon nanotubes is no easy feat, despite the growing number of published reports. Previous difficulties in testing individual carbon nanotubes stem from the dis-aggregation and isolation of a single nanotube. Frustration also arises from the seemingly impossible task of gripping an individual nanotube for mechanical testing. Additionally, the resolution of many characterization techniques (until recently) cannot account for measurements on such small materials. Even partial characterization of carbon nanotubes requires great ingenuity and creativity.

The unique sp^2 hybridization bonding within the carbon nanotubes increases the binding energy of a single carbon – carbon bond; thus, carbon nanotubes should theoretically possess superior mechanical properties compared to other carbon forms. [91] To test this theory, several techniques including atomic force microscopy [102-104], observation of thermal vibration [105, 106], *in situ* straining in transmission electron microscopy [107] and scanning electron microscopy [108], and theoretical molecular dynamic simulations [109] are used to measure and predict the elastic modulus and tensile strength of both single and multiwall carbon nanotubes. Testing results show that the mechanical properties of carbon nanotubes are indeed extraordinary with modulus values on the order of the TerraPascal (TPa). The elastic modulus of single wall carbon nanotubes and SWNT ropes are reported as 1 TPa [103] and 1.25 TPa [105], respectively. Alternatively, reported values for the elastic modulus of MWNTs range from 0.2 to 1.8 TPa. [96, 104, 106-108] Despite the high elastic modulus values, carbon nanotubes are relatively flexible because of their high aspect ratios. Equally as impressive, the tensile strengths of MWNTs vary between 11 and 150 MPa. [107, 108] These numbers suggest that carbon nanotubes are stronger than steel at only a fraction of the weight!

In addition to impressive mechanical strengths, carbon nanotubes are known to possess excellent transport properties. Specifically, the transport of heat through a carbon nanotube is anisotropic and warrants comparison to that of diamond. [81, 110-113] Similarly, the transport of electrons down the long axis of the carbon nanotube facilitates the anisotropic flow of electrical current. Thus, the electrical conductivity of carbon nanotubes surpasses some metal wires of similar dimensions [113] and in cold environments single wall carbon nanotubes possess superconductive behavior. [114] The combination of strength, stiffness, electrical conductivity, and thermal conductivity make carbon nanotubes versatile and necessitates the development of applications for

these nanomaterials. Current applications for carbon nanotubes are nanowires, field emission displays, energy storage devices, semiconductor devices, probes, sensors, and conductive and high-strength composites. [115]

3.3 Carbon Nanotube Composites

The mechanical and transport properties of carbon nanotubes are unmistakably unique; however, their nanoscale dimensions limit their use in real world applications. One solution to this dilemma involves mixing limited amounts of carbon nanotubes into a matrix material. Carbon nanotube composites are attractive because they exploit the mechanical and transport properties of the carbon nanotubes while retaining the structural and processing capabilities of the matrix. The end result is a lightweight, high performance material with improved mechanical, thermal, and/or electrical properties. Matrix materials for consideration include, but are not limited to, polystyrene (PS), polymethylmethacrylate (PMMA), poly(vinyl alcohol) (PVA), polyethylene (PE), polyethylene terephthalate (PET), carbon (fibers, pitches, etc), and epoxy resin.

3.3.1 Dis-aggregation and dispersion of carbon nanotubes

Production of such lightweight, high performance composite materials is not an elementary process, especially considering the entangled mats of as-produced carbon nanotubes. The success of carbon nanotube composites depends on the dis-aggregation and dispersion of the carbon nanotubes. Whether aligned or unaligned, the uniform spatial and angular distribution of carbon nanotubes is necessary for maximizing the interfacial bonding between the matrix and filler. The requirements for high strength composites and electrically/thermally conductive composites are slightly different. For the former, the interface between the matrix and CNTs is critical for stress transfer, the known mechanism of reinforcement in composite materials. [116] For the latter, the CNTs must create an intercalation network (a network of overlapping or touching CNTs) for transport of electrons, phonons, etc. In either case, sub-par dispersion limits the effectiveness of the resulting composite material.

A wide variety of processing techniques exist for forming uniformly dispersed composites. Two of the more common techniques include sonicating CNTs into solution and high temperature shear mixing. The goal of these techniques is to, first, break apart the entanglements of the as-produced nanotubes and, second, disperse the individual nanotubes throughout the matrix. These techniques work well for small concentrations of CNTs; however, mixing higher concentrations of CNTs (>5% by weight) often

increases the viscosity of the mixture regardless of the state of the polymer (in solution or molten). Elevated viscosity discourages the effective dispersion of the CNTs into the polymer; thus, the energy inputted into the mixing process must be elevated at the risk of shortening the CNTs or irreversibly damaging the matrix material. [99] As previously mentioned, the dispersion of the CNTs is critical to the success of the composite. Less than ideal dispersion creates several problems including the formation agglomerates within the bulk of the nanocomposite. (Figure 3.5) In the case of high strength composites, the presence of such agglomerates counteracts the reinforcing capabilities of the carbon nanotubes. For imperfectly dispersed composites, the resulting mechanical properties are the net sum of the positive reinforcing effects of adequately dispersed CNTs and the negative effects of agglomerates.

Figure 3.4 MWNT Agglomeration

This micrograph represents imperfectly dispersed multiwall carbon nanotubes in a methyl methacrylate – styrene copolymer matrix. The agglomeration is roughly 15 microns in diameter. It should also be noted that the MWNTs in the surrounding matrix are adequately dispersed.

3.3.2 The carbon nanotube – matrix interface

In order to best exploit the mechanical properties of carbon nanotubes, an intimate connection must be made between the individual nanotubes and the matrix. The improved mechanical performance of the composite is realized through the transfer of stress from the weaker matrix to the much stronger, stiffer nanotubes [117]; therefore, the interface between the two phases must be large and good. Poor wetting of the CNTs in the matrix creates a deficient interface with little to no interaction and minimal stress transfer. To test the strength of the CNT – matrix interface, individual CNTs are pulled out of the matrix using atomic force microscopy. The resistance of CNT pull-out is directly correlated to the interfacial strength. For example, the strength required to pull a CNT from a polyethylene-butene matrix is around 47 MPa, which is greater than the yield stress of some polymers. [118] This suggests that stress transfer from the matrix to the CNTs enables the matrix to resist stresses that would otherwise result in plastic deformation. However, once the interfacial strength is surpassed, the CNTs lose their reinforcing effect; thus, the most dramatic improvements in mechanical performance are likely limited to the elastic regime.

3.3.3 Mechanical properties of carbon nanotube composites

Many carbon nanotube composites exhibit enhanced mechanical performance. [96, 119, 120] In general, the properties of CNT composites depend on the type, concentration, dispersion, and alignment of CNTs, the matrix material, the composite form, and the mode of mechanical testing (monotonic or dynamic). To date, the monotonic (quasi-static) mechanical performance of carbon nanotube composite is more widely reported than the dynamic (fatigue) performance. The effect of CNTs on the monotonic and dynamic properties of the composite should be different given that the mechanisms of plastic deformation and failure attributed to each mode of testing differ in most respects. Therefore, each mode of testing should be considered when characterizing the mechanical performance of CNT composites.

Reports on the monotonic (quasi-static) properties of CNT composites overwhelmingly dominate the current literature. Surveying these reports, which study a variety of matrices, CNTs, and testing modes, provides valuable insight into the reinforcing capabilities of CNTs. For example, Moore [121] and Kearns [122] show in separate studies that inclusion of 1wt% SWNTs increases the tensile strength of polypropylene (PP) fibers by 45% and 40%, respectively. In the same study, Kearns

shows a 55% increase in the elastic modulus of the SWNT – PP fibers. [122] Haggenmueller et al. [123] shows that 8wt% SWNT increases the tensile strength and elastic modulus of PMMA films by 10 – 30% and 160 – 230%, respectively. An addition of less than 1wt% MWNTs increase the tensile strength and elastic modulus of poly(vinyl alcohol) (PVC) films by 330% and 270%, respectively [124]; whereas, a different study shows that adding 9.1wt% MWNTs increases the tensile strength and elastic modulus of PVC films by 170% and 350%, respectively. [125] Although there are discrepancies between the two studies, they both show that MWNTs dramatically affect the mechanical performance of PVC. Multiwall carbon nanotubes also enhance the tensile strength, flexural strength, and flexural modulus of methyl methacrylate – stryrene copolymer based bone cements. [126, 127] Alternatively, the addition of CNTs modestly alters the tensile strength and elastic modulus of polystyrene. [99] In polymethylmethacrylate (PMMA), small amounts of single wall carbon nanotubes significantly increase the impact strength, which is often correlated to the fracture toughness. [128] Increases in toughness also accompany the addition of several concentrations of carbon nanotubes and appear to be dose dependent with toughness values increasing with increasing concentration of MWNTs. [124, 125, 129] Thostenson shows that the forced alignment of the carbon nanotubes in the direction of the principal stress can dramatically enhance the reinforcing effect of the nanotubes. [130] Successful mechanical reinforcement is not limited to polymer matrices however; Andrews et al show that the ultimate tensile strength and elastic modulus of pitch-based carbon fibers improves with the addition of modest amounts of single wall carbon nanotubes. [131]

The dynamic performance of CNT composites is significantly less reported, although it is by no means less important. Typical dynamic tests include fatigue testing and dynamic mechanical analysis. In the former, the composite is cycled to failure under constant amplitude of load or deformation; in the latter, the dynamic mechanical properties are measured as a function of frequency. For example, large amounts (>17wt%) of CNTs increase the storage modulus of PMMA by 170%. [132] Disappointingly, the fatigue properties of CNT composites are grossly underreported in the literature. Of the few reports on fatigue, Ren et al. show that the fatigue performance of epoxy resin reinforced with single wall carbon nanotubes exceeds that for unidirectional carbon fiber reinforced epoxy. [133] It is likely that the reinforcing mechanisms of CNTs are similar for dynamic and monotonic loading; however, there must be mechanisms that are more prevalent in dynamic loading than in monotonic

loading. To understand fatigue failure of CNT composites, the fatigue failure of unreinforced matrices must be understood. The fatigue of polymers, metals, and ceramics is a culmination of microscopic and sub-microscopic events. [72] The result of these events is fast or slow accumulation of damage that ultimately leads to the catastrophic failure of the matrix. For polymers, fatigue failure can be divided into three distinct phases: 1) crack initiation, 2) crack propagation, and 3) fast, catastrophic failure. Due to the microscale and nanoscale levels of damage resulting from dynamic testing, carbon nanotubes offer new opportunities for directly addressing the mechanisms of fatigue. Additionally, the sub-critical stresses associated with dynamic loading should magnify the effect of the MWNTs. In the early stages of dynamic loading, microscale plastic deformation is at a minimum and the local stresses at the MWNT – matrix interface are theoretically less than the interfacial strength; thus, the MWNTs absorb most of the energy of dynamic loading without damaging the surrounding matrix. The presence of MWNTs likely prevents the rapid onset of damage accumulation and subsequent elevation of the local stresses, which can lead to interfacial failure.

3.4 Carbon Nanotube – Bone Cement Composites

Understanding the reinforcing capabilities of CNTs is important for the development new high performance materials. Optimizing the interface between the CNTs and matrix, the locale of stress transfer, will maximize the mechanical performance of the CNT composite. Without stress transfer, the CNTs do little to alter the mechanical properties of the composite. Thus, the interface is important for both monotonic and dynamic loading. Given the previous successes of CNT composites, it is reasonable to assume that similar enhancements will result from the addition of multiwall carbon nanotubes to the polymer component of bone cement. Improving the monotonic properties of bone cement is important, but would be overshadowed by improvements in the fatigue performance, which would have direct implications to the clinical life of this implantable material.

Chapter Four Augmentation of Acrylic Bone Cement with Multiwall Carbon Nanotubes

4.1 Introduction

Polymethylmethacrylate (PMMA) is the principal material ingredient of bone cement and dental prostheses (dentures). Bone cement is a grouting agent which serves an important interfacial role between metallic total joint prostheses and host bone, and is also being increasingly used as an injectable supportive material for collapsing vertebrae. [134, 135] Although bone cement has an admirable record of performance, it suffers from fatigue related cracking or impact induced breakage. Active or overweight total joint patients with implants fixed with bone cement are at risk for cement mantle failure [18]: this occurs in approximately 5% of all such patients by 10 years postoperatively and failure rates as high as 67% have been noted after 16 years in patients younger than 45 years. [17] Bone cement failure is responsible for a portion of the estimated 50,000 revision total knee and hip joint surgeries performed in 1996. [136]

To improve the properties of bone cement, many have tried to incorporate small amounts of various additive materials (especially fibers) into this polymer. Specifically, stainless steel fibers [62], glass fibers [44, 46, 137], long macroscopic carbon fibers [38, 44, 45], polyethylene fibers [36, 60, 61, 138, 139], aramid (kevlar-related) fibers [59], metal wires [42, 137, 140], and titanium fibers [63, 80, 141] have all been added to bone cement in attempts to bridge incipient fatigue cracks and arrest their propagation. Large fiber size, poor fiber – bone cement matrix bonding (and subsequent debonding), viscosity increases, ductile fiber deformation and fracture, nonuniform additive material distribution, and the adverse effects such materials have had on the mixing of bone cement are among the reasons why these efforts have been less than ideally successful. [141]

The introduction of nanoscale materials, particularly carbon nanotubes [142, 143], offers new promise for augmenting the properties of polymer systems, including PMMA-based bone cement. Carbon nanotubes, in both single and multiwall varieties, have emerged as one of the most exciting [144] and unusual materials found to date. Multiwall carbon nanotubes (MWNTs) are flexible and resilient [102] hollow tubular structures 10 to 40 nanometers in diameter, 10 μm to 100 μm long, and 50 to 100 times stronger than steel at 1/6 of the weight. The tensile modulus of MWNTs is on the order of a terraPascal. [107] In addition to their outstanding mechanical properties, carbon

nanotubes also have remarkable electrical, thermal (their on-axis heat conductivity rivals diamond) and magnetic properties (due to encapsulated catalyst metals). [143] Because carbon nanotubes have extremely high surface area to volume ratios, which in turn may permit the polymer to nucleate at the nanotube's surface thereby forming dominant nanotube – polymer crystalline interphase regions within the composite, it is believed that carbon nanotubes offer new promise for improving the mechanical properties of bone cement and thereby succeeding where other material augmentation efforts have failed. Preliminary testing in other polymer systems, i.e., polystyrene, showed that a small (1%) amount of carbon nanotubes increased the tensile modulus of this polymer by 25% [145], thereby motivating inquiry into the affects of MWNTs on the mechanical properties of PMMA-based bone cement. The goals of the present study were to test the null hypotheses that the addition of small (10% or less by weight) quantities of carbon nanotubes does not alter the quasi-static bending or fatigue properties of bone cement.

4.2 Methods

4.2.1 Nanotube production

Carbon nanotubes were synthesized on a polished quartz substrate in an argon-hydrogen atmosphere. [99, 101] The process began by injecting xylene into a furnace at a controlled rate in the presence of a ferrocene catalyst. This chemical vapor deposition process required precise control of the argon-hydrogen atmosphere, reactor zone temperature, feed material purity, catalyst particle size, catalyst-to-carbon ratio, preheater temperature, etc. These parameters (especially furnace temperature) governed the type (single wall or multiwall), diameter, and length of the resulting nanotubes, as well as the percentage of undesirable amorphous carbon. The typical multiwall carbon nanotube produced consisted of numerous concentric tubes axially aligned like the layers of a coaxial cable (Figure 4.1). Each tube was constructed like a seamless cylinder formed from a series of carbon hexagons that resembles the structure of a graphene sheet. Use of the as-produced nanotubes began by first mechanically harvesting them from the quartz substrate. [99] Since the nanotubes grew parallel to each other, they had a strong tendency to adhere to one another in a parallel long-axis arrangement. Such aggregated nanotubes were first isolated preparatory to uniform spatial and directional dispersion in the polymer system. [101]

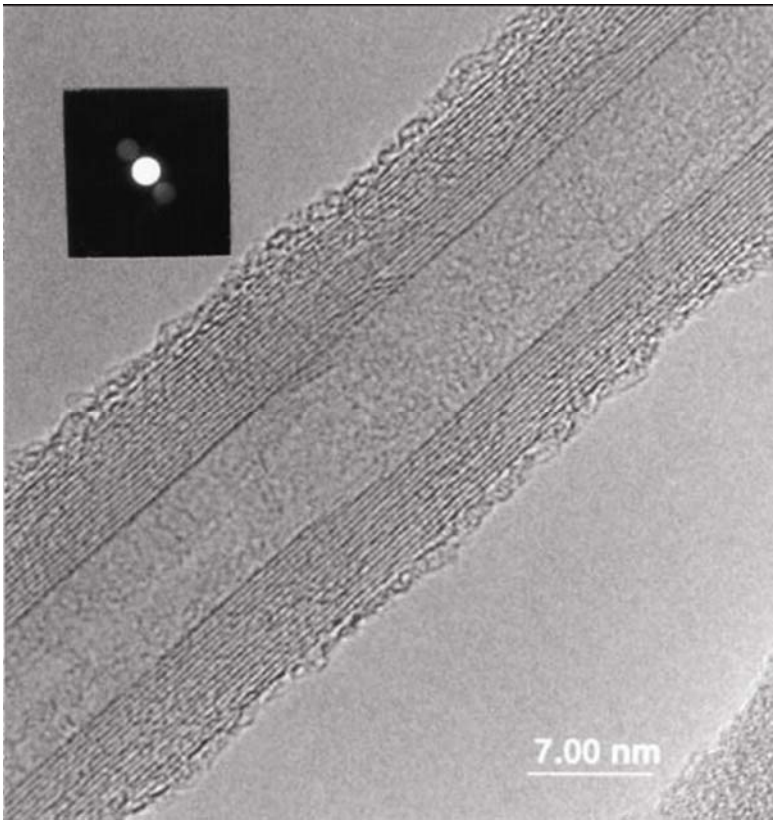

Figure 4.1 MWNT Structure

A typical multiwall carbon nanotube viewed in high-resolution transmission electron microscopy. Note the approximately 4 nm inner diameter and the 16-wall thickness. The x-ray diffraction data (upper left corner) shows a high degree of crystallinity from the clear and distinct reflections from the 002 crystallographic plane.

4.2.2 Specimen preparation

The as-produced multiwall carbon nanotubes (MWNTs) were dispersed throughout the molten matrix of pre-polymerized commercial bone cement powder. The two materials were combined in the heated (220ºC) chamber of a Haake Rheomix (Haake, GMBH, Germany) and subjected to high-shear mixing with two stainless steel counter-rotating (20 rpm) sigma-shaped rotors. Beginning with the greatest concentration of carbon nanotubes, a dilution method was employed to produce composite materials of 0.5%, 1%, 2%, 5%, and 10% (by weight) MWNTs. This dilution method replaced a portion of the larger concentration material with an equal portion of fresh bone cement, thereby reducing the percentage of carbon nanotubes in each

subsequent batch of material. The aspect ratios (length/diameter) of the multiwall carbon nanotubes remained large even though the high-shear mixing process can shorten the nanotubes. [146] After ample time was given for adequate mixing of the two components, the molten composite polymer was allowed to cool in air (25ºC) and harden to a solid. Pure bone cement (0wt% MWNTs) was also processed in the mixer to eliminate any effect the processing procedure may have had on the structure or properties of the control PMMA-only polymer.

The hardened material was then crushed and sieved to a particle size of ≤ 2 mm. These crushed particles were then hot-pressed under vacuum into films of uniform thickness (1.62 mm) with a 12-ton laboratory press. The platens of the press were heated above 140°C (T_m of PMMA) and used to apply 8,896 Newtons (2,000 lbs) of pressure for five minutes. The resulting films were allowed to cool to room temperature, and then they were cut to rough shape and machined into bar-shaped specimens suitable for quasi-static 3-point bending to failure (ASTM D790) and 4-point bending fatigue (ASTM D6272). Each specimen was then annealed (at 125ºC) for a minimum of fifteen hours to remove any surface flaws or micro-cracks that may have formed during the machining process, and then allowed to cure in air (25ºC) for 24 hours. Prior to mechanical testing, each specimen's width and thickness were measured multiple times with a precision caliper to quantify specimen dimensions preparatory to mechanical testing.

4.2.3 Mechanical testing

Bar specimens of the composite materials were tested to failure in 3-point bending by using a Q Test™ 10 Elite (MTS Inc. Minneapolis, MN) materials testing system. The span of the support rods was set to 60 mm and the specimens were deformed at a strain rate of 0.0135 min^{-1}. Flexural strength, flexural yield strength, bending modulus, and strain were recorded for each specimen. Fatigue testing in 4-point bending was then performed in air at room temperature (70º±3ºC; 60%±20% humidity) with an Instron 1331 servo-hydraulic materials testing system (Instron Corp. Canton, MA). The actuator moved according to a sinusoidal wave profile applying maximum and minimum loads of 40 N and 4 N, respectively. An accelerated fatigue protocol [71, 75, 77, 78, 147-150] was used at a test frequency of 5 Hz [148] as a screening tool for comparative evaluation of fatigue performance as a function of MWNT concentration. Although some prior studies [151] suggest that fatigue performance

depends upon test frequency, other studies [148] refute this claim. While contemporary reports suggest that the issue remains controversial [71], the preponderance of prior studies uses a 5 Hz test frequency. For this reason, the 5 Hz test frequency was also used in the present study. All specimens were cool to the touch after fatigue testing and no evidence was obtained indicating that any abnormal specimen heating occurred in response to these tests (thereby aiding justification of the 5 Hz test frequency). The number of cycles to failure was recorded for each specimen.

Fracture surfaces of failed specimens were randomly selected to be viewed with a scanning electron microscope (Hitachi S-2700). Micrographs of such specimens were recorded and observations were made regarding the dispersion of the multiwall carbon nanotubes and whether any evidence was present regarding the interactions between the carbon nanotubes and the bone cement matrix.

4.2.4 Data analysis

Both the quasi-static testing results and the fatigue life data from each sample were compared by using an Analysis of Variance and Fisher's PLSD Post Hoc Correction. The fatigue data for each sample were further analyzed by using the linear form of the three-parameter Weibull model to calculate Weibull parameters, the Weibull mean, and generate probability of survival curves for each sample. [6, 71, 148, 152] Each sample contained at least twelve specimens; prior studies showed that this number was adequate for producing a meaningful analysis with this type of Weibull model [150]. The number of cycles to failure (N_f) was analyzed with this Weibull model, which presented the data as the probability of failure, $P(N_f)$, due to fatigue after N_f cycles and was calculated by

$$P\left(N_f\right) = 1 - \exp\left[-\left(\frac{N_f - N_o}{\beta - N_o}\right)^{\alpha}\right] \qquad (1)$$

where N_o is the minimum fatigue life (a calculation of the baseline number of cycles for the sample at a given load amplitude), β is the characteristic fatigue life (defined as the number of cycles to failure below which 63.2% of the specimens do not survive), and α is the Weibull modulus, or shape parameter. Equation (1) was transformed into the more recognizable form of the equation for a line (Y = mX+B), vis:

$$\ln\ln\left[\frac{1}{\left(1 - P(N_f)\right)}\right] = \alpha\ln\left(N_f - N_o\right) - \alpha\ln\left(\beta - N_o\right) \quad (2)$$

The probability of failure was calculated by ranking the cycles to failure from least to greatest, assigning each data point a rank number M, and substituting the ranks into Equation 3:

$$P(N_f) = (M - 0.3)/(G + 0.4), \qquad (3)$$

where M=0,1,2,..G and G is the total number of specimens in each sample. The minimum fatigue life, N_o, was calculated by computing the inverse natural log of a graphic estimation of the vertical asymptote of the curve formed when plotting ln ln [1/(1-P(N_f))] versus ln N_f. A similar plot was generated with the lone exception that the ln N_f data was corrected by a factor equal to the minimum fatigue life, i.e., ln (N_f – N_o). The linear best fit line to this data yielded the value for the Weibull modulus (α). The characteristic fatigue life (β) was then obtained from Equation 4.

$$\beta = N_o + \exp(-C/\alpha) \qquad (4)$$

where C is the y-intercept value from the linear best fit line.

All three Weibull parameters were combined to calculate the Weibull mean (N_{WM}), a single parameter indicative of the fatigue performance of each sample studied. This number accounted for the minimum number of cycles to failure (N_f) of the data set, the central location of the data set (β), and the variance within the data set (α). The Weibull mean was regarded as a good measure for comparing the fatigue life performance of the various MWNT loadings and was calculated by using Equation 5

$$N_{WM} = N_o + (\beta - N_o)\Gamma\left(1 + 1/\alpha\right) \qquad (5)$$

where Γ is the Gamma function that was previously reported. [6, 71, 148, 152] Probability of survival (reliability) curves were generated by substituting the Weibull parameters into Equation 1 and plotting the results as a function of the number of cycles to failure.

4.3 Results

The quasi-static test results showed that the 2wt% MWNT concentration was nearly optimal for enhancing the quasi-static mechanical properties of bone cement in 3-point bending (Table 4.1). This MWNT loading enhanced flexural strength by 12.9% (p = 0.003) and produced a 13.1% enhancement (p = 0.002) in flexural yield strength. Bending modulus increased slightly with the smaller (< 5wt% MWNT) concentrations, but increased sharply at the 5wt% and 10wt% loadings to as much as a 24.1% increase

($p<0.001$) at the 10wt% loading. None of the other loadings were associated with significant increases in any measured parameter.

Table 4-1 Mean ± Standard Deviation of Mechanical Test Parameters Obtained from Quasi-Static 3-Point Bending Testing of Bone Cement Augmented with MWNTs

% MWNTs (by wt)	Flexural Strength (MPa)	Bending Modulus (MPa)	Flexural Yield Strength (MPa)	Strain (mm/mm)
0	80.3 ± 6.2	3402 ± 44	79.4 ± 5.6	0.035 ± 0.007
0.5	85.7 ± 3.8	3405 ± 44	85.6 ± 2.4	0.038 ± 0.005
1	78.3 ± 7.4	3500 ± 58	77.3 ± 9.2	0.027 ± 0.004
2	90.6 ± 3.2	3528 ± 66	89.8 ± 2.6	0.036 ± 0.006
5	84.9 ± 5.6	3823 ± 127	83.6 ± 5.9	0.027 ± 0.004
10	85.1 ± 6.1	4222 ± 99	79.9 ± 2.6	0.024 ± 0.004

Unlike the small but significant changes to selected quasi-static parameters, the 2wt% loading of multiwall carbon nanotubes was associated with substantial enhancement of bone cement's fatigue performance. Specimens with the 2wt% MWNT concentration showed a 3.1 fold increase in the mean actual fatigue life. (Figure 4.2)

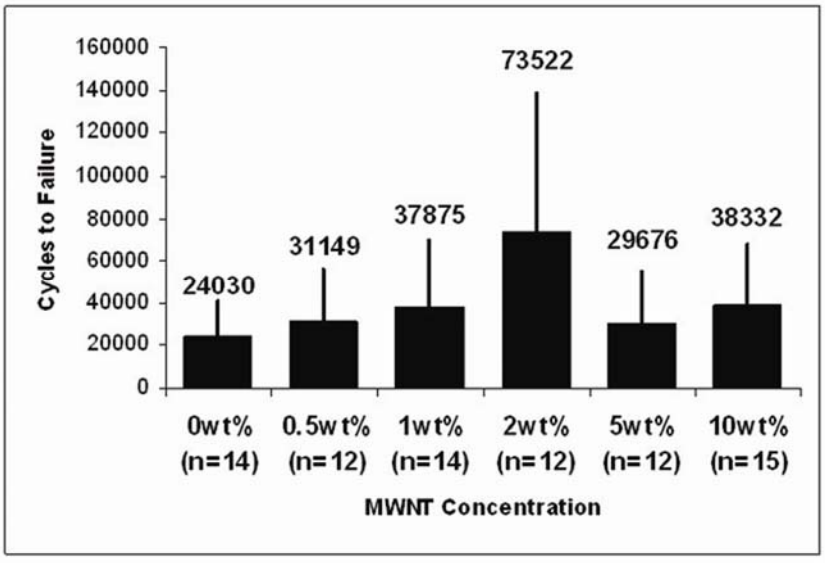

Figure 4.2 Cycles to Failure

The mean (± standard deviation) number of cycles to failure as a function of MWNT loading.

The fatigue data was also analyzed by using the 3-parameter Weibull method. This enabled calculation of the: a) Weibull minimum fatigue life (N_o), b) Weibull modulus (α), c) characteristic fatigue life (β), and d) Weibull mean (N_{WM}). (Table 4.2) The Weibull modulus can be used as a gauge of the data set's variance (i.e. as α increases, the variance within the set decreases). The best indicator of fatigue life performance for each loading was considered to be the Weibull mean fatigue lifetime (N_{WM}). Calculation of N_{WM} requires β, N_o, and α (equation 5). As shown, the 2wt% addition of MWNTs resulted in a 3.3 times enhancement in N_{WM} and this concentration appeared to be optimal when the natural log of the N_{WM} was plotted versus MWNT concentration (Figure 4.3).

Table 4-2 Summarized Fatigue Data and Weibull Parameters for Each MWNT Concentration Studied

	Weibull Parameters			
	Minimum Fatigue Life (N_o)	**Weibull Modulus (α)**	**Characteristic Fatigue Life (β)**	**Weibull Mean (N_{WM})**
0wt% (n=14)	3541	1.100	25848	25069
0.5wt% (n=12)	812	0.780	34651	39873
1wt% (n=14)	1339	0.796	43306	49068
2wt% (n=12)	1097	0.959	80440	81935
5wt% (n=12)	1339	0.937	33590	34556
10wt% (n=14)	665	0.784	46208	53014

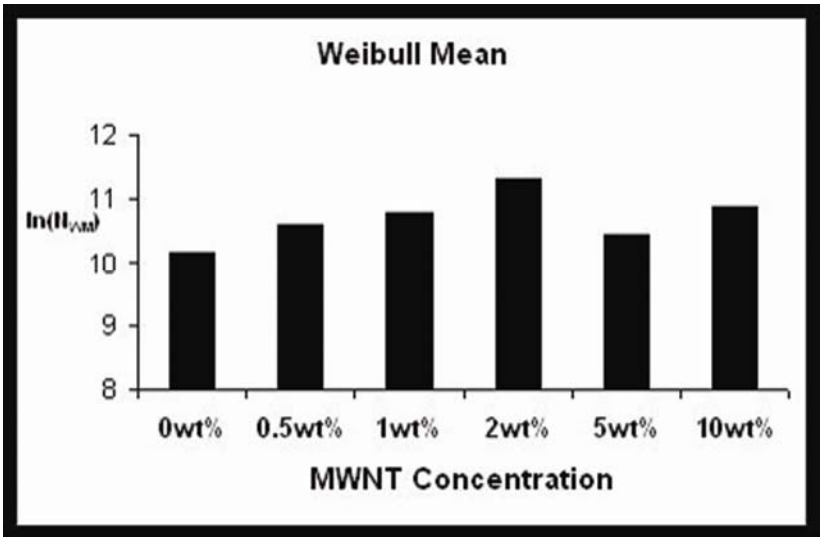

Figure 4.3 Weibull Means

The natural log of the Weibull mean (ln N_{WM}) as a function of the concentration of multiwall carbon nanotubes.

Although N_{WM} is a valuable tool for comparing the mean lifetime of the various MWNT loadings, the other Weibull parameters, especially the Weibull modulus (α), provide additional performance insights that are based upon data variances. Specifically, alpha values equal to 1 are associated with events that follow a course consistent with a "normal" fatigue failure. Alpha values less than 1 are associated with events that are better known as burn-in or run-in fatigue. Alpha values greater than 1 are associated with events describing specimens that are in the process of "wearing out" and which will have a failure rate that will increase with time.

The values for the Weibull parameters were more pronounced when they were presented in the form of reliability curves. (Figure 4.4) The Weibull modulus (α) contributed to the shape of the curve and the characteristic fatigue life (β) determined the positioning of the curve. As noted previously, the 2wt% MWNT loading was associated with an improving fatigue performance and this was evident in the right hand shift of the curve. (Figure 4.4) It is interesting to note that additional increases in MWNTs beyond the 2wt% loading produced effects that were not as pronounced; this suggested that those MWNT loadings in bone cement were associated with inferior fatigue performance.

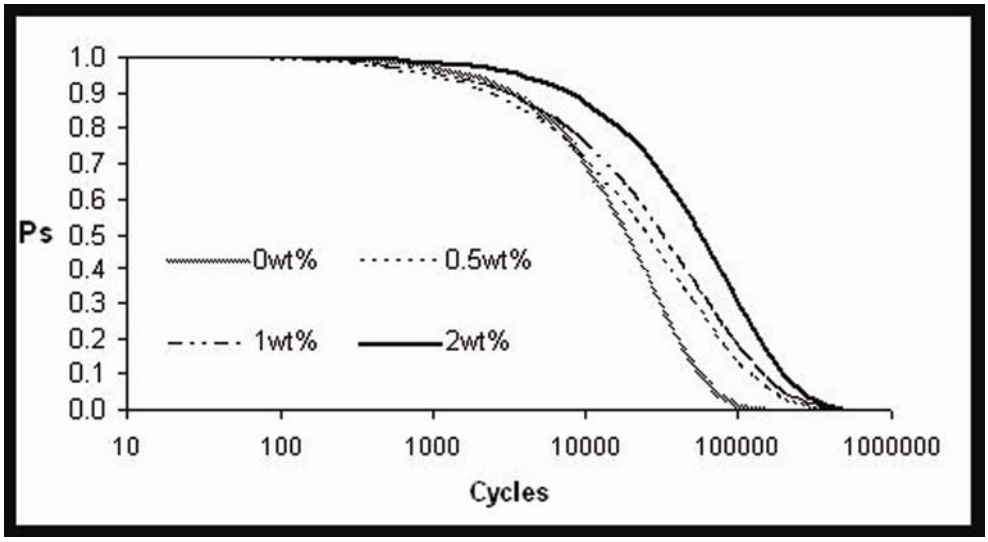

Figure 4.4 Probability of Survival

Probability-of-Survival (P_S) curves corresponding to the 0wt%, 0.5wt%, 1wt%, and 2wt% loading groups. The increased fatigue performance of the 2wt% loading is evident by the shift of the curve to the right.

A scanning electron microscopic image of the fractured surface of a fatigue-failed specimen (Figure 4.5) shows multiwall carbon nanotubes protruding from the bone cement matrix as long fingerlike projections. While there is no gold standard for quantifying the degree of dispersion of multiwall carbon nanotubes in a polymer matrix, or for fibrils embedded in any matrix, visual observation can result in useful information regarding the spatial dispersion of these materials. These nanotubes appear to be randomly spaced but aligned along the direction of loading (perpendicular to the direction of cracking) as expected. It is believed that this alignment was a result of the MWNTs reorienting such that they offered resistance to crack growth by spanning the crack in a direction perpendicular to the plane of crack growth. The hollow cylindrical voids present in the surface of the specimen were created by MWNTs that dislodged from the matrix during failure. While this type of MWNT–matrix failure would typically be indicative of a weak interaction, it is believed that in this case the local stresses became excessive for the individual nanotube–matrix interaction even though enough resistance to crack growth was given to increase the quasi-static strength. In this case, the applied load vastly exceeded material strength led to the fractured surfaces shown, from which all types of failure mechanisms (MWNT-matrix pullout, matrix pullout from matrix while

attached to a MWNT, etc.) were observed (Figure 4.6) but no one mechanism seemed predominate.

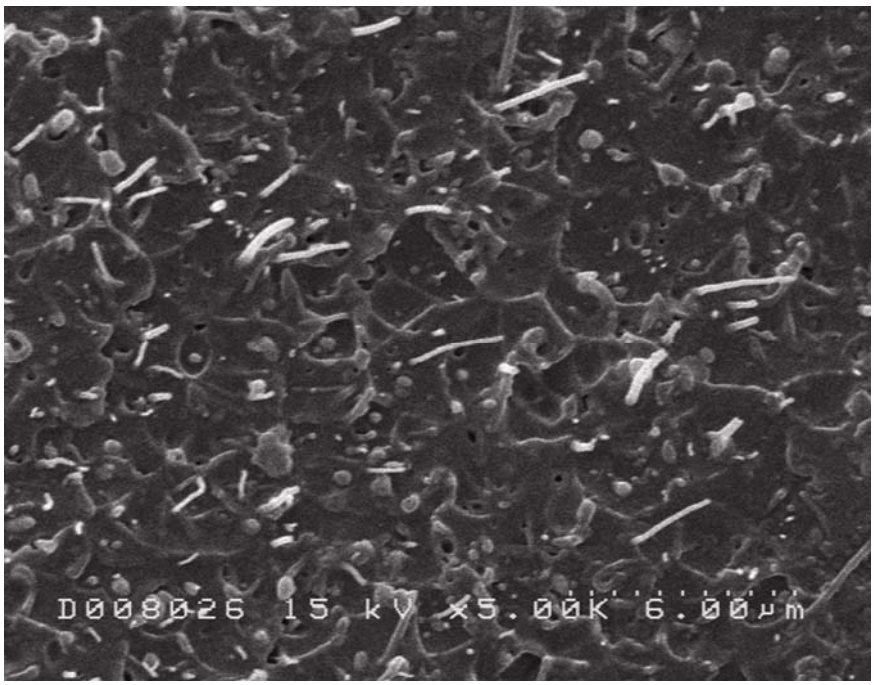

Figure 4.5 MWNT - Bone Cement Composite

SEM image of a typical fractured surface of a randomly selected specimen. The long, finger-like projections are MWNTs protruding from the fracture site.

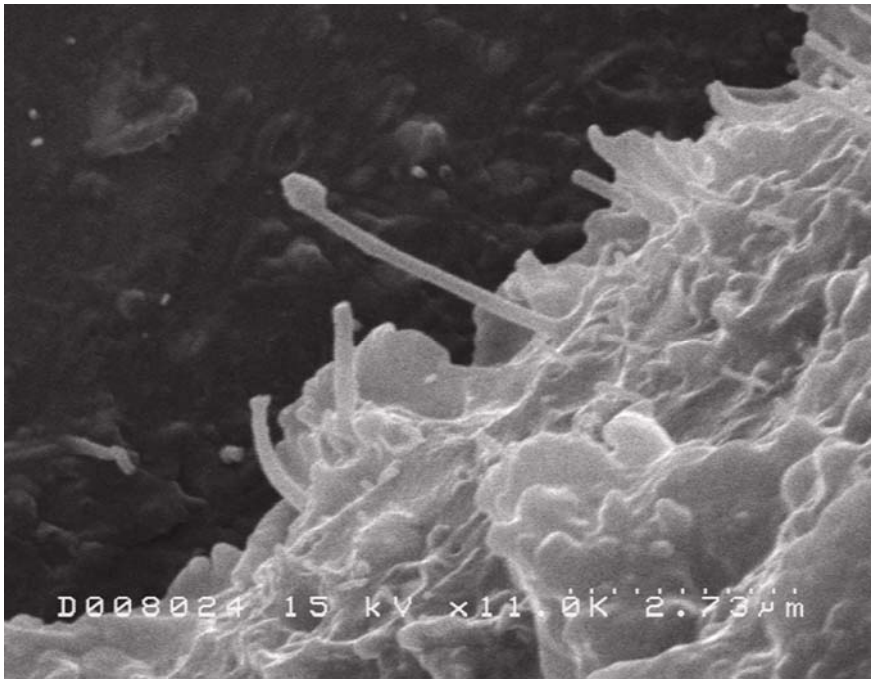

Figure 4.6 Polymer Sheathing

SEM of an isolated multiwall nanotube with what is believed to be bone cement matrix adhering to the tip of the nanotube.

4.4 Discussion

This study clearly showed that small percentages of multiwall carbon nanotubes improved the mechanical (notably fatigue) properties of bone cement. This is noteworthy because mechanical fatigue failure of the cement mantle likely remains one of the chief drawbacks of bone cement. [54] Like typical fiber reinforced composites, fatigue failure of bone cement is believed to occur in three phases, i.e. 1) crack initiation due to a flaw in material continuity, 2) slow crack propagation, and 3) rapid propagation to failure. [80] Although "third and fourth generation" cementing techniques have extended the fatigue life of bone cement, residual material voids or surgical errors in component positioning can cause weak or thin regions that render these regions susceptible to fatigue failure. The presence of well-dispersed nanotubes in bone cement, in conjunction with their anticipated strong nanotube-matrix bonding (due to their high surface area/volume ratio) and extremely strong tensile properties, suggests that some of these nanotubes would have their long axis oriented perpendicular to the plane of the incipient crack. Such nanotubes would act to arrest crack growth and thereby further enhance the longevity of the cement mantle. Also, because the dimensions of the cement mantle have an important role in implant-bone stress transfer, use of MWNTs in bone cement and the

resulting improvement in mechanical properties may result in greater “forgiveness” to suboptimal intraoperative implant placement. This is noteworthy because improper stem placement continues to be cited as a factor which may reduce implant longevity. [153] Finally, dental prostheses are also known to fracture by fatigue failure through the palette. Cast metal is occasionally incorporated into these prostheses [42, 137] in specific thin or high stress areas to reduce the chance of breakage. MWNTs may reduce or eliminate the need for such metal reinforcement and thereby also enhance the fatigue performance of denture-based acrylic materials.

It appears that the larger concentrations of MWNTs do not produce the enhancements observed with the 2wt% loading, thereby suggesting that the optimal concentration is near 2wt%. Although we do not yet understand the nanotube-matrix interactions that occur, we speculate that perhaps the observed decreases in material property enhancement with increasing MWNT loading are due to the beneficial effects of MWNT material augmentation competing against the adverse effects of sporadic inadequately dispersed (still agglomerated) “clumps” of MWNTs. These MWNT clumps, which given sufficient incidence manifested in the 5% and 10% loadings, may act as fracture initiation sites. A sufficient number of such clumps, as may be found in the larger loading, may create enough detrimental effects that they compete with the beneficial effects of well-dispersed and isolated MWNTs. Another possible explanation for the MWNT weight percentage dose-response data observed is that there may be changes in the short or medium-range crystallinity of the polymer matrix that act to decrease the fatigue performance at these higher loadings. [124, 154, 155] Specifically, if a crystalline phase forms in the immediate area around each nanotube, then perhaps at the larger concentrations of MWNTs studied, growth of these crystalline regions could intersect. These intersecting interfaces could lead to decreases in flexural strength, increases in modulus, and reduced fatigue performance. Recall that these were the findings observed with the 5% and 10% loadings.

Nanotube pullout from the matrix is the predominant mode of overload failure and this seems reasonable because the interfacial (MWNT-bone cement) shear strength is believed to be less than the nanotubes tensile strength. Elastic recoil of a tensile strained region of matrix material near the nanotubes outer surface may also be responsible for the accumulated material visible at the end of the “pulled-out” nanotube and may explain some of the data observed. (Figure 4.6). Specifically, Ding et al [156] have shown that the material like that visible on the end of the nanotube in Figure 6 is

actually polymer matrix that formed a sheath around the isolated carbon nanotube during composite production. Once tensile failure occurred, this sheath was energetically released from one end of the nanotube and "balled up" on the opposite tip. While the interface between carbon nanotubes and polymer matrices is not clearly understood, this "sheathing" phenomenon may provide additional information regarding the nature of the interaction between the individual nanotubes and the adjacent bone cement matrix**.** It is again worthy to note that all of the preceding are preliminary speculations regarding the possible mechanisms that may explain MWNT-bone cement interactions and subsequent failure. Additional study is needed to understand the mechanism(s) responsible for the effects observed as a function of MWNT loading and the phenomenon of MWNT-matrix pullout.

No prior studies of MWNTs in PMMA exist against which the results of the present study can be compared, but several prior studies (Lewis et al [6, 148], Murphy et al [77], and Dunne et al [152]) have examined the fatigue performance of unaugmented PMMA-based bone cements by using the Weibull analytical methods reported presently. Although the actual number of cycles to failure is a necessary metric, the variance in the data renders this an incomplete measure. The Weibull life-analysis methods offer additional insights into fatigue performance and should be used to analyze and compare the results. Although both two-parameter and three-parameter Weibull models provide quantification of the α and β parameters, only the three-parameter model calculates a baseline for each sample (N_o) instead of assuming a zero baseline. The 3-parameter model also enables calculation of the Weibull mean fatigue lifetime (N_{WM}) and it has been said that this metric should receive more widespread use as a gauge of fatigue performance.[71] The actual number of cycles to failure and all Weibull derived parameters, including the survival probability curves, support the claim that multiwall carbon nanotubes have a positive affect on the fatigue performance of PMMA-based bone cement.

The addition of carbon nanotubes to bone cement may also offer a thermal benefits (as yet unstudied) which promotes enhanced implant longevity. Due to their high axial thermal conductivity, [157] MWNTs may reduce the high temperatures (70 - 90°C) observed at cement-bone interfaces [158] during in vivo polymerization via improved conduction of the heat of polymerization to the metallic stem. Support for this potential benefit is obtained from a recent study showing that the addition of steel fibers (5 – 15%) reduced the peak temperature of curing PMMA. [62] Thus, the addition of

MWNTs to bone cement may help avoid polymerization induced “hot” spots and subsequent hyperthermia-based destruction of bone adjacent to the cement mantle that is believed to be observed radiographically. [159] This may improve the mechanical integrity of the cement-bone interface and thereby promote enhanced implant performance.

Limitations to the present study include the non-clinically relevant manner in which MWNTs were dispersed in bone cement and the techniques used to prepare the specimens. This limits immediate applicability of the material and necessitates additional work aimed at suspending MWNTs in one or both of the two-phase cement components presently mixed intraoperatively. Also, like many other bone cement studies, only fresh non-oxidized materials were studied. The effects of MWNTs on oxidized bone cement matrices remain unknown. Room temperature fatigue testing in air is clearly non-physiological, but present work is ongoing to remedy this limitation. Finally, concerns have been raised that carbon nanotubes may have adverse effects on living cells. [160] To date, no definitive studies regarding these concerns have appeared in the literature, although studies are emerging which use nanotubes in contact with cells and for which no adverse events have been noted. [161] Although biocompatibility assessment of MWNTs was beyond the scope of the present investigation, such biocompatibility testing was considered irrelevant (at the outset of this study) in the absence of data showing MWNTs enhanced material performance. It is also important to note that there are two varieties of nanotubes (single and multiwall) and they have different morphologies, properties, and perhaps, different levels of biocompatibility (which remain to be quantified).

In conclusion, we reject the null hypothesis and conclude from these early results that specific loadings of multiwall carbon nanotubes favorably alter the static and fatigue mechanical properties of acrylic bone cement.

Chapter Five Multiwall Carbon Nanotubes Enhance the Fatigue Performance of Physiologically Maintained Methyl Methacrylate – Styrene Copolymer

5.1 Introduction

The copolymer of methyl methacrylate and styrene (MMA-co-Sty) is an important polymeric biomaterial that has many uses in medicine, especially orthopaedics. Bone cement, which is primarily composed of either polymethylmethacrylate or MMA-co-Sty, is a widely used polymer whose principal orthopaedic use is to: 1) provide a mechanical interface between native bone and a metallic joint prosthesis, 2) replace bone in cranial and maxillofacial surgeries [162], or 3) restore the load bearing capabilities of collapsed vertebrae. [135, 163] While the overall performance of bone cement is commendable, the longevity of clinical devices fixed with cement is partially limited by fatigue failure of this material. [10] Fatigue failure of bone cement results in implant loosening, pain, the need for revision total joint replacement surgery, and substantially increased healthcare expenditures.

The mechanism of bone cement fatigue failure is thought to occur in 3-phases: 1) initiation of cracks, 2) accumulation of damage and coalescence of cracks, and 3) catastrophic failure. [64] Fatigue cracks nucleate at pores or material inhomogeneities, and then grow at a slow, steady rate. [54, 82] This period of slow crack growth is directly linked to the formation of crazes near the tip of the advancing crack. [72] Crazing is a phenomenon observed in amorphous polymers (e.g., PMMA, MMA-co-Sty) whereby elevated stresses cause localized realignment of the polymer chains along the principal stress direction. While this initially toughens the polymer [72], continued crazing and chain realignment into fibrils results in the formation of microscopic recesses within the polymer just ahead of the crack tip. As loading continues, more polymer chains are drawn into the fibrils from the surfaces of these recesses. [82] Eventually, the fibrils fail and the recesses coalesce. This in turn causes the crack to advance through the entire craze zone whereby multiple micro-cracks meet and coalesce, form large cracks, then rapidly lead to brittle failure. [65]

Many have tried to improve the mechanical properties of bone cement by adding small amounts of metal [62, 80, 140], glass [41], polymer [59, 60], or carbon [38, 44, 81] fibers as reinforcing materials, but these efforts resulted in limited success. Inadequate dispersion, poor fiber- matrix bonding, and filler – damage scale mismatch are potential reasons to explain these sub-satisfactory results. Scale mismatch pertains to the

dimensional incompatibility between the diameters of the reinforcing fibers and the size of the fatigue damage in the matrix; fibers that were orders of magnitude larger than the scale of the damage were considered ineffective for preventing or arresting damage accumulation.

Scale compatibility is one of the key reasons why the discovery of multiwall carbon nanotubes (MWCNTs) gives new hope for fiber reinforcement of bone cement. [93] (Figure 5.1) The small diameter (~ 10^1 nm) of this nanomaterial is far more comparable to the size of the polymer chains and the scale of fatigue damage compared to the size of conventional (~10^4-10^6 nm) fibers. Small diameters, in conjunction with long (~10^5 nm) fiber lengths, confer MWCNTs with large surface area/volume ratios. This increases the physical interface between the MWCNTs and the polymer matrix, which boosts the efficiency of MWCNT – MMA-co-Sty matrix stress transfer compared to conventional fibers. The advantageous dimensions of MWCNTs would be of limited utility were it not for their extraordinary (~ 0.1 TPa) tensile strength. [164] These features strongly support the use of MWCNTs for augmenting various polymer matrices. This use is also supported by prior experimental data in other polymer systems. [119, 120, 124, 165, 166] To evaluate the potential of MWCNTs to enhance the fatigue performance of bone cement, this study sought to test the effect of adding small amounts of MWCNTs (≤ 10wt%) on the fatigue performance of MMA-co-Sty under physiologically relevant conditions.

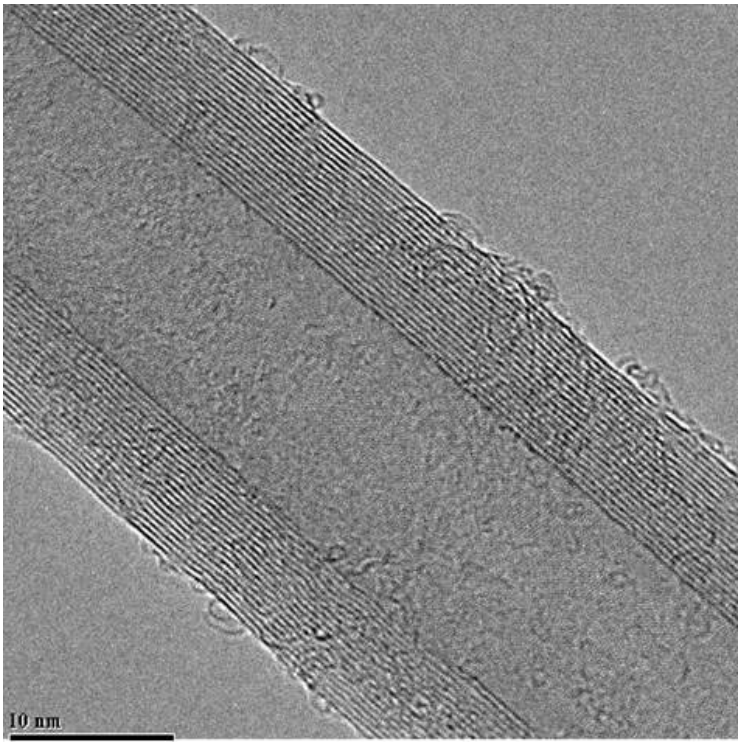

Figure 5.7 Multiwall Carbon Nanotube

This transmission electron micrograph shows the highly ordered walls of a multiwall carbon nanotube whose outer diameter is ~ 20nm.

5.2 Experimental

5.2.1 Sample preparation

Multiwall carbon nanotubes were synthesized by using a chemical vapor deposition process [99], which injected a mixture of ferrocene catalyst and xylene into a multi-zone, heated furnace under a hydrogen-argon atmosphere. Iron from the decomposed ferrocene acted as a catalyst for the formation of the ordered lattice structure of the carbon nanotubes. The as-produced carbon nanotubes were harvested in clusters that required disaggregation preparatory to and during dispersion into the polymer matrix. The as-produced multiwall carbon nanotubes (MWCNTs) were dispersed throughout the molten matrix of MMA-co-Sty [165] with two heated (220ºC) stainless steel, counter-rotating sigma rotors in the mixing chamber of a Haake Rheomix (Haake, GMBH, Germany). The powder, taken from a clinically used bone cement system and containing a substantial portion (~10wt%) of the radiopacifying agent barium sulfate, was added to the mixing chamber followed by an appropriate addition of as-produced MWCNTs. The two materials were then shear mixed [146] by the sigma rotors

(20 rpm) to disentangle and thoroughly disperse the MWCNTs throughout the molten polymer thereby producing nanocomposites consisting of 0.5%, 1%, 2%, 5%, and 10% (by weight) MWCNTs. Although shear mixing could shorten the lengths of the MWCNTs, the aspect ratios (length/diameter) remained large because the potency of the shear-mixing induced MWCNT shortening mechanism diminished as the nanotubes were dispersed. [146] At completion, the molten material was collected and allowed to cool in air (25ºC) until solid. A control group (0wt% MWCNTs) was prepared by a similar shear mixing process, but without the addition of MWCNTs.

Each hard nanocomposite material was crushed into pellets and hot-pressed (~200ºC; 0.9 metric tons) under vacuum into films of uniform thickness (1.6 mm). The cool, hard films were then machined into dog-bone-shaped specimens suitable for constant amplitude-of-force, fully reversed tension-compression fatigue testing (ASTM F2118). Each specimen was annealed at 125ºC for a minimum of fifteen hours to alleviate any residual stresses that formed during machining. The width and thickness of each specimen were measured in several locations along the gauge length with a precision caliper to quantify specimen dimensions. Each specimen was then aged in Dulbecco's Phosphate Buffered Saline (PBS) (Gibco, Invitrogen Corp. Carlsbad, CA) at 37ºC for a minimum of six days and a maximum of sixty days.

5.2.2 Fatigue testing and scanning electron microscopy

Fully reversed tension-compression fatigue testing was performed in a heated (37ºC) Dulbecco's PBS environment with an Instron servo-hydraulic materials testing system (model 8521; Instron Corp. Canton, MA). An accelerated (5 Hz) fatigue testing protocol was developed based upon prior studies [71, 77], which sinusoidally loaded test specimens to peak tensile/compressive stress amplitudes of 20, 30, and 35 MPa (0 MPA mean stress value) until failure or to a run-out value of 2 million cycles. The number of cycles to failure was recorded for each specimen. Specimens that failed prior to achieving 1,000 cycles at any stress amplitude were considered unrepresentative of the population and were excluded from consideration.

Scanning electron microscopy (Hitachi S-2700) was used on arbitrarily selected specimens to observe the positioning of individual MWCNTs within the nanocomposite matrix after fatigue testing was completed. Additionally, the surfaces of these failed specimens were prepared by manual fracture in liquid nitrogen at sites along their undamaged gauge length. Micrographs of such freeze-fractured specimens were

examined for any secondary fatigue cracks that may have formed during fatigue testing and qualitative conclusions were drawn regarding the interactions between the MWCNTs and the matrix as well as the mechanism of failure.

5.2.3 3-parameter Weibull analysis

Fatigue testing measures the lifetime of a device or a material and, frequently, cycles to failure data are not normally distributed. Therefore, non-normal based data analytical methods are used, the most useful and widespread of which is based upon the Weibull distribution. This method is recommended for analyzing fatigue data from bone cement specimens. [71] Thus, the cycles to failure for each sample were analyzed by using the linear version of the three-parameter Weibull model. This analysis technique produced three parameters, namely the minimum fatigue life (N_o), the shape parameter (α), and the location parameter (β), each of which were calculated from a step-wise procedure that converted the cycles to failure into a set of ranks and natural logs. The cycles to failure (N_f) for each sample were converted into a probability of failure $P(N_f)$, defined as the probability of a specimen failing by cycle number N_f and calculated by:

$$P\left(N_f\right) = 1 - \exp\left[-\left(\frac{N_f - N_o}{\beta - N_o}\right)^{\alpha}\right] \qquad (1)$$

where N_o was the minimum fatigue life (the baseline number of cycles for the sample at a given load amplitude), β was the location parameter (the number of cycles to failure below which 63.2% of the specimens fail), and α was the Weibull modulus, or shape parameter (an indicator of the variance within the sample).

For calculating the three parameters, Equation (1) was transformed into linear form (Y = mX+B), vis:

$$\ln\ln\left[\frac{1}{\left(1 - P(N_f)\right)}\right] = \alpha \ln\left(N_f - N_o\right) - \alpha \ln\left(\beta - N_o\right) \qquad (2)$$

The numbers of cycles to failure were ranked from least to greatest (M=1,2,...,G) and substituted into Equation 3:

$$P\left(N_f\right) = \left(M - 0.3\right)/\left(G + 0.4\right) \qquad (3)$$

where G was the total number of specimens in each sample. The minimum fatigue life (N_o) was calculated by applying a least squares regression to the plot of ln[ln(1/(1-$P(N_f)$))] versus ln(N_f) to produce a best fit 2nd order polynomial. [167] The vertical asymptote of this best fit line was used to determine N_o. Subsequently, the minimum

fatigue life was used to correct the cycles to failure data, $\ln(N_f - N_o)$, for the remainder of the analysis. The shape parameter (α) was calculated as the slope of the best-fit line to the corrected data and the location parameter (β) was obtained from Equation 4:

$$\beta = N_o + \exp(-C/\alpha) \qquad (4)$$

where C is the y-intercept of this best fit line. (Figure 5.2)

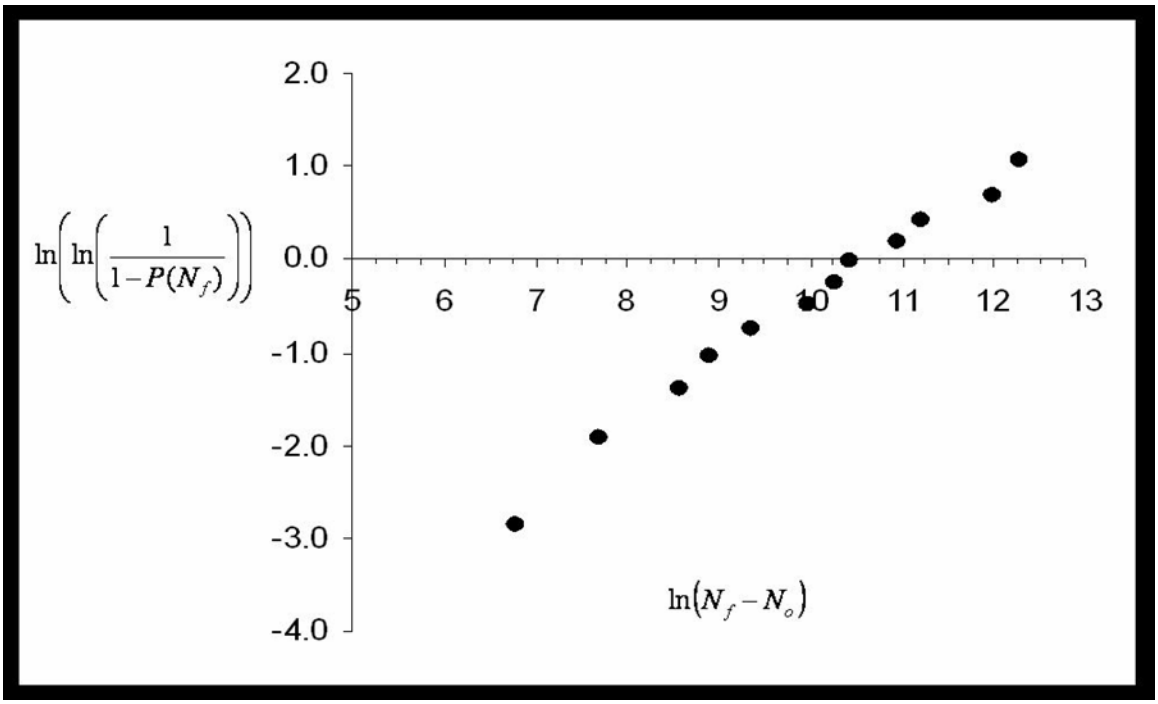

Figure 5.8 Minimum Fatigue Life

Data points in this figure show the effect of variability on the calculation of the minimum fatigue life (N_o). The two smallest values in the data (furthest left on the graph) forced the 2nd order polynomial to assume an upwards concavity and no vertical asymptote. The procedure presented by Janna et al [167] called for values of zero to be assigned for such conditions. This explains the zero values for minimum fatigue life (N_o) presented in Tables 5.1, 5.2, and 5.3.

All three Weibull parameters were used to calculate the Weibull mean (N_{WM}), an indicator of the fatigue performance of each sample. Calculation of this indicator incorporated the minimum value (N_o) of the range, norm (β), and variance (α) of the sample. The Weibull mean (N_{wm}) was considered the best parameter for comparing the

fatigue performance of the MWCNT – MMA-co-Sty nanocomposites, and was calculated by:

$$N_{WM} = N_o + (\beta - N_o)\Gamma\left(1 + 1/\alpha\right) \qquad (5)$$

where Γ is the Gamma function as previously reported. [71]

5.3 Results and Discussion

5.3.1 Fatigue testing results

Testing at the 20 MPa peak stress amplitude showed that the addition of 2wt% and 5wt% MWCNTs produced the largest increases in Weibull mean (N_{wm}) value, i.e., 565% and 592% greater fatigue lives than the control (0wt%) group. (Table 5.1) The 0.5wt% MWCNT loading resulted in the smallest improvement in N_{wm}, yet this value was still 307% greater than that observed from the control group. Although the 2wt% MWCNTs sample generated the optimal enhancement in the Weibull minimum fatigue life (N_o) parameter, this effect may be due to the increased difficulty in mixing higher loadings of MWCNTs. Calculated location parameter (β) values varied with MWCNT loading similarly as that shown for N_{wm}. The low α values observed suggested high variances within the 1wt%, 2wt%, and 10wt% MWCNT loading groups while the variance within the 0.5wt% MWCNT loading group (α = 1.25) was low.

Table 5-3 Weibull Test Parameters vs MWCNT Loading at 20 MPa Peak Stress

MWNT Concentration	Minimum Fatigue Life (N_o)	Shape Parameter (α)	Location Parameter (β)	Weibull Mean (N_{WM})
0wt% (n=12)	17,763	1.0	124,145	124,754
0.5wt% (n=11)	0	1.2	544,863	507,953
1wt% (n=11)	45,877	0.7	533,213	714,810
2wt% (n=11)	107,661	0.8	742,933	830,028
5wt% (n=11)	23,266	0.9	836,413	863,216
10wt% (n=11)	27,514	0.6	356,925	563,449

At 30 MPa, the 1wt%, 2wt%, and 5wt% MWCNTs loadings were associated with N_{wm} increases of 148%, 247%, and 171%, respectively, as compared to the control group. (Table 5.2) Based upon the particulars of the Weibull analytical technique, the 0wt% sample demonstrated a minimum fatigue life (N_o) value of zero while the 2wt% and 5wt% MWCNTs samples produced the largest N_o values. Similarly, the magnitudes of

the location parameter (β) and the Weibull mean (N_{wm}) peaked at concentrations of 2wt% and 5wt% MWCNTs. The 0wt% and 10wt% MWCNTs samples had low variances (α = 1.35 and 1.33, respectively) while the 2wt% MWCNTs sample showed the highest variance (α = 0.67).

Table 5-4 Weibull Test Parameters vs MWCNT Loading at 30 MPa Peak Stress

MWNT Concentration	Minimum Fatigue Life (N_o)	Shape Parameter (α)	Location Parameter (β)	Weibull Mean (N_{WM})
0wt% (n=12)	0	1.4	21,929	20,097
0.5wt% (n=12)	1,943	0.9	28,607	29,943
1wt% (n=12)	4,253	1.0	49,730	49,782
2wt% (n=12)	14,170	0.7	56,499	59,784
5wt% (n=11)	16,928	0.9	51,740	54,417
10wt% (n=11)	1,571	1.3	28,882	26,668

Testing at the highest stress amplitude, 35 MPa, revealed that N_{wm} decreased slightly with increasing concentration of MWCNTs up to and including 2wt%. (Table 5.3) Conversely, the location parameters (β) for the 0wt%, 0.5wt%, 1wt% and 2wt% MWCNTs samples remained consistent. At 5wt% MWCNT, the Weibull mean decreased sharply whereas the Weibull parameters and N_{wm} could not be calculated for the 10wt% MWCNT sample because the specimens failed prior to reaching 1,000 cycles. The values for the minimum fatigue lives (N_o) for each nanocomposite were far less than that of the control group, especially for the 2wt% MWCNTs sample (N_o= 0).

Table 5-5 Weibull Test Parameters vs MWCNT Loading at 35 MPa Peak Stress

MWNT Concentration	Minimum Fatigue Life (N_o)	Shape Parameter (α)	Location Parameter (β)	Weibull Mean (N_{WM})
0wt% (n=12)	2,970	0.7	13,435	16,055
0.5wt% (n=11)	572	0.7	12,457	15,209
1wt% (n=11)	710	1.1	11,159	10,959
2wt% (n=11)	0	1.2	14,316	13,467
5wt% (n=11)	943	0.9	3,337	3,508
10wt% (n=11)	****	****	****	****

Examination of a freeze fractured specimen loaded with 5wt% MWCNTs (Figures 5.3A and B) revealed a secondary crack in the surface. The MWCNTs were observed to protrude from the crack faces into the crack wake normal to the direction of crack growth. Magnification of the secondary crack (Figures 5.3C and D) showed some of the MWCNTs bridging the growing crack. Similarly, a SEM image of a freeze-fractured 0.5wt% MWCNT loaded specimen also showed MWCNTs obtruding into the crack wake. (Figure 5.4)

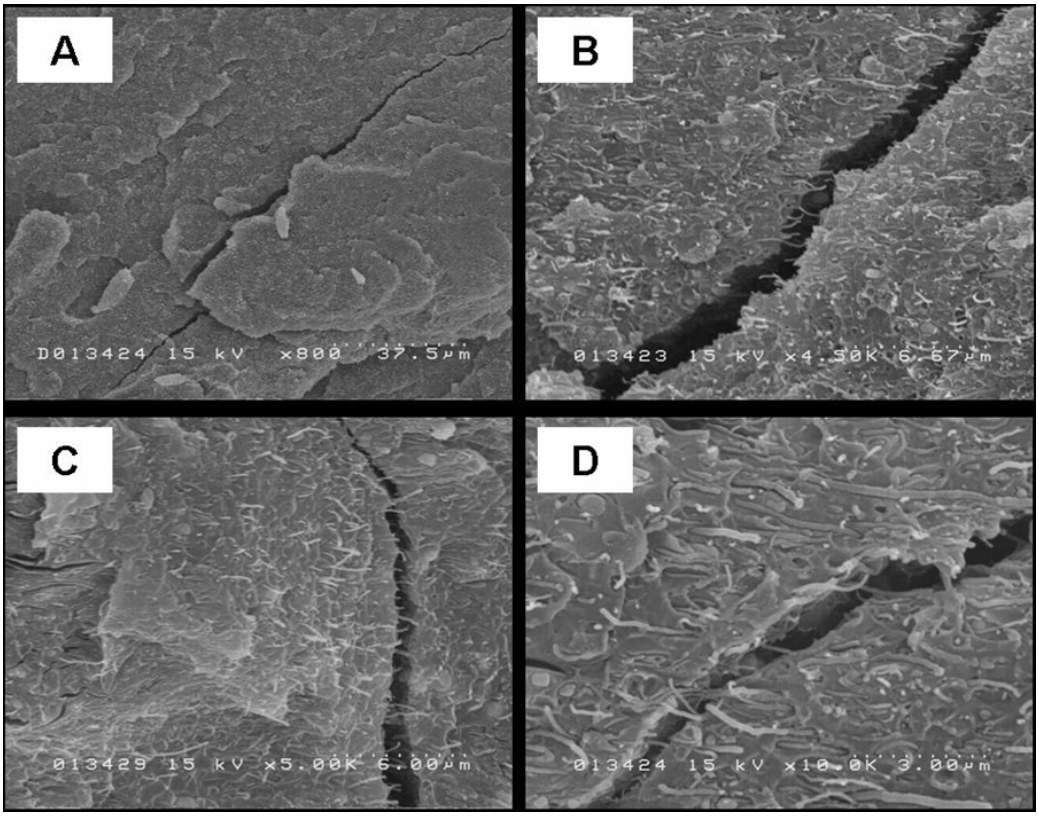

Figure 5.9 Micro-crack

A series of SEM images documenting one micro-crack (**A**) observed on the freeze fractured surface of a test specimen loaded with 5wt% MWCNTs and stressed at 20 MPa. Magnification of the crack in images **B**, **C**, and **D** revealed the matrix-reinforcing behavior of the MWCNTs in response to crack growth. The MWCNTs are clearly observed as finger-like projections protruding into the wake of the crack normal to the direction of crack growth.

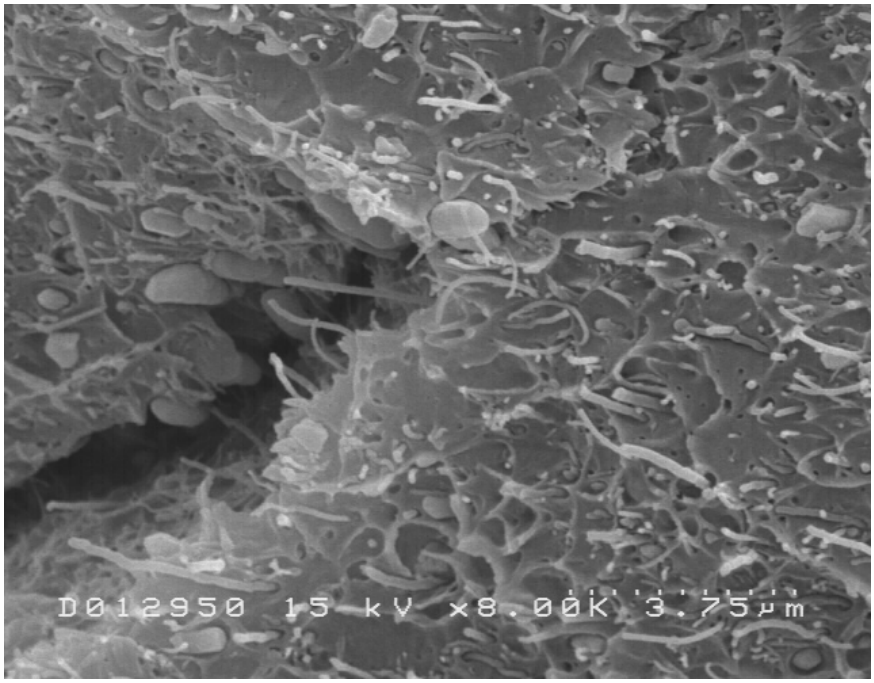

Figure 5.10 MWNT - Bone Cement Composite

This SEM image of a specimen loaded with 0.5wt% MWCNTs and stressed at 20 MPa clearly shows MWCNTs in the crack wake that have reoriented perpendicularly to the crack face. Particles of barium sulfate, a radiopacifier commonly used in bone cement, are also seen and provide a size comparison to the MWCNTs.

5.3.2 Mechanisms of reinforcement

The quantitative fatigue results and qualitative image data clearly show that multiwall carbon nanotubes enhance the fatigue performance of MMA-co-Sty. These data support the working hypothesis that MWCNTs retard the mechanism of fatigue failure by preventing or minimizing the initiation of catastrophic cracks and by slowing damage accumulation of existing or newly forming cracks. That is, the MWCNTs are believed to effectively bridge cracks and reduce the extent of plastic deformation experienced by the matrix. Although crazing related plastic deformation is inevitable in highly stressed polymer matrices [54, 64, 72, 82], MWCNTs can successfully reinforce the craze by strengthening the fibrils and bridging the recesses or sub-micron voids to prevent their coalescence. Thus, there are three components to the hypothesized mechanism of improving the fatigue performance of MMA-co-Sty. First, the addition of MWCNTs induces the nucleation of polymer chains into interstitial regions of crystallinity [156, 165, 168] that maximize the efficiency of stress transfer between the matrix and

the MWCNTs. Second, their nanoscale dimensions enable MWCNTs to reinforce the fibrils of the craze [169] and bridge the microcracks in the craze zone. The elevated local stresses in the craze zone and around the crack tip are blunted by their conversion into small local strains by stress transfer from the weak matrix to the strong MWCNTs via Hooke's Law. Lastly, the high surface area to volume ratio of the MWCNTs implies a greater number of interfacial bonds between the MWCNTs and the matrix as compared to other fiber reinforced polymers, including bone cement [62]; thus, MWCNT pull-out from the matrix requires the breaking of the interfacial bonds, which absorbs energy that would otherwise result in damage accumulation and subsequent growth of the fatigue crack. (Figures 5.3 and 5.4) It remains unclear which mechanism, if any, is dominant; however, it can be inferred that each mechanism plays a role in enhancing the fatigue performance of MMA-co-Sty.

MWCNTs clearly produce larger increases in fatigue life at lower stress amplitudes. This finding may be explained by considering the stress intensity factor K (a measure describing the local stresses relative to the applied stress based on the geometry and size of the fatigue crack or other damage). If the applied stress is maintained at a constant level then the stress intensity factor will increase as damage accumulates in the form of crazing beyond the crack tip. [65, 72] A large craze zone implies an elevated stress intensity factor, which suggests that the fatigue crack will grow at much faster rates and failure will occur sooner; furthermore, it is known that a fatigue crack will grow with every cycle at high rates of damage accumulation and elevated stresses. [170] We postulate that at these higher levels of stress the onset of damage overcomes the ability of MWCNTs to slow crack growth via the aforementioned mechanisms. However, it should be noted that comparing the methods of this study with those of other bone cement studies revealed that the lowest stress amplitude here (20 MPa) is greater than the majority of the maximum stresses (10 – 15 MPa) studied elsewhere [71]; thus, we believe that testing at 35 MPa approaches the extreme upper limit of stress amplitudes commonly attributed to bone cement. Furthermore, we also postulate that testing at stress amplitudes below 20 MPa, which is common to the study of bone cement, will result in fatigue performance that exceeds the results presented in this study.

5.3.3 Carbon fibers versus multiwall carbon nanotubes

Previous work showed that the addition of 2wt% untreated, milled carbon fibers (150 μm lengths; 8 μm diameters) did not substantially increase the fatigue performance of bone cement containing an untreated radiopacifying agent. [81] Furthermore, adding untreated, milled carbon fibers negated the positive effect of plasma treating the radiopacifying agent and decreased the fatigue performance of the bone cement. In the same study, plasma treating the milled carbon fibers (enriching the surface of the fibers with oxygen functional groups) in combination with a treated radiopacifier improved the fatigue performance of bone cement by ~600%, which was comparable to the effect of adding 2wt% untreated MWCNTs to MMA-co-Sty with an untreated radiopacifier. Thus, the untreated MWCNTs outperformed the untreated carbon fibers and, at the very least, matched the performance of the treated carbon fibers. Plasma treating the surfaces of the carbon fibers was believed to improve the adhesion of the filler in the bone cement matrix. Perhaps treating the surfaces of MWCNTs in such a manner would magnify their effect on the fatigue performance of MMA-co-Sty. If so, the combination of improved wettability and nanoscale dimensions would make MWCNTs better candidates than traditional carbon fibers for improving the fatigue performance of polymers such as MMA-co-Sty.

5.3.4 Effects of aging and testing in a physiologically relevant environment

Aging and testing the samples in a physiologically relevant environment (i.e. phosphate buffered saline, 37ºC) is known to improve bone cement's resistance to crack formation [50] and propagation. [50, 67] Additionally, the phosphate buffered saline may improve the lubricating properties of MWCNTs much in the same way as a humid environment increases the lubricity of graphite. [171] It is likely that the combined plasticization of the matrix and lubrication of the MWCNTs led to improvements in fatigue performance greater in magnitude than those presented for fatigue testing a similar MWCNT – polymer nanocomposite in air at room temperature (25ºC). [165] Although the mode of testing in the previous work differs from this study (i.e. 4-point bending versus fully reversed tension – compression), they both incorporate elements of tension and compression. Therefore, it is likely that the combined effects of the MWCNTs and the testing environment led to elevated fatigue performances of MMA-co-Sty loaded with MWCNTs.

5.3.5 The effects of MWCNTs is reduced at high concentrations

Despite the reported positive effects of MWCNT addition, the data collected for the highest concentration of MWCNTs (10wt%) showed less than ideal results. At the 20 and 30 MPa applied peak stress levels, the Weibull means for these samples sharply decreased. These irregularities are believed to be due to imperfectly disaggregating and dispersing large amounts of MWCNTs (i.e. 10% by weight loadings) into the MMA-co-Sty matrix. Agglomerations of MWCNTs can nucleate pores and other non-homogeneous regions in the resulting nanocomposite. While individual nanotubes and perhaps even clumps of nanotubes can reinforce polymer matrices, clumps of such nanotubes also can have a detrimental role. The observed fatigue behavior therefore represents the net of both the improvements made by well dispersed nanotubes and detractions made by clumped nanotubes. Thus, it is believed that the limitations of the aforementioned shear mixing protocol were met with the addition of 10wt% MWCNTs. Perhaps increasing the shear during mixing or mixing for a longer period of time would further disaggregate such entanglements of MWCNTs, but the likelihood of irreversible damage to polymer matrix would become too great.

5.4 Conclusions

The addition of multiwall carbon nanotubes substantially improves the fatigue performance of MMA-co-Sty when cyclically stressed under physiologically relevant conditions. Furthermore, the effectiveness of MWCNT reinforcement is dependent on the concentration of MWCNTs, the dispersion of the MWCNTs, and the peak stress of the dynamic loading cycle. Subsequent efforts need to be focused on dispersing MWCNTs into the commercial bone cement system (both liquid and powder phases) and thereby allow testing of the effect of MWCNTs on bone cement as it is prepared in the operating room. Regardless of the route taken to disperse MWCNTs into the MMA-co-Sty matrix, the results of this study show that further efforts to develop a clinically relevant material formulation with appropriate mixing techniques are justified given the benefits of nanotube reinforcement of the present polymer matrix. Additionally, the results obtained in this study have broader implications for numerous other applications in Orthopaedics and the medical industry as well as sporting goods, aerospace, and structural applications.

Chapter Six Monotonic and Dynamic Fracture Properties of Single Phase Bone Cement Reinforced with Multiwall Carbon Nanotubes

6.1 Introduction

Acrylic bone cement is widely used in orthopaedics, dentistry, and orofacial surgery. This multi-component, polymer based system provides mechanical stability to metallic joint prosthesis (total joint arthroplasty), restores structure to vertebral column fractures (vertebroplasty/kyphoplasty) [135, 163], and fills cranial and maxillofacial defects [162]. Although the clinical performance of bone cement is commendable, it is susceptible to fatigue failure. Everyday activities, such as walking and stair climbing, generate dynamic loads that contribute to the mechanistic accumulation of microscale fatigue related damage. Catastrophic failure of bone cement loosens the implant, necessitates revision surgery, and elevates healthcare expenditures.

Understanding fracture mechanics and fatigue failure is beneficial for engineering new, high performance bone cements. Fatigue failure of bone cement can be divided into three distinct stages: 1) crack initiation, 2) crack propagation, and 3) fast, catastrophic failure. [64, 72, 82, 84, 87] Debate continues regarding which stage is dominant, though propagation is more widely reported. Crack propagation involves the nonlinear accumulation of fatigue related damage and is typically more complex than initiation. Once a fatigue crack nucleates, the crack front serves as a site for stress localization. These elevated stresses are counteracted through the development of an energy dissipation zone, which often includes crazing and micro-cracking. [50, 72, 83, 84, 86] Crazing, a material phenomenon common to amorphous polymers, is attributed to the redistribution and alignment of molecules at local sites of elevated stress. Crack growth is often preceded by craze development; thus, craze failure is one of the rate limiting steps in the progression of fatigue cracks through the bulk material. With regard to linear elastic fracture mechanics (LEFM), the stress intensity factor (K) is used to describe the combinatorial effect of applied load and crack size. The common denominator between monotonic and dynamic fracture properties is dependence on the stress intensity factor (K). For monotonic loading, a critical value of the stress intensity factor, termed the fracture toughness (K_{IC}), is a material property that describes the resistance to fracture. The probability of catastrophic failure increases as the crack grows and as K approaches K_{IC}. For dynamic loading, the stress intensity factor is reported as a range, ΔK ($K_{max} - K_{min}$), and is related to the rate of crack growth (da/dN).

The stress intensity range (ΔK) during fatigue crack propagation testing is typically well below the K_{IC} value for the material and is directly related to the rate of fatigue crack growth. ΔK increases as damage accumulates ahead of the crack tip and the fatigue crack grows. Eventually, stable crack growth gives way to unstable crack growth and, ultimately, failure. Therefore, the ideal high performance bone cement not only exhibits improved resistance to crack initiation, but also demonstrates elevated fracture toughness and resistance to crack propagation.

The fatigue performance and fracture mechanics of bone cement are widely reported and many factors, extrinsic and intrinsic, are shown to affect the results. [2, 49, 50, 70, 71, 78, 152] Several solutions for improving the fatigue and fracture properties of bone cement include (but not limited to) vacuum mixing [52, 76, 77], alternative radiopacifiers [7, 66], and reinforcing fibers and particles [58, 62, 80, 81, 172]. The effects of fiber reinforcement are limited by fiber ductility and elevated viscosity as well as size discrepancy between the fiber diameters and the scale of fatigue related damage. Fiber – matrix de-bonding contributes to less than ideal fatigue results; yet, ironically, the dissipation of energy attributed to de-bonding is thought to increase resistance to fracture. [48, 62, 63] Recent studies report enhanced fatigue performance of bone cement reinforced with multiwall carbon nanotubes (MWNTs). [165, 173] MWNTs (10^{-9} – 10^{-8} m diameters) have aspect ratios (length/diameter) greater than 1,000 and large surface area to volume ratios, which confer these nanomaterials with unique reinforcing capabilities. (Figure 1) Although the quasi-static mechanical properties of carbon nanotube composites are well established [119, 120, 166], the fatigue and fracture mechanics of such materials are seldom reported. Theoretical mechanisms of MWNT reinforcement include matrix shielding, craze reinforcement, crack deflection, and crack bridging; yet, no data exists linking these mechanisms with the fracture properties of single phase bone cement. Therefore, the goals of the current study are to measure the fracture toughness and characterize the fatigue crack propagation behavior of single phase bone cement reinforced with small amounts of multiwall carbon nanotubes.

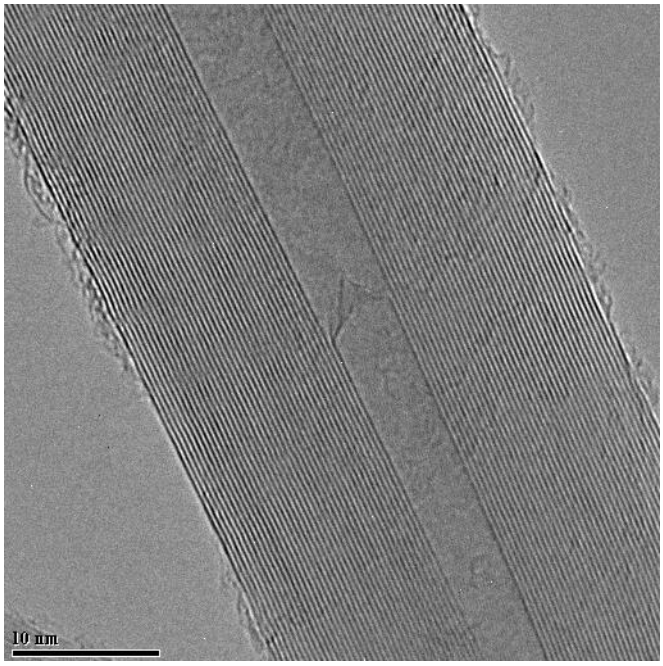

Figure 6.1 Multiwall Carbon Nanotube
This transmission electron micrograph reveals the highly ordered, concentric structure of a multiwall carbon nanotube.

6.2 Experimental

6.2.1 Multiwall carbon nanotubes

Multiwall carbon nanotubes were produced using a chemical vapor deposition process. [99] Iron nanoparticles catalyzed the formation of the ordered lattice structure of the carbon nanotubes. The as-produced carbon nanotubes were harvested in clusters that required disaggregation preparatory to and during dispersion into the polymer matrix. As-produced multiwall carbon nanotubes (MWNTs) were dis-aggregated and dispersed in molten single phase bone cement [165] with two heated (220ºC) stainless steel, counter-rotating sigma rotors in the mixing chamber of a Haake Rheomix (Haake, GMBH, Germany). The powder, taken from a clinically used bone cement system and containing a substantial portion (~10wt%) of barium sulfate radipacifier, and MWNTs were thoroughly shear mixed in the heated chamber [146] by the sigma rotors (20 rpm) thereby producing nanocomposites consisting of 0.5%, 2%, and 5% (by weight) MWNTs. The aspect ratios (length/diameter) of the MWNTs were not greatly affected by shear mixing because shear induced MWNT shortening diminished as the nanotubes were dispersed. [146] After mixing, the molten material

was harvested and cooled in air (25ºC) until hard. A control group (0wt% MWNTs) was prepared with identical methods, except for the addition of MWNTs.

6.2.2 Specimen production

Hard nanocomposite material (0wt%, 2wt% MWNT) was crushed into pellets and hot-pressed (~200ºC; 0.9 metric tons) under vacuum into films. The cool, hard films were then machined into rectangular specimens suitable for constant amplitude-of-force, 4-point bend crack propagation testing.[174] Parallel edges were created with a slow turning diamond blade (Buehler Ltd; Lake Bluff, IL) with the thickness of the specimen (W) approximately equal to four times the width (B). A single notch (1 mm) was machined into one of the long edges of each specimen. The width and thickness of each specimen were measured in several locations with a precision vernier caliper. The faces of the specimens were thoroughly cleaned and two crack propagation gages (RDS22; HBM, Darmstadt, Germany) were mounted onto either face of each specimen. Each gage was comprised of 50 conductive ties in parallel spaced 100 microns apart. The gages were mounted close to the notch tip with quick setting resin. Conductive leads were soldered onto each end of the gages.

For fracture toughness, hard nanocomposite material (0wt%, 0.5wt%, 2wt%, and 5wt% MWNTs) was hot-pressed under vacuum into rectangular molds. The faces of the specimen were polished using rotary polishing wheels (600 grit; 1000 grit). Each specimen was machined once down the length to ensure the thickness (W) of each specimen was twice the width (B) (as per ASTM D5045). The width and thickness of each specimen were measured at several locations using a high precision vernier caliper. A single notch equal to one half of the thickness (B) was machined into each specimen using a slow turning diamond blade (Buehler Ltd, Lake Bluff, IL). Preparatory to testing, each specimen was pre-cracked by either tapping or slicing a fresh, industrial razor blade into the notch.

6.2.3 Fracture toughness

Fracture toughness testing was performed on a MTS QTest (MTS) in accordance with ASTM D5045. [175] Specimens were loaded to failure in 3-point bending (10 mm/min) and the load – deformation curves were recorded. The length of the pre-crack was measured post-fracture in three locations with optical microscopy. The load at fracture was used to calculate the fracture toughness (K_{IC}) (Equation 1):

$$K_{IC} = \frac{P}{BW^{1/2}} f\left(a/W\right) \qquad (1)$$

where P is max load, B is the specimen width, W is the specimen thickness, and a is the length of the pre-crack. The function f (a/W) was calculated with Equation 2.

$$f(x) = \frac{6x^{1/2}}{\left[(1+2x)(1-x)^{3/2}\right]}\left[1.99 - x(1-x)\left(2.15 - 3.93x + 2.7x^2\right)\right] \qquad (2)$$

where x equals a/W. Each sample was checked for outliers and analyzed for significance using Analysis of Variance and Fischer's PLSD post-hoc correction. Additionally, the effect of pre-cracking method was analyzed for significant difference.

6.2.4 Fatigue crack propagation

Each specimen was mounted onto a 4-point bending fixture of an Instron servohydraulic materials testing system (Instron, Canton, MA). A conservative, increasing ΔK (da/daN > 10^{-9} m/cycle) protocol for testing the specimens to failure was developed to ensure adequate pre-crack growth. The actuator was cycled (5 Hz) in load control with a maximum load of 100 N and an R value of 0.1. If the pre-crack did not form after 100,000 cycles, the applied load was increased by 10%. Resistance across the crack gages were recorded with a real time data logger (dataTaker DT80; Grant Instruments Ltd, Shepreth, UK). Data acquisition was started simultaneous to the start of the fatigue test. The rate of crack growth (da/dN) was calculated with the secant method in accordance with BS ISO 12108:

$$\frac{da}{dN} = \frac{\left(a_n - a_{n-1}\right)}{\left(N_n - N_{n-1}\right)} \qquad (3)$$

The stress intensity factor (ΔK) was calculated with Equation 4:

$$K = \left(\frac{20}{2W}\right)\frac{P}{BW^{1/2}} f\left(a_{ave}/W\right) \qquad (4)$$

where 20 is the difference between the support span and loading span, P is the maximum load, B is the specimen thickness, W is the specimen width, and a_{ave} is the average crack length over the increment $a_n - a_{n-1}$. The function f(a/W) is defined for a single edge notch three point bend specimen (SENB4):

$$f(\theta) = 3(2\tan\theta)^{1/2}\left[\frac{0.923 + 0.199(1-\sin\theta)^4}{\cos\theta}\right] \qquad (5)$$

where θ = πa/2W. The rates of crack growth (da/dN) were plotted against the corresponding ΔK values. The Paris Law regression was applied to each sample. The Paris Law model (Equation 6) assumes that the slope (m) and the intercept (C) of the regression line are material constants.

$$da/dN = C(\Delta K)^m \qquad (6)$$

6.2.5 Scanning electron microscopy

Scanning electron microscopy (Hitachi S-2700) was used to observe the mechanisms of crack growth and the relative positioning of individual MWCNTs within the nanocomposite matrix. The micrographs were used to formulate postulations regarding the reinforcing capabilities of the MWNTs. Additionally, the micrographs were used to delineate the different regions of crack growth (i.e. pre-cracking, fatigue related crack propagation, brittle fracture).

6.3 Results

Results of fracture toughness testing for four MWNT – bone cement composites (0wt%, 0.5wt%, 2wt%, and 5wt% MWNTs) are shown in Table 1. Specimens with a crack length to width ratio (a/W) outside the preferred range of 0.45 – 0.55 were excluded from the data set (as per ASTM D 5045). The effect of pre-cracking method (tapping or sawing) did not significantly affect the fracture toughness of each composite (not shown); therefore, the data were combined for each MWNT – single phase bone cement composite and the effects of MWNT concentration were tested for significance. The mean fracture toughness values decreased with increasing concentration of MWNTs; however, none of the decreases were significant.

Table 6-1 Fracture Toughness of MWNT - Single Phase Bone Cement Composites

MWNT Concentration	K_{IC} (MPa$\sqrt{m}$)	P-value
0wt% (n=11)	1.34 ± 0.18	
0.5wt% (n=9)	1.28 ± 0.16	0.521
2wt% (n=14)	1.23 ± 0.22	0.232
5wt% (n=14)	1.20 ± 0.25	0.110

The crack propagation behavior of each MWNT – single phase bone cement composite was characterized by measuring the change in gage resistance. A change in resistance denoted a growth of the fatigue crack (a) by 100 microns (the known distance between ties in the gage). Crack length was measured on both sides of the specimen to validate symmetry and the results obtained from each gage were averaged. The crack length was plotted against number of cycles (Figure 6.2) and the secant method was used to calculate the fatigue crack growth rate (da/dN). [174] The stress intensity factor (ΔK) associated with each growth rate was calculated using Equation 2. The combined data for each sample were combined and the crack propagation rate (da/dN) was plotted against the stress intensity factor (ΔK). (Figure 6.3) The Paris Law regression was applied to each sample. The material constants, C and m, were recorded and are presented in Table 6.2 along with the correlation coefficient of each sample. The slope of the regression line (m) for the 2wt% MWNT – single phase bone cement sample was 187% greater than that for the control (0wt% MWNT – single phase bone cement). Alternatively, the intercept of the regression (C) for 2wt% MWNT – single phase bone cement was nearly an order of magnitude less than the control. The 0wt% and 2wt% MWNT – single phase bone cement samples were reasonably represented by the Paris Law regression.

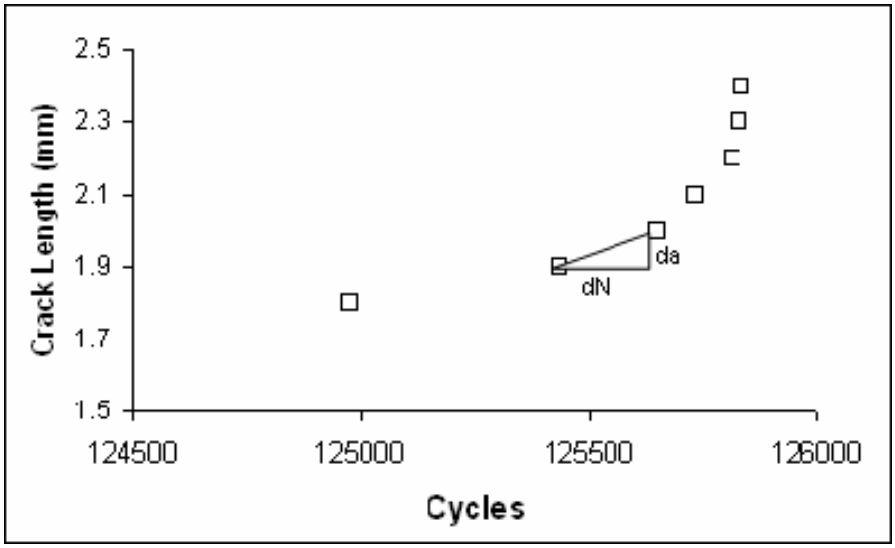

Figure 6.2 Secant Method for Measuring Growth Rate

The rate of crack growth (da/dN) for a given increment is calculated as the change in crack length per change in cycle number. The average of the two crack lengths (a_{ave}) is used to calculate the corresponding ΔK.

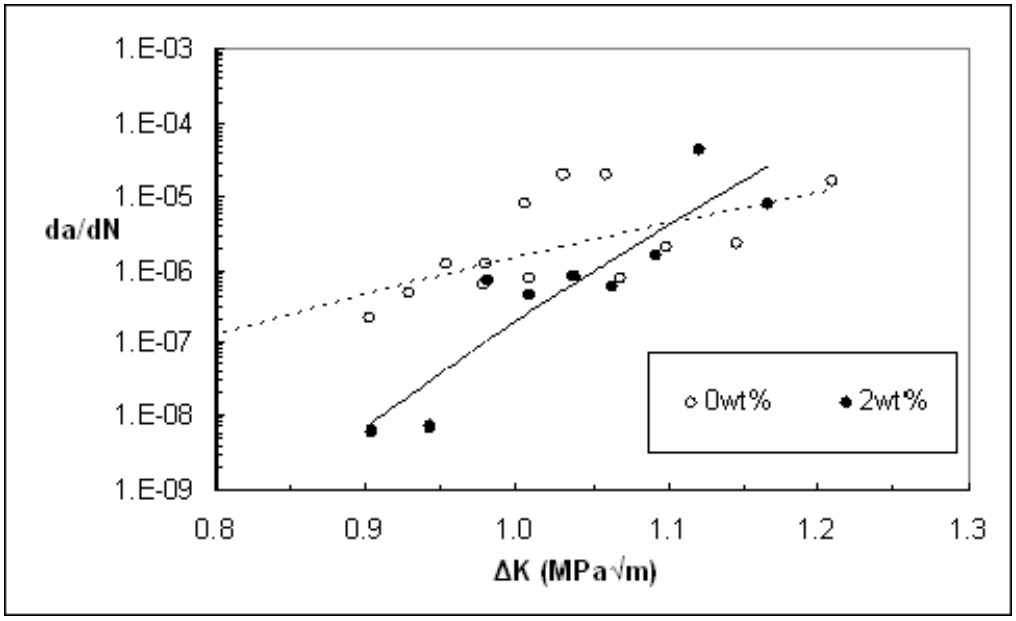

Figure 6.3 Fatigue Crack Propagation

The fatigue crack propagation behavior of unreinforced (0wt%) and reinforced (2wt%) single phase bone cement. The Paris Law regression is applied to each sample.

Table 6-2 Paris Law Parameters

	C	m
0wt% MWNT	1.0E-06	11.02
2wt% MWNT	2.0E-07	31.62

6.4 Discussion

The results reported in Table 6.1 reveal that MWNTs have little effect on the fracture toughness of single phase bone cement. This is probably due to the ineffective stress transfer between the matrix and the MWNTs. At high values of K, the elevated local stress near the crack tip likely exceeds the strength of the interfacial bonding between the two phases. Thus, the MWNTs ineffectively shield the matrix from damage accumulation. As the crack lengthens and the stress intensity factor increases, the probability of interfacial failure is heightened; thus, the reinforcing capabilities of MWNTs are diminished and the fracture toughness is not increased. In addition to interfacial failure, the prevalence of small MWNT agglomerations also contributes to the lack of improvement and may account for the decreasing trend (though not statistically significant). Agglomerations result from less than ideal dis-aggregation of MWNT clumps. (Figure 6.4) Since agglomerates provide little reinforcement, they behave as sites of stress concentration and may accelerate crack growth at high stress intensity factors. Thus, the mechanical performance of MWNT composites containing agglomerations is the net sum of the positive reinforcing effects of well dispersed MWNTs and the negative effects of poorly dis-aggregated MWNTs. Elevated stress intensities likely magnify the negative effects of agglomerates; thus, agglomerates serve to accelerate fracture rather than resist it.

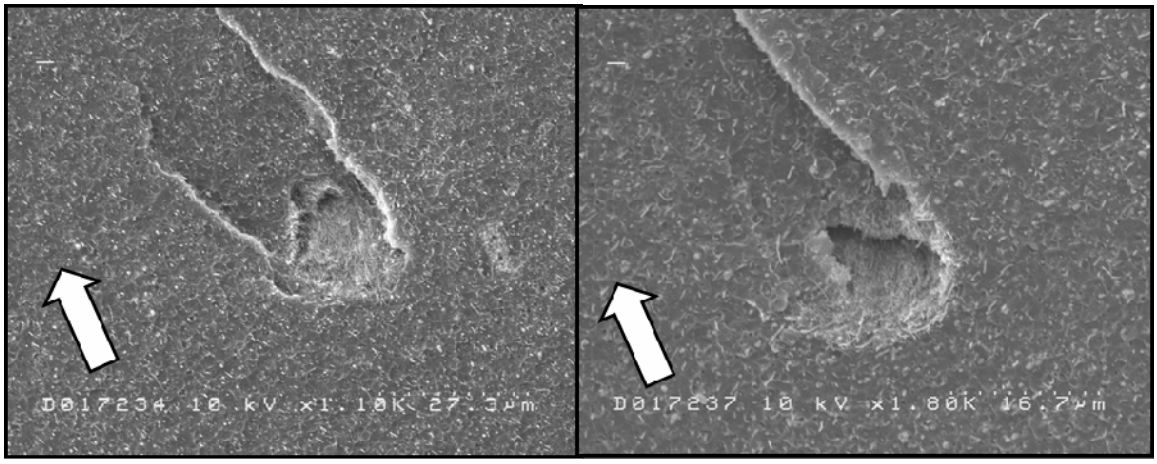

Figure 6.4 MWNT Agglomerations

Agglomerations of MWNTs were present in the fracture surfaces of MWNT – bone cement composites. The role of the agglomerates in the resistance to fracture is dependent on the stress intensity factor, K. The white arrows indicate the direction of crack growth.

The results from fatigue crack propagation testing echo the interdependence of MWNT reinforcement, agglomerations, and stress intensity. The combination of higher slope (m) and smaller intercept (C) for the fatigue crack propagation regression of the 2wt% MWNT sample suggests that at lower values of ΔK (< 1.1 MPa$\sqrt{m}$) the MWNTs effectively reinforce the single phase bone cement matrix. As the regression lines converge (Figure 6.3), the reinforcing effect of the MWNTs diminishes and, momentarily, the crack growth behaviors of the 0wt% and 2wt% MWNT samples are similar. As ΔK increases, the reinforced single phase bone cement exhibits higher crack growth rates than unreinforced single phase bone cement. Although this is unexpected, it is not surprising, especially considering the results from fracture toughness testing. For both materials, the probability of fracture increases as ΔK approaches K_{IC}. From Table 6.1, the fracture toughness of the reinforced (2wt% MWNT) single phase bone cement is less than that of unreinforced single phase bone cement, which possibly explains why the reinforced material experiences greater rates of crack growth for similar ΔK values. The elevated slope of the regression line for 2wt% MWNT – single phase bone cement points to the magnification of the agglomerates' effect with increasing ΔK. Agglomerates must be playing a role in the crack growth behavior of the reinforced material; otherwise, the two regression lines would converge at higher ΔK's. Disregarding the presence of agglomerates, the reinforcing effect of MWNTs likely diminishes with increasing stress

intensity; thus, the combination of reduced reinforcement and agglomerate magnification serves to accelerate crack growth.

The reinforcing effect of MWNTs is strongly dependent on the stress intensity factor as evidenced by the dramatic increases in crack growth rate over a small range of ΔK values. Following the regression line for the 2wt% MWNT sample at lower values of ΔK, it can be inferred that the MWNTs dramatically improve the resistance of single phase bone cement to crack growth when the crack size is relatively small. Well dispersed MWNTs shield the matrix from elevated stresses and prevent or slow the formation of crazes, which is a known mechanism of damage accumulation in polymers. Additionally, the MWNTs strengthen the fibrils of the craze [169] and interfacial de-bonding (Figure 6.5) provides an additional mechanism of energy dissipation. The collective effort of these mechanisms improves the resistance of single phase bone cement to crack growth. Agglomerates of MWNTs may also have a positive effect on the crack propagation behavior. Previous reports on the contradictory roles of porosity in the mechanical reinforcement of bone cement [69] can be extended to include MWNT agglomerations. Thus, at smaller ΔK values the agglomerates may blunt crack growth or force the crack path to deviate. In both instances, the rate of crack growth would be slowed. Considering the previously reported dramatic improvements in the fatigue performance of bone cement [165, 173], it is reasonable to postulate that MWNTs more effectively reinforce the initiation stage of fatigue failure than the propagation stage.

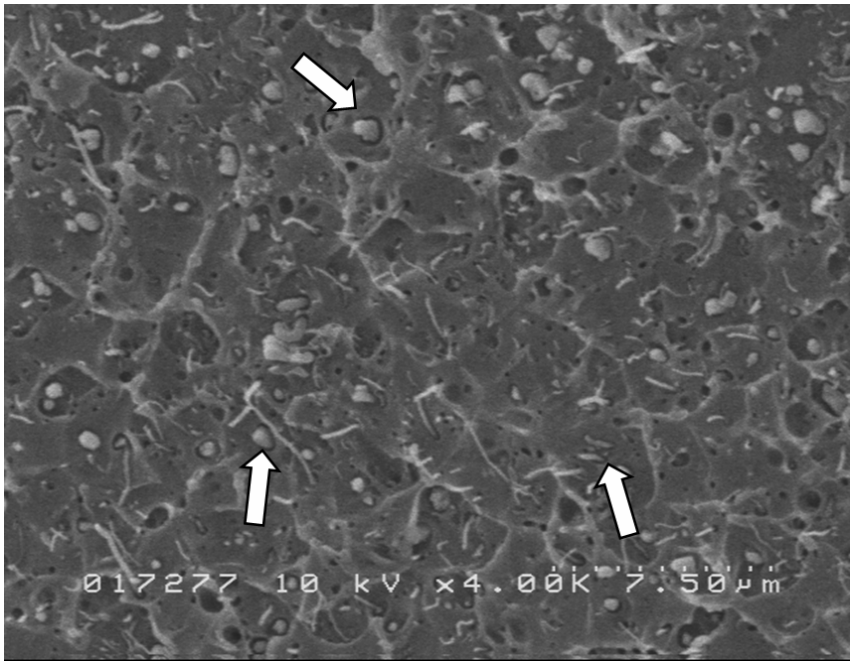

Figure 6.5 MWNT – Matrix De-Bonding

This high magnification image shows de-bonding between the radiopacifier and the matrix as well as between the MWNTs and the matrix. Nanotube – matrix de-bonding is thought to improve the resistance of single phase bone cement to crack growth by dissipating energy associated with dynamic loading. The white arrows point to sites of de-bonding.

Current evidence suggests that MWNTs positively affect the crack propagation stage when the effect of agglomerations is limited; thus, it is reasonable to speculate that reducing or eliminating MWNT agglomerations would further improve the fracture and fatigue performance of single phase bone cement. In order to fully exploit the mechanical strengths of MWNTs, dis-aggregation and dispersion technologies must be improved. The prevalence of MWNT agglomerations limits current technique of consolidation despite previously reported enhancements to the quasi-static and fatigue performance of bone cement polymer. [165, 173] Improving the dis-aggregation of MWNT clumps in the current model would require more energy; however, increasing the shear rate of the mixing process would likely damage the polymer. Increased shearing could also severely shorten the MWNTs, which would detract from their reinforcing capabilities. The method for consolidating the MWNT – bone cement composites is a limitation of this study. The shear mixing method is not clinically relevant for mixing

commercial bone cement; however, the results obtained from shear mixed materials provide a baseline understanding of the role of multiwall carbon nanotubes in the fracture and fatigue performance of a related polymer system. Additionally, failure of commercial bone cement includes some mechanisms that are not present in the current single phase bone cement model (i.e. failure at the interstitial polymer – polymer bead interface); yet, they likely share similar micro-mechanisms of damage accumulation, which can be altered by incorporating MWNTs. The current results provide valuable insight into the effects of MWNTs on the fracture toughness and fatigue crack propagation of single phase bone cement. These results especially highlight the role of agglomerations and, thus, have implications for a number of MWNT – polymer composites.

In conclusion, the addition of small amounts of multiwall carbon nanotubes affects the monotonic and dynamic fracture and fatigue crack growth behavior of single phase bone cement. Furthermore, these effects are strongly dependent on the stress intensity factor, K. Agglomerations of MWNTs also affect the mechanical performance – at high values of K, the negative effects of MWNT agglomerates are magnified. Future work should consider more clinically relevant methods of consolidation that maximize the dis-aggregation of MWNT clumps.

Unequivocally, multiwall carbon nanotubes enhance the mechanical performance of single phase bone cement. This is significant because the clinical performance of bone cement is limited by less than ideal fatigue and fracture properties, which often lead to premature clinical failure and elevated healthcare expenditures. One proposed solution to this quandary involves reinforcing bone cement with high strength fibers and particles. Current reports on such composites are promising, but room for improvement still exists. The limitations of reinforced bone cements include fiber ductility, fiber – matrix de-bonding, and mismatch between fiber size and the scale of fatigue related damage. For these reasons, multiwall carbon nanotubes are excellent candidates for improving the performance of bone cement.

7.1 Mechanisms of Reinforcement

Success of MWNT – reinforced composites depends on the transfer of stress from the weaker matrix to the stiffer, stronger MWNTs. Stress transfer is promoted by strong interfacial bonding between the two phases and it enables the composite to withstand higher loads without deforming plastically. The shielding effect of MWNTs is especially magnified at stresses that are well below the interfacial strength of the MWNT – matrix bond. The MWNTs are able to absorb the strain energy from loading (monotonic or dynamic) without leaving the composite's elastic regime. Eventually, increased loading causes the composite to fail. In the ideal case, fracture of the composite would entail failure through nanotubes (i.e. telescopic fracture) rather than MWNT de-bonding and pull-out. This type of failure suggests that the interfacial strength of the MWNT – matrix bond is superior to the strength of the nanotube. Alternatively, MWNTs that pull out of the matrix might suggest that the interfacial bond is weak and, thus, stress transfer is poor; however, this is not necessarily true. De-bonding and pull-out are evident in the scanning electron micrographs of failed composites that exhibited enhanced quasi-static and fatigue performance. (Figures 4.5, 5.4, and 6.5) In most cases, the strain energy associated with loading exceeds the strength of resisting crack formation/propagation along the MWNT – matrix interface; thus, de-bonding is not truly reflective of the reinforcing capabilities of MWNTs. In fact, de-bonding is a valid energy dissipating mechanism that in itself resists crack growth and fracture. The shielding effect of MWNTs extends the elastic limit of the matrix, thus, increasing the yield

strength of the composite and, most likely, contributing to the modest increases in quasi-static properties and dramatic enhancements to fatigue performance. In monotonic loading, the yield stress of the composite is guaranteed to be surpassed, but extending the elastic limit enables the composite to withstand greater loads prior to plastic deformation and failure. Alternatively, the stress amplitudes associated with dynamic testing are well below the yield strength of the polymer; thus, increasing the elastic limit increases the time taken to plastically deform the composite through crack growth or cyclic deformation.

7.1.1 Crack initiation

Recall that fatigue failure of bone cement is divided into three stages: 1) crack initiation, 2) crack propagation, and 3) fast fracture. It is reasonable to assume that multiwall carbon nanotubes alter the mechanisms of damage accumulation during each stage (although the likelihood of MWNT reinforcement during fast fracture is far less than the other two stages). During sub-critical (elastic) monotonic loading, little to no plastic deformation forms; however, stress begins to concentrate at local points of weakness within the composite (pores, voids, etc). The presence of MWNTs counteracts localized stress elevation by shielding the matrix. This enables the reinforced single phase bone cement to withstand higher loadings before damage begins to accumulate. The stress associated with monotonic loading continually rises and localizes at weak points within the matrix. Irreversible damage in the matrix signifies the early stages of fracture. Similarly, the shielding effects of MWNTs delay the initiation of fatigue cracks during dynamic loading. Dynamic testing is typically performed at stress amplitudes well below the yield and ultimate strengths of the material; therefore, the MWNTs are able to effectively absorb the strain energy of the test without plastically deforming the matrix. Additionally, MWNT reinforcement gains effectiveness as the stress amplitude decreases. (Table 5-1, Table 5-2, Table 5-3) Over time and loading cycles, the matrix plastically deforms via the collective effort of stress concentration and local heating. Accumulation of plastic damage, albeit on a small scale, leads to the initiation of a fatigue crack. This signals entrance into the crack propagation stage of fatigue failure.

7.1.2 Plastic deformation and crack propagation

Although there are some similarities between the reinforcing mechanisms of crack initiation and propagation, the role of MWNTs in resisting crack growth is

expanded beyond stress shielding. Stress shielding delays the formation of crazes and micro-cracks, which retard the growth of cracks, but it is not as dominant a mechanism of reinforcement as in crack initiation. In the presence of plastic deformation, which invariably involves some form of micro-cracking, the MWNTs counteract the crack growth by bridging the micro-cracks. In such cases, the MWNTs provide resistance to separation of the micro-crack faces (which increases the stress intensity at the crack tip); thus, the MWNTs frustrate the accumulation of damage and crack propagation by shielding the crack tip. In a sense, the shielding effect of MWNTs is two-fold – the matrix is shielded ahead of the crack tip and the crack tip is shielded by the resistance to separation of the crack faces.

Even though the reinforcing mechanisms associated with dynamic loading are quite different from those of monotonic loading, they do share some similarities. Typically, a zone of energy dissipation, which usually manifests as crazing, develops around the crack front. Although crazing is present in some forms of monotonic deformation, its role is magnified in dynamic loading because the loading rates and magnitudes of the applied loads are much lower. The MWNTs slow the development of such zones by providing an alternative mechanism of energy dissipation (i.e. stress transfer from the matrix to the MWNTs). Craze formation is inevitable and it is likely that MWNTs strengthen the craze by reinforcing the fibrils and bridging the associated micro-cracks. Since the fatigue crack cannot advance until the craze breaks down (i.e. the craze strength is surpassed), the MWNTs slow the rate of crack propagation. Slowing the development of crazes and subsequent crack growth limits the stress intensity factor (ΔK); therefore, this reinforcing effect of MWNTs can be sustained for longer periods of time. This mechanism is especially prevalent at low values ΔK (Figure 6.3). In bone cements reinforced with traditional fibers, little to no craze reinforcement is achieved because the discrepancy in size between the diameters of the fibers and sub-micron crazes is too great.

With time, crazes break down and the fatigue crack grows. The resulting crack faces are rough due to fibril failure and MWNT pull-out. Recall that dynamic loading includes phases of crack separation (tensile swing) and crack closure (compressive swing). During closure, the crack faces are forced into close proximity and the rough faces may physically interact via mechanical interlocking or MWNT entanglement. The physical interaction between crack faces provides a secondary mechanism of reinforcement.

7.1.3 Stress Intensity Factor (K)

The initiation of cracks gives rise to the stress intensity factor (K), which alters the role of MWNTs in the matrix. As damage accumulates in the form of plastic deformation or crack growth, the stress intensity factor (K) increases exponentially until the fracture toughness (K_{IC}) of the material is reached. The reinforcing effect of the MWNTs is inversely proportional to the stress intensity factor, which is best explained by the localization of stress at the MWNT – matrix interface. At some stress intensity, the strain energy linked to the applied load exceeds the energy required to propagate a crack along the MWNT – matrix interface. Although energy is dissipated during de-bonding, the effect on the overall resistance to fracture is overshadowed by the continual development of the stress intensity factor during monotonic loading. Regardless of loading mode, the reinforcing effect of MWNTs seems to diminish as the stress intensity (and extent of damage accumulation) increases. This is likely caused by interfacial de-bonding due to elevated local apparent stress.

The current results strongly suggest that the positive effects of MWNTs are more dominant during crack initiation and the early stages of propagation than during the later stages of crack propagation. Increases in the quasi-static strength of single phase bone cement (Table 4.1) are shown despite non-significant decreases in fracture toughness. (Table 6.1) This suggests that, in monotonic loading, the MWNTs do more to slow or prevent the initiation and nucleation of cracks than to prevent crack growth once cracks do form. Similar postulations can be drawn for dynamic testing – large increases in fatigue performance (Figure 4.7, Table 5-1, and Table 5-2) coupled with sharp increases in crack growth rate with increasing ΔK (Figure 6.3) suggest that MWNTs more effectively reinforce single phase bone cement during initiation and propagation at low values of ΔK. The larger slope of the regression line for reinforced single phase bone cement points to 1) the diminishing effect of well dispersed MWNTs with increasing ΔK and 2) the magnification of the negative roles of agglomerates at high ΔK's. When viewed collectively, the current results point to the strong K-dependency of MWNT reinforcement.

7.1.4 MWNT Agglomerations

Agglomerations also contribute to (or detract from) the reinforcing capabilities of MWNTs. Agglomerates result from the less than ideal dis-aggregation of MWNT clumps. (Figure 6.4) Since they offer little to no reinforcing effect, agglomerates are

treated similar to pores. In both monotonic and dynamic loading, the negative effects of agglomerates magnify as the stress intensity increases. At low stress intensities, the agglomerates may reinforce the matrix by blunting crack growth or deflecting the crack path. Alternatively, the agglomerates are stress risers and accelerate crack growth at high stress intensities. Thus, the mechanical performance of the MWNT – single phase bone cement composites is the net sum of the reinforcing effects of well dispersed MWNTs and the negative effects of MWNT agglomerations. As stress intensity increases and the reinforcing effects of MWNTs diminish, the balance between positive and negative is tipped in favor of the agglomerations. The acceleration of crack growth through the agglomerates is used to explain the decreasing fracture toughness values.

7.2 Effect of Stress Amplitude

Stress intensity is the combinatorial effect of damage accumulation and applied load. Given the K-dependency of MWNT reinforcement, it is easy to presume that MWNT reinforcement is also strongly dependent on the amplitude of the applied stress. This is directly evidenced by the decreasing magnitude of increase in fatigue performance of reinforced single phase bone cement with increasing stress amplitude. (Table 5-1, Table 5-2, and Table 5-3) Recall Figure 2.3, which plots stress amplitude versus number of cycles. As the magnitude of the applied stress decreases, the material's fatigue performance shifts to the right in Region II; this is known to be dominated more by crack initiation than by crack propagation. This shift in fatigue performance is corroborated by the current results.

Given the known shielding effects of MWNTs during the initiation stage of fatigue failure, it is no surprise that their reinforcing effect is heightened at lower stress amplitudes. The MWNTs are able to absorb the mechanical energy associated with low stress cycling through stress transfer because the interfacial strength between the MWNTs and the matrix is superior to the elevated local stresses. Even after crack initiation, the stress intensity factor increases slowly and plays a minor role for the majority of the fatigue life. As the stress intensity increases, either through damage accumulation or increasing applied stress, it more directly affects the fatigue performance of the composite (i.e. the reinforcing effect of MWNTs is known to decrease at high stress intensities). Elevated stresses also expose and magnify the negative effects of MWNT agglomerations. At high stress amplitudes, agglomerates serve as sites of crack initiation, nucleation, and acceleration. The prevalence of agglomerations

increases with concentration of MWNTs; thus, the combined effect of stress amplitude and presence of agglomerations accounts for the sub-par fatigue performance of 5wt% and 10wt% MWNT – single phase bone cement composites at a stress amplitude of 35 MPa. (Table 5-3) Alternatively, agglomerates may serve to extend the period of crack propagation by altering the path of the fatigue crack or blunting crack growth at low stress intensity factors (ΔK) [69]; however, any positive effect rapidly turns negative as ΔK increases and the agglomerations accelerate crack growth.

7.3 Interstitial Crystallinity

Several works report the formation of an interstitial region of crystallinity for a variety of polymers in the presence of carbon nanotubes. [124, 154-156, 176, 177] It is unclear whether this interstitial region arises from the polymerization of the polymer at the surface of the carbon nanotube or the wrapping of polymer molecules around the nanotubes. Either way, a polymer sheath is created. Since the work reported here does not involve polymerization, it must be assumed that the polymer orientates around the MWNTs during shear mixing and subsequent cooling. This polymer sheath, which is represented in Figure 4.6, likely magnifies the reinforcing capabilities of the MWNTs by enhancing stress transfer. This interstitial region would have different material properties (most likely modulus) from the bulk given the ordering of the polymer molecules and provides a buffer between the carbon nanotubes and the bulk matrix enabling efficient stress transfer.

7.4 Dose Dependency

The effect of MWNTs on the mechanical performance of single phase bone cement is dose dependent, regardless of monotonic or dynamic loading. For nearly all tests, the optimal range appears to be 2wt% - 5wt% MWNTs. Previous reports suggest that smaller concentrations of MWNTs are optimal, but their results are likely limited by less than ideal dispersion of MWNTs in highly concentrated composites. Adding larger amounts of MWNTs (>2wt%) increases the viscosity of the mixture and frustrates the dis-aggregation and dispersion of MWNT clumps. With current methods, the prevalence of MWNT agglomerations increases with increasing concentration of MWNTs. Thus, more energetic mixing protocols are needed to properly disperse high doses of MWNTs. Aggressive mixing increases the risk of irreversibly damaging the matrix or shortening the nanotubes, which would contradict the purpose for adding MWNTs. Conversely, conservative, low energy mixing methods do not damage the matrix, but do not achieve

the level of dispersion needed for maximizing the reinforcing effects of MWNTs. Thus, the optimum range clearly shown here (2wt% - 5wt% MWNTs) may be an effect of the current mixing methods rather than a true effect of concentration.

Previous reports of matrix crystallization induced by carbon nanotubes [124, 154-156, 176, 177] offer another possible explanation for decreased performance at high concentrations of MWNTs. As the molecules of the polymer preferentially align at the surface of individual nanotubes, an interstitial region of higher ordered matrix is created. At high MWNT concentrations, these regions may be underdeveloped or may butt against each other creating local discontinuities or zones of mismatch, which may detract from the overall performance of the resulting composite; thus, the full reinforcing effect of MWNTs would not be realized at high concentrations.

7.5 Limitations

Despite the multiple positive outcomes of this report, several limitations exist that should be addressed. First and foremost, the single phase bone cement model is not clinically relevant. Although the current model is used to predict the behavior of MWNTs in the clinical system, there are several differences between clinical bone cement and single phase bone cement. The former is a two phase system that involves the polymerization of methyl methacrylate monomer around polymer beads and radiopacifiers; whereas, single phase bone cement is a combination of radiopacifier and methyl methacrylate –styrene copolymer (MMA-co-Sty). Although the two systems are markedly different, the mechanisms of reinforcement reported here should carry over and be applicable in the two phase system. Additionally, to maximize the fatigue performance of bone cement, MWNTs should be added to both phases considering recent evidence showing indiscriminate fatigue crack propagation through both phases of the two phase system. [178]

Secondly, the method of consolidation is not clinically relevant. Shear mixing is not proposed for use in the clinical setting, yet it is used here because it is the best currently available method for adequately dispersing MWNTs into a polymer matrix. Gathering insight into the reinforcing effects of MWNTs was deemed more important than mastering a clinically relevant mixing method at the start of this investigation. Rather than struggle with the large and numerous agglomerations, shear mixing is used to minimize agglomerate formation and magnify the effect of adequately dispersed MWNTs. Now that some of the basic questions regarding the mechanical performance

of MWNT – single phase bone cement are answered, future efforts can focus on dispersing MWNTs into the clinically relevant bone cement system.

7.6 Implications

The future implications for MWNT – bone cement composites are quite clear. Enhanced fatigue performance can directly lead to improved longevity of the clinical life of the implant, which will reduce the risk for premature failure, limit case numbers of revisions surgeries, and reduce healthcare expenditures. The current results also have implications for a number of structural, aerospace, and other medical applications, especially those that call for lightweight, high performance materials. To date, reports on the fatigue performance of carbon nanotube composites, other than those reported here, are limited to one other group that investigates the effect of single wall carbon nanotubes on the fatigue performance of epoxy.[133] Additionally, no known reports exist regarding the fatigue crack propagation of CNT – containing composites. Although the quasi-static strengths and fracture toughness are widely reported for a variety of matrices, few relate them to fatigue performance and fracture mechanics. Therefore, the current results might be extended to a number of alternative polymer matrices that serve many functions and applications.

7.7 Conclusions

Based on the current results, I conclude that:

I. Multiwall carbon nanotubes positively affect the flexural strength and bending modulus of single phase bone cement.
II. Multiwall carbon nanotubes enhance the fatigue performance of single phase bone cement when tested in ambient and physiologically relevant conditions.
III. The effects of multiwall carbon nanotubes on the quasi-static and fatigue properties of single phase bone cement are dose dependent with an optimal concentration of 2 – 5wt% MWNTs.
IV. The effect of multiwall carbon nanotubes on the fatigue performance of single phase bone cement is magnified as the amplitude of the applied stress decreases.
V. The reinforcing effects of MWNTs are strongly K-dependent.
VI. The effect of MWNT agglomerations on the fracture properties of bone cement magnifies with increasing stress intensity factor.

APPENDIX

A. Weibull Analysis

The results of fatigue testing were analyzed using the 3-Parameter Weibull models. Example calculations are presented. The minimum fatigue life (N_o) in Manuscript 1 was calculated through visual estimation of the vertical asymptote. Alternatively, the minimum fatigue life (N_o) in Manuscript 2 was calculated using a technique reported by Janna et al[1] This technique was not publish until after Manuscript 1 was submitted for publication.

A.1 3-Parameter Weibull Analysis with Visual Estimation of N_o

Cycles	Rank	Median Ranks P(Nf)	1/(1-Median Rank)	ln(ln(1/(1-Median Rank)))	$\ln(N_f)$
5409	1	0.0486	1.051	-2.999	8.596
6633	2	0.1181	1.134	-2.074	8.800
9388	3	0.1875	1.231	-1.572	9.147
11012	4	0.2569	1.346	-1.214	9.307
11935	5	0.3264	1.485	-0.929	9.387
14063	6	0.3958	1.655	-0.685	9.551
16368	7	0.4653	1.870	-0.468	9.703
21715	8	0.5347	2.149	-0.268	9.986
26064	9	0.6042	2.526	-0.076	10.168
27070	10	0.6736	3.064	0.113	10.206
40627	11	0.7431	3.892	0.307	10.612
46310	12	0.8125	5.333	0.515	10.743
47237	13	0.8819	8.471	0.759	10.763
52597	14	0.9514	20.571	1.107	10.870

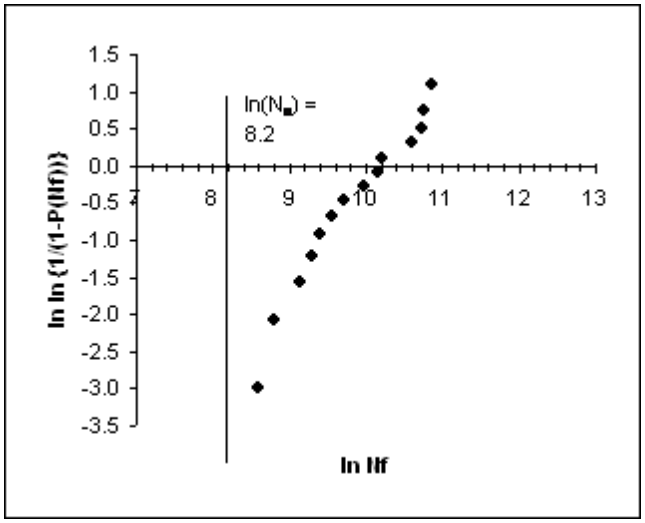

From visual estimation of the vertical asymptote

$\ln(N_o) = 8.2$

$N_o = 3641$

$\ln(N_f - N_O)$
7.478
8.004
8.656
8.905
9.023
9.252
9.451
9.802
10.018
10.062
10.518
10.661
10.683
10.799

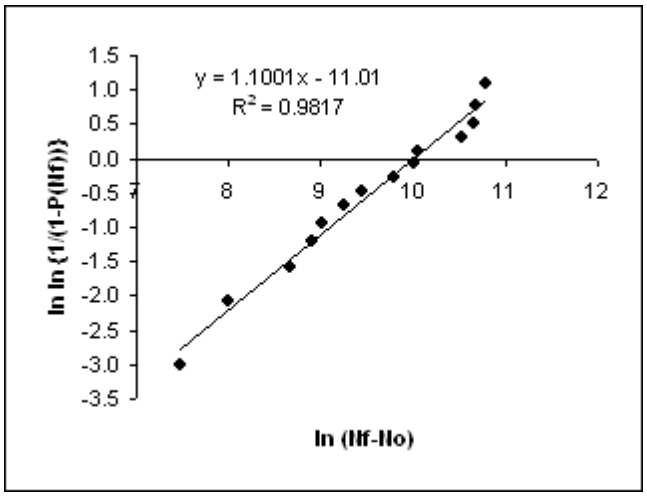

$\alpha = 1.1001$

$\beta = 22207$

$N_{WM} = 21428$

A.2 3-Parameter Weibull Analysis with Calculated N_o

Cycles	Rank	Median Ranks P(Nf)	1/(1-Median Rank)	ln(ln(1/(1-Median Rank)))	ln(Nf)
23412	1	0.0565	1.060	-2.845	10.061
45146	2	0.1371	1.159	-1.914	10.718
48461	3	0.2177	1.278	-1.404	10.789
49939	4	0.2984	1.425	-1.037	10.819
60030	5	0.3790	1.610	-0.741	11.003
70537	6	0.4597	1.851	-0.485	11.164
82379	7	0.5403	2.175	-0.252	11.319
105619	8	0.6210	2.638	-0.030	11.568
140486	9	0.7016	3.351	0.190	11.853
185728	10	0.7823	4.593	0.422	12.132
277651	11	0.8629	7.294	0.687	12.534
341564	12	0.9435	17.714	1.056	12.741

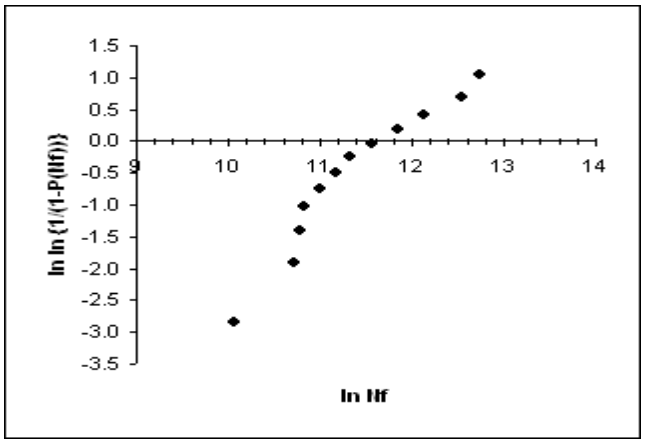

	ln(Nf - NO)
	8.639
Calculated based on	10.218
methods from Janna	10.332
	10.379
No = 17763	10.652
	10.874
	11.076
	11.383
	11.718
	12.032
	12.468
	12.688

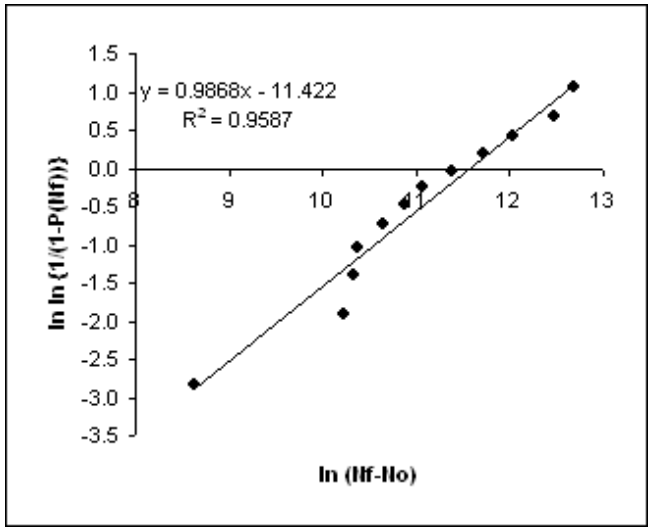

α = slope of best fit line	α = 0.9868
β = exp(C/α) + No	β = 106392
N_{WM} = No + (β - No)Γ(1+(1/α))	N_{WM} = 107001

References

[1] Baleani M, Cristofolini L, Minari C, Toni A. Fatigue strength of PMMA bone cement mixed with gentamicin and barium sulphate vs pure PMMA. Proc Inst Mech Eng [H]. 2003;217(1):9-12.

[2] Molino LN, Topoleski LD. Effect of BaSO4 on the fatigue crack propagation rate of PMMA bone cement. J Biomed Mater Res. 1996 May;31(1):131-7.

[3] Gilbert J, Hasenwinkel J, Mroczkowski M, Lautenschlager E, Wixson R. Two-Solution PMMA Bone Cement: Effect of Barium Sulfate Inclusion Size on Mechanical Properties. Society For Biomaterials 28th Annual Meeting Transactions; 2002; 2002. p. 392.

[4] Artola A, Gurruchaga M, Vazquez B, Roman JS, Goni I. Elimination of barium sulfate from acrylic bone cements. Use of two iodine-containing monomers. Biomaterials. 2003;24:4071-80.

[5] Ginebra MP, Albuixech L, Fernandez-Barragan E, Aparicio C, Gil FJ, San RJ, et al. Mechanical performance of acrylic bone cements containing different radiopacifying agents. Biomaterials. 2002 Apr;23(8):1873-82.

[6] Lewis G, Janna S, Bhattaram A. Influence of the method of blending an antibiotic powder with an acrylic bone cement powder on physical, mechanical, and thermal properties of the cured cement. Biomaterials. 2005 Jul;26(20):4317-25.

[7] van Hooy-Corstjens CSJ, Govaert LE, Spoelstra AB, Bulstra SK, Wetzels GMR, Koole LH. Mechanical behaviour of a new acrylic radiopaque iodine-containing bone cement. Biomaterials. 2004;25(13):2657.

[8] Charnley J. Anchorage of the femoral head prosthesis to the shaft of the femur. The Journal of Bone and Joint Surgery. 1960 February 1960;42B(1):28.

[9] Bauer TW, Schils J. The pathology of total joint arthroplasty. I. Mechanisms of implant fixation. Skeletal Radiol. 1999 Aug;28(8):423-32.

[10] Lewis G. Properties of acrylic bone cement: state of the art review. J Biomed Mater Res. 1997 Summer;38(2):155-82.

[11] Bauer TW, Schils J. The pathology of total joint arthroplasty II. Mechanisms of implant failure. Skeletal Radiology. 1999;28(9):483.

[12] Mohler CG, Callaghan JJ, Collis DK, Johnston RC. Early loosening of the femoral component at the cement-prosthesis interface after total hip replacement. J Bone Joint Surg Am. 1995 September 1, 1995;77(9):1315-22.

[13] Berry DJ, Harmsen WS, Ilstrup DM. The Natural History of Debonding of the Femoral Component from the Cement and Its Effect on Long-Term Survival of Charnley Total Hip Replacements. J Bone Joint Surg Am. 1998 May 1, 1998;80(5):715-21.

[14] Kurtz S, Mowat F, Ong K, Chan N, Lau E, Halpern M. Prevalence of Primary and Revision Total Hip and Knee Arthroplasty in the United States From 1990 Through 2002. J Bone Joint Surg Am. 2005 July 1, 2005;87(7):1487-97.

[15] Bauer GS, Murthi AM, Bigliani LU. Fixation for the millennium: The shoulder. The Journal of Arthroplasty. 2002;17(4, Supplement 1):9.

[16] Kozak TKW, Adams RA, Morrey BF. Total elbow arthroplasty in primary osteoarthritis of the elbow. The Journal of Arthroplasty. 1998;13(7):837.

[17] Dorr LD, Kane TJ, 3rd, Conaty JP. Long-term results of cemented total hip arthroplasty in patients 45 years old or younger. A 16-year follow-up study. J Arthroplasty. 1994 Oct;9(5):453-6.

[18] Schurman D, Bloch D, Segal M, Tanner C. Conventional Cemented Total Hip Arthroplasty. Clinical Orthopaedics and Related Research. 1989 March 1989;240:173-9.
[19] AAOS. Orthopaedic Patients and Conditions. 2006 June 23, 2006 [cited; Available from: http://www.aaos.org/wordhtml/research/stats/patientstats.htm
[20] Burns A, Bourne R, Chesworth B, MacDonald S, Rorabeck C. Cost Effectiveness of Revision Total Knee Arthroplasty. Clinical Orthopaedics and Related Research. 2006;446:29-33.
[21] Phillips FM. Minimally Invasive Treatments of Osteoporotic Vertebral Compression Fractures. Spine. 2003;28(15S):S45-S53.
[22] Hadjipavlou AG, Tzermiadianos MN, Katonis PG, Szpalski M. Percutaneous vertebroplasty and balloon kyphoplasty for the treatment of osteoporotic vertebral compression fractures and osteolytic tumours. J Bone Joint Surg Br. 2005 December 1, 2005;87-B(12):1595-604.
[23] Lewis G. Injectable bone cements for use in vertebroplasty and kyphoplasty: State-of-the-art review. Journal of Biomedical Materials Research Part B: Applied Biomaterials. 2006;76B(2):456-68.
[24] Mathis JM, Barr JD, Belkoff SM, Barr MS, Jensen ME, Deramond H. Percutaneous Vertebroplasty: A Developing Standard of Care for Vertebral Compression Fractures. AJNR Am J Neuroradiol. 2001 February 1, 2001;22(2):373-81.
[25] Kurtz SM, Villarraga ML, Zhao K, Edidin AA. Static and fatigue mechanical behavior of bone cement with elevated barium sulfate content for treatment of vertebral compression fractures. Biomaterials. 2005;26(17):3699.
[26] FDA. 510(k) Database. 2006.
[27] Lieberman I, Reinhardt M. Vertebroplasty and kyphoplasty for osteolytic vertebral collapse. Clinical Orthopaedics and Related Research. 2003;415 Supplement:S176-86.
[28] Darbar UR, Huggett R, Harrison A. Denture fracture--a survey. Br Dent J. 1994 May 7;176(9):342-5.
[29] Standard Specification for Acrylic Bone Cement. West Conshocken, PA: ASTM International; 1999. Report No.: ASTM F451-99ae1.
[30] Kuehn K-D, Ege W, Gopp U. Acrylic bone cements: mechanical and physical properties. Orthopedic Clinics of North America. 2005;36:29-39.
[31] Lewis G, Nyman JS, Trieu HH. Effect of mixing method on selected properties of acrylic bone cement. J Biomed Mater Res. 1997 Fall;38(3):221-8.
[32] Lidgren L, Drar H, Moller J. Strength of polymethylmethacrylate increased by vacuum mixing. Acta Orthop Scand. 1984;55(5):536-41.
[33] Wixson RL, Lautenschlager EP, Novak MA. Vacuum mixing of acrylic bone cement. Journal of Arthroplasty. 1987;2(2):141-9.
[34] Lewis G, Mladsi S. Effect of sterilization method on properties of Palacos R acrylic bone cement. Biomaterials. 1998 Jan-Feb;19(1-3):117-24.
[35] Harper EJ, Braden M, Bonfield W, Dingeldein E, Wahlig H. Influence of sterilization upon a range of properties of experimental bone cements. Journal of Materials Science: Materials in Medicine. 1997;8(12):849.
[36] Pourdeyhimi B, Wagner HD. Elastic and ultimate properties of acrylic bone cement reinforced with ultra-high-molecular-weight polyethylene fibers. J Biomed Mater Res. 1989 Jan;23(1):63-80.
[37] Yang JM, Huang PY, Yang MC, Lo SK. Effect of MMA-g-UHMWPE grafted fiber on mechanical properties of acrylic bone cement. J Biomed Mater Res. 1997 Winter;38(4):361-9.

[38] Saha S, Pal S. Mechanical characterization of commercially made carbon-fiber-reinforced polymethylmethacrylate. J Biomed Mater Res. 1986 Jul-Aug;20(6):817-26.
[39] Gilbert JL, Ney DS, Lautenschlager EP. Self-reinforced composite poly(methyl methacrylate): static and fatigue properties. Biomaterials. 1995 Sep;16(14):1043-55.
[40] Wright DD, Lautenschlager EP, Gilbert JL. Bending and fracture toughness of woven self-reinforced composite poly(methyl methacrylate). J Biomed Mater Res. 1997 Sep 15;36(4):441-53.
[41] Vallittu PK. A review of fiber-reinforced denture base resins. J Prosthodont. 1996 Dec;5(4):270-6.
[42] Polyzois GL, Andreopoulos AG, Lagouvardos PE. Acrylic resin denture repair with adhesive resin and metal wires: effects on strength parameters. J Prosthet Dent. 1996 Apr;75(4):381-7.
[43] Grosland N, Kim JK, Park JB. Reinforcement of bone cement around prostheses by pre-coated wire coil: a finite element model study. Biomed Mater Eng. 1995;5(1):29-36.
[44] Bowman AJ, Manley TR. The elimination of breakages in upper dentures by reinforcement with carbon fibre. Br Dent J. 1984 Feb 11;156(3):87-9.
[45] Manley TR, Bowman AJ, Cook M. Denture bases reinforced with carbon fibres. Br Dent J. 1979 Jan 2;146(1):25.
[46] Stipho HD. Effect of glass fiber reinforcement on some mechanical properties of autopolymerizing polymethyl methacrylate. J Prosthet Dent. 1998 May;79(5):580-4.
[47] Polyzois GL, Tarantili PA, Frangou MJ, Andreopoulos AG. Fracture force, deflection at fracture, and toughness of repaired denture resin subjected to microwave polymerization or reinforced with wire or glass fiber. J Prosthet Dent. 2001 Dec;86(6):613-9.
[48] Vallo CI. Influence of filler content on static properties of glass-reinforced bone cement. J Biomed Mater Res. 2000;53(6):717-27.
[49] Lewis G, Nyman JS. Toward standardization of methods of determination of fracture properties of acrylic bone cement and statistical analysis of test results. J Biomed Mater Res. 2000;53(6):748-68.
[50] Nguyen NC, Maloney WJ, Dauskardt RH. Reliability of PMMA bone cement fixation: fracture and fatigue crack-growth behaviour. J Mater Sci Mater Med. 1997 Aug;8(8):473-83.
[51] Vila MM, Ginebra MP, Gil FJ, Planell JA. Effect of porosity and environment on the mechanical behavior of acrylic bone cement modified with acrylonitrile-butadiene-styrene particles: I. Fracture toughness. Journal of Biomedical Materials Research. 1999;48(2):121-7.
[52] Graham J, Pruitt L, Ries M, Gundiah N. Fracture and fatigue properties of acrylic bone cement. The Journal of Arthroplasty. 2000;15(8):1028.
[53] Lewis G. Relative influence of composition and viscosity of acrylic bone cement on its apparent fracture toughness. Bio-Medical Materials and Engineering. 2000;10(1):1-11.
[54] Topoleski LD, Ducheyne P, Cuckler JM. A fractographic analysis of in vivo poly(methyl methacrylate) bone cement failure mechanisms. J Biomed Mater Res. 1990 Feb;24(2):135-54.
[55] Deb S, Lewis G, Janna SW, Vazquez B, San Roman J. Fatigue and fracture toughness of acrylic bone cements modified with long-chain amine activators. J Biomed Mater Res A. 2003 Nov 1;67(2):571-7.

[56] Lewis G. Apparent fracture toughness of acrylic bone cement: effect of test specimen configuration and sterilization method. Biomaterials. 1999;20(1):69.
[57] Ries MD, Young E, Al-Marashi L, Goldstein P, Hetherington A, Petrie T, et al. In vivo behavior of acrylic bone cement in total hip arthroplasty. Biomaterials. 2006 Jan;27(2):256-61.
[58] Pourdeyhimi B, Robinson HHt, Schwartz P, Wagner HD. Fracture toughness of Kevlar 29/poly(methyl methacrylate) composite materials for surgical implantations. Ann Biomed Eng. 1986;14(3):277-94.
[59] Pourdeyhimi B, Wagner H, Schwartz P. A comparison of mechanical properties of discontinuous Kevlar 29 fibre reinforced bone and dental cements. Journal of Materials Science. 1986;21:4468-74.
[60] Ramos V, Jr., Runyan DA, Christensen LC. The effect of plasma-treated polyethylene fiber on the fracture strength of polymethyl methacrylate. J Prosthet Dent. 1996 Jul;76(1):94-6.
[61] Samadzadeh A, Kugel G, Hurley E, Aboushala A. Fracture strengths of provisional restorations reinforced with plasma-treated woven polyethylene fiber. J Prosthet Dent. 1997 Nov;78(5):447-50.
[62] Kotha SP, Li C, Schmid SR, Mason JJ. Fracture toughness of steel-fiber-reinforced bone cement. J Biomed Mater Res A. 2004 Sep 1;70(3):514-21.
[63] Topoleski LD, Ducheyne P, Cuckler JM. Flow intrusion characteristics and fracture properties of titanium-fibre-reinforced bone cement. Biomaterials. 1998 Sep;19(17):1569-77.
[64] Topoleski LD, Ducheyne P, Cuckler JM. Microstructural pathway of fracture in poly(methyl methacrylate) bone cement. Biomaterials. 1993 Dec;14(15):1165-72.
[65] Jeffers JR, Browne M, Taylor M. Damage accumulation, fatigue and creep behaviour of vacuum mixed bone cement. Biomaterials. 2005 Sep;26(27):5532-41.
[66] Manero J, Ginebra M, Gil F, Planell J, Delgado J, Morejon L, et al. Propagation of fatigue cracks in acrylic bone cements containing different radiopaque agents. Proc Inst Mech Eng [H]. 2004;218(3):167-72.
[67] Vila MM, Ginebra MP, Gil FJ, Planell JA. Effect of porosity and environment on the mechanical behavior of acrylic bone cement modified with acrylonitrile-butadiene-styrene particles: Part II. Fatigue crack propagation. Journal of Biomedical Materials Research. 1999;48(2):128-34.
[68] Jeffers JR, Browne M, Roques A, Taylor M. On the importance of considering porosity when simulating the fatigue of bone cement. J Biomech Eng. 2005 Aug;127(4):563-70.
[69] Janssen D, Aquarius R, Stolk J, Verdonschot N. The contradictory effects of pores on fatigue cracking of bone cement. Journal of Biomedical Materials Research Part B: Applied Biomaterials. 2005;74B(2):747-53.
[70] Ishihara S, McEvily AJ, Goshima T, Kanekasu K, Nara T. On fatigue lifetimes and fatigue crack growth behavior of bone cement. Journal of Materials Science: Materials in Medicine. 2000;11(10):661.
[71] Lewis G. Fatigue testing and performance of acrylic bone-cement materials: state-of-the-art review. J Biomed Mater Res B Appl Biomater. 2003 Jul 15;66(1):457-86.
[72] Suresh S. Fatigue of Materials. 2nd ed. Cambridge: Cambridge University Press 1998.
[73] Lewis G. Effect of mixing method and storage temperature of cement constituents on the fatigue and porosity of acrylic bone cement. J Biomed Mater Res. 1999;48(2):143-9.

[74] Lewis G. Relative roles of cement molecular weight and mixing method on the fatigue performance of acrylic bone cement: Simplex P versus Osteopal. J Biomed Mater Res. 2000;53(1):119-30.
[75] Lewis G, Janna S. Effect of test specimen cross-sectional shape on the in vitro fatigue life of acrylic bone cement. Biomaterials. 2003 Oct;24(23):4315-21.
[76] Lewis G. Effect of two variables on the fatigue performance of acrylic bone cement: mixing method and viscosity. Biomed Mater Eng. 1999;9(4):197-207.
[77] Murphy B, Prendergast P. On the magnitude and variability of the fatigue strength of acrylic bone cement. International Journal of Fatigue. 2002;22:855-64.
[78] Murphy BP, Prendergast PJ. The relationship between stress, porosity, and nonlinear damage accumulation in acrylic bone cement. J Biomed Mater Res. 2002 Mar 15;59(4):646-54.
[79] Gilbert JL, Hasenwinkel JM, Wixson RL, Lautenschlager EP. A theoretical and experimental analysis of polymerization shrinkage of bone cement: A potential major source of porosity. J Biomed Mater Res. 2000 Oct;52(1):210-8.
[80] Topoleski LD, Ducheyne P, Cuckler JM. The effects of centrifugation and titanium fiber reinforcement on fatigue failure mechanisms in poly(methyl methacrylate) bone cement. J Biomed Mater Res. 1995 Mar;29(3):299-307.
[81] Kim HY, Yasuda HK. Improvement of fatigue properties of poly(methyl methacrylate) bone cement by means of plasma surface treatment of fillers. J Biomed Mater Res. 1999;48(2):135-42.
[82] Scheirs J. Compositional and Failure Analysis of Polymers: A Practical Approach. Chichester: John Wiley & Sons, Ltd 2000.
[83] Beardmore P, Rabinowitz S. Fatigue Deformation of Polymers. In: Arsenault R, ed. *Treatise on Materials Science and Technology: Plastic Deformation of Materials*. New York: Academic Press 1975:267-332.
[84] Schultz J. Fatigue Behavior of Engineering Polymers. In: Schultz J, ed. *Treatise on Materials Science and Technology: Properties of Solid Polymeric Materials Part B* New York: Academic Press 1977:599-636.
[85] Paris P, Erdogan F. A critical analysis of crack propagation laws. Journal of Basic Engineering, Transactions of the American Society fo Mechanical Engineers. 1963:528-34.
[86] Kausch H. Polymer Fracture. 2nd ed. Berlin: Springer-Verlag 1987.
[87] Rabinowitz S, Beardmore P. Cyclic deformation and fracture of polymers. Journal of Materials Science. 1974;9:81-99.
[88] Michler G. Crazing in Amorphous Polymers - Formation of Fibrillated Crazes Near the Glass Transition Temperature. In: Grellman W, Seider S, eds. *Deformation and Fracture Behaviour of Polymers*. Berlin: Springer 2001:193-208.
[89] Drexler KE. Engines of Creation: The Coming Era of Nanotechnology. New York: Anchor Books 1986.
[90] Kroto H, Heath J, Obrien S, Curl R, Smalley R. C-60 - Buckminsterfullerene. Nature. 1985;318:162-3.
[91] Saito R, Dresselhaus G, Dresselhaus M. Physical Properties of Carbon Nanotubes. London: Imperial College Press 1998.
[92] Dresselhaus M, Dresselhaus G, Saito R. Carbon fibers based on C60 and their symmetry. Physical Review B. 1992 15 March 1992;45(11):6234-42.
[93] Iijima S. Helical microtubules fo graphitic carbon. Nature. 1991 7 November 1991;354:56-8.
[94] Kiang CH, Endo M, Ajayan PM, Dresselhaus G, Dresselhaus MS. Size Effects in Carbon Nanotubes. Physical Review Letters. 1998;81(9):1869.

[95] Cumings J, Zettl A. Low-friction nanoscale linear bearing realized from multiwall carbon nanotubes. Science. 2000 Jul 28;289(5479):602-4.
[96] Sinnott SB, Andrews R. Carbon Nanotubes: Synthesis, Properties, and Applications. Critical Reviews in Solid State and Materials Science. 2001;26(3):145-249.
[97] Thess A, Lee R, Nikolaev P, Dai H, Petit P, Robert J, et al. Crystalline Ropes of Metallic Carbon Nanotubes. 1996:483-7.
[98] Journet C, Maser WK, Bernier P, Loiseau A, de la Chapelle ML, Lefrant S, et al. Large-scale production of single-walled carbon nanotubes by the electric-arc technique. Nature. 1997;388(6644):756-8.
[99] Andrews R, Jacques D, Qian D, Rantell T. Multiwall carbon nanotubes: synthesis and application. Accounts of Chemistry Research. 2002 Dec;35(12):1008-17.
[100] Andrews R, Jacques D, Rao A, Derbyshire F, Qian D, Fan X, et al. Continuous production of carbon nanotubes: a step closer to commercial realization. Chem Phys Letters. 1999;303:467-74.
[101] Qian D, Andrews R, Jacques D, Kichambare P, Lian G, Dickey EC. Low-temperature synthesis of large-area CNx nanotube arrays. J Nanosci Nanotechnol. 2003 Feb-Apr;3(1-2):93-7.
[102] Falvo MR, Clary GJ, Taylor RM, 2nd, Chi V, Brooks FP, Jr., Washburn S, et al. Bending and buckling of carbon nanotubes under large strain. Nature. 1997 Oct 9;389(6651):582-4.
[103] Salvetat J-P, Briggs GAD, Bonard J-M, Bacsa RR, Kulik AJ, StÃckli T, et al. Elastic and Shear Moduli of Single-Walled Carbon Nanotube Ropes. Physical Review Letters. 1999;82(5):944.
[104] Wong EW, Sheehan PE, Liebart CM. Nanobeam Mechanics: Elasticity, Strength, and Toughness of Nanorods and Nanotubes. Science. 1997;277:1971-5.
[105] Krishnan A, Dujardin E, Ebbesen TW, Yianilos PN, Treacy MMJ. Young's modulus of single-walled nanotubes. Physical Review B. 1998;58(20):14013.
[106] Treacy MMJ, Ebbesen TW, Gibson JM. Exceptionally high Young's modulus observed for individual carbon nanotubes. Nature. 1996;381(6584):678-80.
[107] Demczyk B, Wang Y, Cumings J, Hetman M, Han W, Zettl A, et al. Direct mechanical measurement of the tensile strength and elastic modulus of multiwalled carbon nanotubes. Materials Science & Engineering. 2002 Sept 1;A334(1-2):173-8.
[108] Yu M-F, Lourie O, Dyer MJ, Moloni K, Kelly TF, Ruoff RS. Strength and Breaking Mechanism of Multiwalled Carbon Nanotubes Under Tensile Load. 2000:637-40.
[109] Nardelli MB, Yakobson BI, Bernholc J. Brittle and Ductile Behavior in Carbon Nanotubes. Physical Review Letters. 1998;81(21):4656.
[110] Che J, Cagin T, III WAG. Thermal conductivity of carbon nanotubes. Nanotechnology. 2000;11:65-9.
[111] Hone J, Whitney M, Piskoti C, Zettl A. Thermal conductivity of single-walled carbon nanotubes. Physical Review B. 1999;59(4):R2514.
[112] Ruoff R, Lorents D. Mechanical and Thermal Properties of Carbon Nanotubes. Carbon. 1995;33(7):925-30.
[113] Yang DJ, Wang SG, Zhang Q, Sellin PJ, Chen G. Thermal and electrical transport in multi-walled carbon nanotubes. Physics Letters A. 2004;329(3):207-13.
[114] Kasumov AY, Deblock R, Kociak M, Reulet B, Bouchiat H, Khodos II, et al. Supercurrents Through Single-Walled Carbon Nanotubes. 1999:1508-11.
[115] Baughman RH, Zakhidov AA, de Heer WA. Carbon nanotubes--the route toward applications. Science. 2002 Aug 2;297(5582):787-92.

[116] Mallick PK. Fiber Reinforced Composites. New York: Marcel Dekker 1993.
[117] Wagner H. Nanotube-polymer adhesion: a mechanics approach. Chemical Physics Letters. 2002 24 July 2002;361:57-61.
[118] Barber AH, Cohen SR, Wagner HD. Measurement of carbon nanotube-polymer interfacial strength. Applied Physics Letters. 2003;82(23):4140-2.
[119] Andrews R, Weisenberger MC. Carbon nanotube polymer composites. Current Opinion in Solid State and Materials Science. 2004;8(1):31.
[120] Thostenson ET, Ren Z, Chou T-W. Advances in the science and technology of carbon nanotubes and their composites: a review. Composites Science and Technology. 2001;61(13):1899.
[121] Moore EM, Ortiz DL, Marla VT, Shambaugh RL, Grady BP. Enhancing the strength of polypropylene fibers with carbon nanotubes. 2004:2926-33.
[122] Kearns JC, Shambaugh RL. Polypropylene fibers reinforced with carbon nanotubes. 2002:2079-84.
[123] Haggenmueller R, Gommans HH, Rinzler AG, Fischer JE, Winey KI. Aligned single-wall carbon nanotubes in composites by melt processing methods. Chemical Physics Letters. 2000;330(3-4):219.
[124] Coleman JN, Cadek M, Blake R, Nicolosi V, Ryan KP, Belton C, et al. High-Performance Nanotube-Reinforced Plastics: Understanding the Mechanism of Strength Increase. Advanced Functional Materials. 2004;14(8):791-8.
[125] Chen W, Tao X, Xue P, Cheng X. Enhanced mechanical properties and morphological characterizations of poly(vinyl alcohol)-carbon nanotube composite films. Applied Surface Science. 2005;252(5):1404-9.
[126] Marrs B, Andrews R, Rantell T, Pienkowski D. Flexural Properties of Polymethylmethacrylate Augmented with Multiwalled Carbon Nanotubes. Orthopaedic Research Society; New Orleans, LA; 2003. p. 1461.
[127] Pienkowski D, Andrews R, Goltz M, Rantell T. Carbon Nanotubes Enhance the Mechanical Properties of Bone Cement. 28th Annual Meeting of the Society for Biomaterials; 2002; Tampa, FL; 2002.
[128] Cooper CA, Ravich D, Lips D, Mayer J, Wagner HD. Distribution and alignment of carbon nanotubes and nanofibrils in a polymer matrix. Composites Science and Technology. 2002;62(7-8):1105.
[129] Dalton AB, Collins S, Razal J, Munoz E, Ebron VH, Kim BG, et al. Continuous carbon nanotube composite fibers: properties, potential applications, and problems. Journal of Materials Chemistry. 2004;14(1-3).
[130] Thostenson ET, Chou T-W. Aligned multi-walled carbon nanotube-reinforce composites: processing and mechanical characterization. Journal of Physics D: Applied Physics. 2002;35:L77-L80.
[131] Andrews R, Jacques D, Rao AM, Rantell T, Derbyshire F, Chen Y, et al. Nanotube composite carbon fibers. Applied Physics Letters. 1999;75(9):1329.
[132] Jin Z, Pramoda KP, Xu G, Goh SH. Dynamic mechanical behavior of melt-processed multi-walled carbon nanotube/poly(methyl methacrylate) composites. Chemical Physics Letters. 2001;337(1-3):43.
[133] Ren Y, Li F, Cheng H-M, Liao K. Tension-tension fatigue behavior of unidirectional single-walled carbon nanotube reinforced epoxy composite. Carbon. 2003;41:2177-9.
[134] Diamond TH, Champion B, Clark WA. Management of acute osteoporotic vertebral fractures: a nonrandomized trial comparing percutaneous vertebroplasty with conservative therapy. Am J Med. 2003 Mar;114(4):257-65.
[135] San Millan Ruiz D, Burkhardt K, Jean B, Muster M, Martin JB, Bouvier J, et al. Pathology findings with acrylic implants. Bone. 1999 Aug;25(2 Suppl):85S-90S.

[136] Praemer A, Furner S, Rice D. Musculoskeletal Conditions in the United States. Rosemont: American Academy of Orthopaedic Surgeons 1999.
[137] Vallittu PK. Dimensional accuracy and stability of polymethyl methacrylate reinforced with metal wire or with continuous glass fiber. J Prosthet Dent. 1996 Jun;75(6):617-21.
[138] Uzun G, Hersek N, Tincer T. Effect of five woven fiber reinforcements on the impact and transverse strength of a denture base resin. J Prosthet Dent. 1999 May;81(5):616-20.
[139] Wang Z, Mo S, Li Y, Zhang Q, Song Z. Mechanical property analysis of polyethylene fiber reinforced polymethyl methacrylate. Hua Xi Kou Qiang Yi Xue Za Zhi. 2004;22:62-4.
[140] Saha S, Kraay MJ. Bending properties of wire-reinforced bone cement for applications in spinal fixation. J Biomed Mater Res. 1979 May;13(3):443-57.
[141] Topoleski LD, Ducheyne P, Cuckler JM. The fracture toughness of titanium-fiber-reinforced bone cement. J Biomed Mater Res. 1992 Dec;26(12):1599-617.
[142] Liu J, Rinzler AG, Dai H, Hafner JH, Bradley RK, Boul PJ, et al. Fullerene pipes. Science. 1998 May 22;280(5367):1253-6.
[143] Smalley R. Nanotech Growth. Research and Development. 1999;41:34-6.
[144] Burkins G. Clinton to Propose More Funding for Research. Wall Street Journal. 2000;240:B10.
[145] Qian D, Dickey EC, Andrews R, Rantell T. Load transfer and deformation mechanisms in carbon nanotube-polystyrene composites. Applied Physics Letters. 2000;76(20):2868.
[146] Andrews R, Jacques D, Minot M, Rantell T. Fabrication of Carbon Multiwall Nantube/Polymer Composites by Shear Mixing. Macromol Mater Eng. 2002;287(6):395-403.
[147] Hasenwinkel JM, Lautenschlager EP, Wixson RL, Gilbert JL. Effect of initiation chemistry on the fracture toughness, fatigue strength, and residual monomer content of a novel high-viscosity, two-solution acrylic bone cement. J Biomed Mater Res. 2002 Mar 5;59(3):411-21.
[148] Lewis G, Janna S, Carroll M. Effect of test frequency on the in vitro fatigue life of acrylic bone cement. Biomaterials. 2003 Mar;24(6):1111-7.
[149] Lewis G, Janna SI. Effect of fabrication pressure on the fatigue performance of Cemex XL acrylic bone cement. Biomaterials. 2004 Mar-Apr;25(7-8):1415-20.
[150] Lewis G, Sadhasivini A. Estimation of the minimum number of test specimens for fatigue testing of acrylic bone cement. Biomaterials. 2004 Aug;25(18):4425-32.
[151] Johnson JA, Provan JW, Krygier JJ, Chan KH, Miller J. Fatigue of acrylic bone cement--effect of frequency and environment. J Biomed Mater Res. 1989 Aug;23(8):819-31.
[152] Dunne NJ, Orr JF, Mushipe MT, Eveleigh RJ. The relationship between porosity and fatigue characteristics of bone cements. Biomaterials. 2003 Jan;24(2):239-45.
[153] Morscher EW, Wirz D. Current state of cement fixation in THR. Acta Orthop Belg. 2002 Feb;68(1):1-12.
[154] Ryan KP, Lipson SM, Drury A, Cadek M, Ruether M, O'Flaherty SM, et al. Carbon-nanotube nucleated crystallinity in a conjugated polymer based composite. Chemical Physics Letters. 2004;391(4-6):329.
[155] Cadek M, Coleman JN, Barron V, Hedicke K, Blau WJ. Morphological and mechanical properties of carbon-nanotube-reinforced semicrystalline and amorphous polymer composites. Applied Physics Letters. 2002;81(27):5123.

[156] Ding W, Eitan A, Fisher FT, Chen X, Dikin DA, Andrews R, et al. Direct Observation of Polymer Sheathing in Carbon Nanotube-Polycarbonate Composites. Nano Lett. 2003 November 12, 2003;3(11):1593-7.
[157] Kim P, Shi L, Majumdar A, McEuen PL. Thermal Transport Measurements of Individual Multiwalled Nanotubes. Physical Review Letters. 2001;87(21):215502.
[158] Homsy CA, Tullos HS, Anderson MS, Diferrante NM, King JW. Some physiological aspects of prosthesis stabilization with acrylic polymer. Clin Orthop. 1972 Mar-Apr;83:317-28.
[159] Linder L. Reaction of bone to the acute chemical trauma of bone cement. J Bone Joint Surg Am. 1977 Jan;59(1):82-7.
[160] Service RF. Nanotoxicology. Nanotechnology grows up. Science. 2004 Jun 18;304(5678):1732-4.
[161] Meng J, Kong H, Xu H, Song L, Wang C, Xie S. Improving the blood compatibility of polyurethane using carbon nanotubes as fillers and its implications to cardiovascular surgery. Journal of Biomedical Materials Research. 2005 5 January 2005;74A:208-14.
[162] Lara W, Schweitzer J, Lewis R, Odum B, Edlich R, Gampper T. Technical considerations in the use of polymethylmethacrylate in cranioplasty. J Long Term Eff Med Implants. 1998;8(1):45-53.
[163] Diamond TH, Clark WA. Percutaneous vertebroplasty: a novel treatment for acute vertebral fractures. Med J Aust. 2001 Apr 16;174(8):398-400.
[164] Barber AH, Andrews R, Schadler LS, Wagner HD. On the tensile strength distribution of multiwalled carbon nanotubes. AIP 2005:203106.
[165] Marrs B, Andrews R, Rantell T, Pienkowski D. Augmentation of acrylic bone cement with multiwall carbon nanotubes. Journal of Biomedical Materials Research Part A. 2006;77A(2):269-76.
[166] Safadi B, Andrews R, Grulke E. Multiwalled Carbon Nanotube Polymer Composites: Synthesis and Characterization of Thin Films. Journal of Applied Polymer Science. 2002;84:2660-9.
[167] Janna S, Dwiggins DP, Lewis G. A new, reliable, and simple-to-use method for the analysis of a population of values of a random variable using the Weibull probability distribution: Application to acrylic bone cement fatigue results. Bio-Medical Materials adn Engineering. 2005 15 March 2004;15:349-55.
[168] Cadek M, Coleman JN, Ryan KP, Nicolosi V, Bister G, Fonseca A, et al. Reinforcement of Polymers with Carbon Nanotubes: The Role of Nanotube Surface Area. Nano Lett. 2004 February 11, 2004;4(2):353-6.
[169] Ye H, Lam H, Titchenal N, Gogotsi Y, Ko F. Reinforcement and rupture behavior of carbon nanotubes--polymer nanofibers. Applied Physics Letters. 2004;85(10):1775.
[170] Roques A, Browne M, Thompson J, Rowland C, Taylor A. Investigation of fatigue crack growth in acrylic bone cement using the acoustic emission technique. Biomaterials. 2004 Feb;25(5):769-78.
[171] Savage RH. Graphite Lubrication. Journal of Applied Physics. 1948;19(1):1-10.
[172] Kotha SP, Li C, Schmid SR, Mason JJ. Reinforcement of Bone Cement Using Zirconia Fibers with and without Acrylic Coating. 52nd Annual Meeting of the Orthopaedic Research Society; 2006; Chicago, IL; 2006. p. 935.
[173] Marrs B, Andrews R, Pienkowski D. Multiwall Carbon Nanotubes Enhance the Fatigue Performance of Physiologically Maintained Bone Cement. The International Carbon Conference; 2006 July 2006; Aberdeen, Scotland; 2006.
[174] Metallic Materials - Fatigue testing - Fatigue crack growth method: British Standards; 2003. Report No.: BS ISO 12108:2002.

[175] Standard Test Methods for Plane-Strain Fracture Toughness and Strain Energy Release Rate of Plastic Materials. West Conshohocken, PA: ASTM International; 2000. Report No.: ASTM Standard D5045.
[176] Ryan KP, Cadek M, Nicolosi V, Walker S, Ruether M, Fonseca A, et al. Multiwalled carbon nanotube nucleated crystallization and reinforcement in poly (vinyl alcohol) composites. Synthetic Metals. 2006;156(2-4):332.
[177] Satapathy BK, Weidisch R, Potschke P, Janke A. Crack Toughness Behaviour of Multiwalled Carbon Nanotube (MWNT)/Polycarbonate Nanocomposites. Macromolecular Rapid Communications. 2005;26:1246-52.
[178] Sinnett-Jones PE, Browne M, Ludwig W, Buffiere JY, Sinclair I. Microtomography assessment of failure in acrylic bone cement. Biomaterials. 2005 Nov;26(33):6460-6.

VITA

Brock Holston Marrs

Born February 26, 1979, Glasgow, KY

EDUCATION

Master of Science, Biomedical Engineering, University of Kentucky, December 2003. Thesis: Augmenting Bone Cement with Multiwall Carbon Nanotubes.

Bachelor of Science, Physics-Engineering, Washington and Lee University, June 2001.

PROFESSIONAL POSITIONS

2000 – 2000 **Research Assistant**, Washington and Lee University, Lexington, VA

2002-current **Graduate Research Associate**, Center for Applied Energy Research, Lexington, KY

2006 - 2006 **Visiting Scientist**, Finsbury, Ltd United Kingdom

HONORS

2005 Nomination for Dissertation Year Fellowship

2007 Society of Biomaterials STAR Award (Honorable Mention)

PUBLICATIONS

Marrs B, Andrews R, Rantell T, Pienkowski D. "Flexural properties of polymethylmethacrylate augmented with multiwalled carbon nanotubes." Presented (poster # 1461) at the 49th Annual meeting of the Orthopaedic Research Society, New Orleans, LA, 1 – 4 February 2003.

Marrs B, Andrews R, Rantell T, and Pienkowski D. "Multiwall Carbon Nanotubes Improve the Fatigue Performance of Bone Cement." Presented (poster # 69) at the International Workshop on Nanomaterials, Lexington, KY 20 – 21 September 2004.

Marrs B, Andrews R, Rantell T, and Pienkowski D. "Multiwall Carbon Nanotubes Enhance the Fatigue Life of Bone Cement." Podium Presentation at the 50th Annual Meeting of the Orthopaedic Research Society, San Francisco, CA, 7 – 10 April 2004.

Marrs B, Andrews R, Rantell T, Pienkowski D. "Augmentation of acrylic bone cement with multiwall carbon nanotubes." Journal of Biomedical Materials Research Part A, 2006; 77A(2): 269-276.

Shaffer W, Margulies J, Cassidy C, **Marrs B**, Seeley M, Pienkowski D, Shapiro R. "Sacroiliac Instability: A Novel Study of Scoliosis Constructs." Harrington Spine Symposium, University of Kansas, 2005.

Shaffer W, Margulies J, Cassidy C, **Marrs B**, Seeley M, Pienkowski D, Shapiro R. "Sacral fracture constructs: how can we understand the complex relationships of the pelvis to the lumbar spine?" 20th Annual Meeting of the North American Spine Society, 2005.

Marrs B, Andrews R, Pienkowski D. "The Fatigue Life of Physiologically Maintained Bone Cement is Enhanced by Multiwall Carbon Nanotubes." Podium Presentation at the International Carbon Conference, Aberdeen, Scotland, 16 – 21 July 2006.

Marrs B, Andrews R, Pienkowski D. "Multiwall Carbon Nanotubes Enhance the Fatigue Performance of Methyl Methacrylate Copolymer." Accepted for Presentation at the Society for Biomaterials 2007 Annual Meeting, Chicago, IL, 18 – 21 April 2007.

Marrs B, Weisenberger M, D Bortz. "Fatigue Performance of Multiwall Carbon Nanotube – Polymer Composites." Accepted for Presentation at the International Carbon Conference, Seattle, WA, 15 – 20 July 2007.

Marrs B, Sinnett-Jones P, Sinclair I, Andrews R, Pienkowski D. "Multiwall Carbon Nanotubes Affect the Fatigue Crack Propagation of Orthopaedic MMA-co-Sty." Accepted for Presentation at the International Carbon Conference, Seattle, WA, 15 -20 July 2007.

Marrs B, Andrews R, Pienkowski D. "Multiwall Carbon Nanotubes Enhance the Fatigue Performance of Physiologically Maintained Methyl Methacrylate – Styrene Copolymer." *Submitted to* Carbon, 2007.